University of Vermont
ScholarWorks @ UVM

Graduate College Dissertations and Theses | Dissertations and Theses

2015

Multi-Satellite Formation Trajectory Design with Topological Constraints over a Region of Interest using Differential Evolution

David William Hinckley
University of Vermont, dhinckle@uvm.edu

Follow this and additional works at: http://scholarworks.uvm.edu/graddis

 Part of the Aerospace Engineering Commons, Computer Sciences Commons, and the Mechanical Engineering Commons

Recommended Citation
Hinckley, David William, "Multi-Satellite Formation Trajectory Design with Topological Constraints over a Region of Interest using Differential Evolution" (2015). *Graduate College Dissertations and Theses*. Paper 404.

This Thesis is brought to you for free and open access by the Dissertations and Theses at ScholarWorks @ UVM. It has been accepted for inclusion in Graduate College Dissertations and Theses by an authorized administrator of ScholarWorks @ UVM. For more information, please contact donna.omalley@uvm.edu.

Multi-Satellite Formation Trajectory Design with Topological Constraints over a Region of Interest using Differential Evolution

A Thesis Presented

by

David Hinckley

to

The Faculty of the Graduate College

of

The University of Vermont

In Partial Fullfillment of the Requirements
for the Degree of Master of Science
Specializing in Mechanical Engineering

October, 2015

Date: March 20th, 2015
Thesis Examination Committee:

Darren Hitt Ph.D., Advisor
Chris Danforth Ph.D., Chairperson
Margaret Eppstein Ph.D.
Cynthia J. Forehand, Ph.D., Dean of the Graduate College

Abstract

Satellite formation missions allow for scientific measurement opportunities that are only otherwise possible with the use of unrealistically large satellites. This work applies the Evolutionary Algorithm (EA), Differential Evolution (DE), to a 4-satellite mission design that borrows heavily from the mission specifications for Phase 1 of NASA's Magnetospheric Multi-Scale Mission (MMS). This mission specifies goals for formation "quality" and size over the arc when scientific measurements are to be taken known as the Region of Interest (ROI). To apply DE to this problem a novel definition of fitness is developed and tailored to trajectory problems of the parameter scales of this mission. This method uses numerical integration of evolved initial conditions for trajectory determination. This approach allows for the inclusion of gravitational perturbations without altering the method. Here, the J2 oblateness correction is considered but other inclusions such as solar radiation pressure and other gravitational bodies are readily possible by amending the governing equations of integration which are stored outside of the method and called only during evaluation. A set of three launch conditions is evaluated using this method. Due to computational limitation, the design is restricted to only single-impulse maneuvers at launch and the ROI is initially restricted but then expanded through a process known here as "staging". The ROIs of tests are expanded until they fail to meet performance criteria; no result was able to stage to the full MMS specified $\pm 20^\circ$ ROI but this is a result of the single-impulse restriction. The number of orbits a launch condition is able to meet performance criteria is also investigated. Revolutions considered and the ROIs therein contained are staged to investigate if the method is able to handle this additional problem space. Evidence of suitable formation trajectories found by this method is here presented.

Acknowledgements

I would first like to thank my advisor Dr. Hitt for all his help and always being willing to answer questions I had concerning orbital mechanics and grad school in general. I also would like to thank Dr. Eppstein for offering the class that started all of the research herein contained. Additionally, thanks to Jacob Englander and Trevor Williams of NASA GSFC for helping with the specifics of the MMS mission. Lastly, I wish to thank Vermont Space Grant Consortium and the Vermont Advanced Computing Core for providing the funds and the means to conduct this research.

Table of Contents

List of Figures

Chapter 1

Introduction

The use of multi-satellite formations to accomplish tasks that would otherwise require monolithic and impractical single satellite designs is an area of growing interest for both scientific and commercial applications. The premise of this technology is taking advantage of the additional information provided by the known large relative displacement of many satellites; information such as measurement variation, signal arrival angle, etc. For example, Stiles, Goodman, and Lin (1) proposed using formation satellites equipped with synthetic aperture radar (SAR) to form a large "virtual" satellite of greater capability. Similarly, Gill (2) discussed the QB50 mission which aims to use multiple (target number of 50) cube-sats for thermospheric measurement. These are just two examples of the ever-expanding realm of opportunity provided by formation flying satellites. Trajectory design for a mission consisting of a single satellite is complicated, thus extending this to multiple satellites with new requirements on relative position (some form of formation constraint is required for many of tasks that benefit from this technology) further complicates the matter. In recent years, the prospect of Evolutionary Algorithms (EA) has been explored in an effort to automate this task and aid in the discovery of optimal trajectories for mission planning. In 2005, Lee et al. (3) applied multi-objective variations of Genetic Algorithms (GA) to low-thrust orbit transfer problem by evolving orbital elements. Bessette and Spencer

(4), in 2006, sought to find alternatives to the fuel optimal Hohmann transfer that better balanced considerations of time of flight as well as fuel expended. They applied Particle Swarm Optimization (PSO), Differential Evolution (DE), and Covariance Matrix Adapted Evolutionary Strategies (CMA-ES) to Low-Earth Orbit (LEO) focused transfer problems. In 2007 Vasile, Miniscil, and Locatelli (5) developed a new variant of DE called Inflationary Differential Evolution which drew upon the heuristics of PSO and the premise of Monotonic Basin Hopping (MBH) to form a method that, given a few assumptions, guarantees convergence to fixed points (which exist under the assumptions) as the number of evolved generations approaches infinity. They applied it the method to interplanetary trajectory design. In 2008, Casalino and Sentinella (6) explored the benefit of having different combinations of GA, DE, and PSO cooperate in designing interplanetary trajectories with gravity assist maneuvers (all done using orbit relations and the patched-conic model). Also in 2008, Cacciatore and Toglia (7) used a GA to find orbit transfers between circular orbits that minimized fuel under the finite-burn thrust model. Yet again in 2008, Vinko and Izzo (8) applied GA, DE, PSO, and Simulate Annealing (SA) to many benchmark problems posed by the European Space Agency (ESA) and found that, similar to Casalino and Sentinella, cooperative approaches have the benefit of covering methodological weaknesses. In 2011, Yam, Lorenzo, and Izzo (9) applied Basin Hopping and SA to interplanetary low-thrust problems. They used the Sims-Flanagan transcription for the low-thrust model and combined their EAs with local optimizers to improve performance. In 2012 Englander et al. (10) used a GA to choose fly-by sequences for interplanetary missions where the trajectories were then found using an alternating combination of DE and PSO.

The work here presented aims to apply the evolutionary optimization method DE to the design of formation-flying satellite trajectories that meet formation requirements akin to those in actual application. The Magnetospheric Multi-Scale Mission (MMS) serves as the inspiration for the mission specifications and a definition of evolutionary "fitness" is

developed that is well suited to conditioning the evolution of formation trajectories that meet the set specifications. Orbit determination will be done using numerical integration so as to allow for the inclusion of perturbations to the traditional gravity model, many of which do not have orbits that can be expressed in closed form. Only the gravitational perturbation caused by the oblate description of the Earth will be considered, as it is the most prominent disturbance for the MMS mission; a description of the physics involved can be found in the Appendix. A select set of initial configurations will be tested to demonstrate the approach. First, optimization will be done for tests that consider only single revolutions about Earth. A method will then be presented and demonstrated for extending these results to multiple revolutions. The ultimate result is a means of finding trajectories for multi-craft formation flying missions with formation constraints over a region of the orbit. In this work, the concern is not so much the discovery of "the optimal" (globally optimal) formation trajectories but rather to show that DE, with the bulk of the effort applied to the development of the fitness function and the adjustment of already available algorithm parameters, is a good candidate for the task when approaching this problem using numerical integration so that incorporation of gravitational perturbations is seamless; the functionality of the basic DE will not be too heavily altered beyond the parameters that already exist. To declare that solutions found in this work are globally optimal would require a deep investigation of the effects of varying the algorithm's parameters and that is beyond the intended scope of this work. All this ignores the fact that mission design of this type is only a medium-fidelity result. High-fidelity mission planning isn't possible with EAs since they are too computationally expensive to be viable. The answer is to locally optimize the medium-fidelity solution in a high-fidelity tool, like NASA's General Mission Analysis Tool (GMAT). This allows for the searching to be conducted in the less computationally expensive search space yet still directly benefit from the result.

1.1 Magnetospheric Multi-Scale Mission Specifications

An exemplar of a multi-satellite mission in which formation is a constraint is NASA's Magnetospheric Multi-Scale Mission (MMS). This soon ready mission (scheduled to launch 3-12-15) plans to use a tetrahedral arrangement of four satellites to take scientific measurements of the Earth's magnetosphere to further our understanding of the Earth as a whole. As Hughes explains, the missions purpose is to take measurements throughout the plasma sheet region of the Earth's magnetosphere; the reference orbit was constructed so as to maximize the time spent in this region (11). The mission's specified reference path about the planet has a perigee of 1.2 Earth Radii (Re), an apogee of 12Re, and an inclination of 28.5°. This corresponds to an eccentricity of 0.82 which means the reference orbit is highly elliptical. The mission consists of different phases with different goals for each. This work focuses on the specifications for Phase 1. For all phases, the satellites are to attempt to meet different size targets for their regular tetrahedral formation. In Phase 1, the smallest target side-length is 10km and the largest target side-length is 160km. It is only necessary to outline the extremes of the target range since they would be the most difficult required side-lengths to meet. These side-length targets need not be strictly met but rather allow a range of permissible values for each. For the target of 10km, the formation is allowed to have any average side-length within the range of 6km to 18km. When 160km is the target, any average side-length of the range 140km to 190km is acceptable. There is also no penalty for non-constant side-lengths. Formation constraints that allow for scientific measurement are only relevant in a region that is symmetric about apogee. The mission specifies that the region of interest (ROI) is the section of the orbit where the orbital radius exceeds 9Re which roughly translates to $\pm 20°$ about around apogee (an illustration of the concept of an ROI is shown in figure 1.1). The measurements would ideally be made while all four

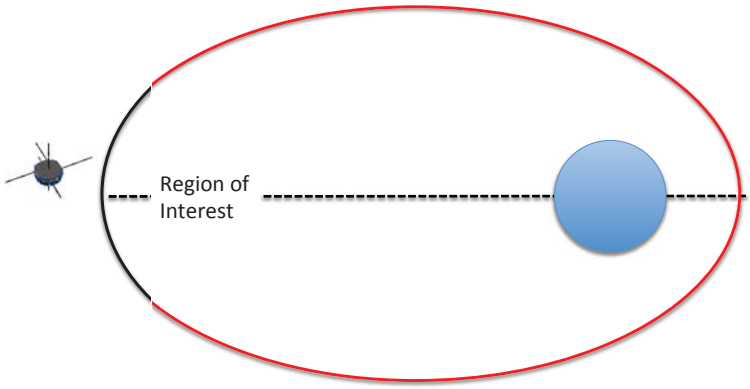

Figure 1.1: Illustration of Differential Evolution's main operator

satellites maintain formation in the shape of a regular tetrahedron but maintaining a constant shape over a region of the orbit is not physically possible; Keplerian motion demands relative drift of the satellites due to their differing orbital radii. A metric known as the quality factor (QF) was established to measure the regularity of the tetrahedron made by the satellites (11)(12). The QF is expressed mathematically as:

$$QF = \frac{V}{V_{reg}} \tag{1.1}$$

where V is the volume of the tetrahedron made by the satellites at a specific time and V_{reg} is the volume of a regular tetrahedron whose side-length is equal to the average side-length of the formation's tetrahedron at the same moment in time. The QF is then always of the range $[0, 1]$ with 1 representing a regular tetrahedron. The MMS mission specifies that the satellite formation is to have a QF that exceeds 0.7 for 80% of the time the satellites spend while in the ROI(13). All of these specifications can be met if active control methods were employed but that would ultimately be too expensive from a fuel standpoint to be viable in application. Satellites are instead given two opportunities to make corrective maneuvers along the orbit, at $\pm 90^{\circ}$ anomaly, so as to meet the stated requirements for as long as

possible; perigee would have been a more efficient choice for conducting corrections due to the Oberth effect but the satellites are moving too fast through perigee for communication with ground control (Trevor Williams, personal communication).

MMS trajectory design has been explored by both Hughes (11) and Roscoe (12). Both optimized equations that contained penalties for trajectories that failed to meet the mission requirements using known orbit relations. In both cases, the satellite trajectories were found by considering only the relative motion of the satellites while a reference path was traveled since the scales of the formation and the scale of the orbit were sufficiently different for them to be determined separately. Hughes used MATLAB's $fmincon$ function to optimize trajectories based on the defining orbital elements using orbit relations. This restricted his analysis to Keplerian motion although the use of such relations does allow for fast calculation. Roscoe made use of the Gim-Alfriend state transition matrix for his calculation of relative motion which incorporates the effects of the J2 oblateness correction (discussed in A.1.2). Roscoe also optimized trajectories considering multiple revolutions using this approach; as was made meaningful with the oblateness inclusion which makes the problem non-trivial. Neither of these methods are extendable beyond the physics initially considered, but this will be discussed later in section 3.1.

The work of Hughes and Roscoe serve to provide many useful elements to consider for this optimization problem. Components of this mission's specifications are used by this work to lend real-world relevance to the task of developing an evolutionary approach.

1.2 Differential Evolution

Differential Evolution (DE) is a population-based Evolutionary Algorithm (EA) in which candidate solutions are found by taking weighted differences of members of the population. Candidate solutions are themselves arrays of values that correspond to a potential solution to the function being optimized (the "fitness function"), which incorporates elements from the

problem domain giving the potential solution meaning. As an EA, the optimization is based off of concepts in biological evolution like "survival of the fittest" and "genetic" construction being responsible for said fitness. The problem is decomposed into a set of values that are used to describe a candidate solution. This is called the "genome" of the problem as it is the "genetic" map that translates into the phenotypic expression known as "fitness". DE has a genome comprised of real-values. As a population-based method, DE maintains several different candidate solutions during optimization. New solutions that provide lower fitness values (problems are often framed for minimization) replace the old solution from which they were made. Thus the population of candidate solutions progressively improves as evolution proceeds. Exact details of the DE parameter values used here are provided in Section 3.5. The implementation DE used here is taken from Storn and Price (14). The basic functionality of this template was only slightly modified to allow for the specific needs of this problem, namely initial seeding of the population was adjusted. The fitness function is entirely new and detailed in Section 3.2.

There are many flavors of DE. Here the basic method DE/rand/1/bin is described. The method starts with initializing a population of trial solutions. Often the initial population is comprised of entirely random solutions drawn from a uniform distribution but for certain applications it may be advantageous to seed the initial population, possibly by applying random noise to an estimated trial solution around which one wishes to explore. Once the population is initialized, "children" solutions are created from the trial solutions in the population ("parents"); a child solution is made for each trial solution in the population. This is done using a stochastic cross-over operation between a parent solution and a weighted combination of one other random solution, and the difference of two other random solutions, taken from the existing population. The parameter that controls the element-wise likelihood of cross-over is called the cross-over rate. To ensure that the child solution has no possibility of being identical to the parent, which has a non-zero probability if only the cross-over rate

were used, one index is chosen at random to cross-over regardless of the cross-over rate.

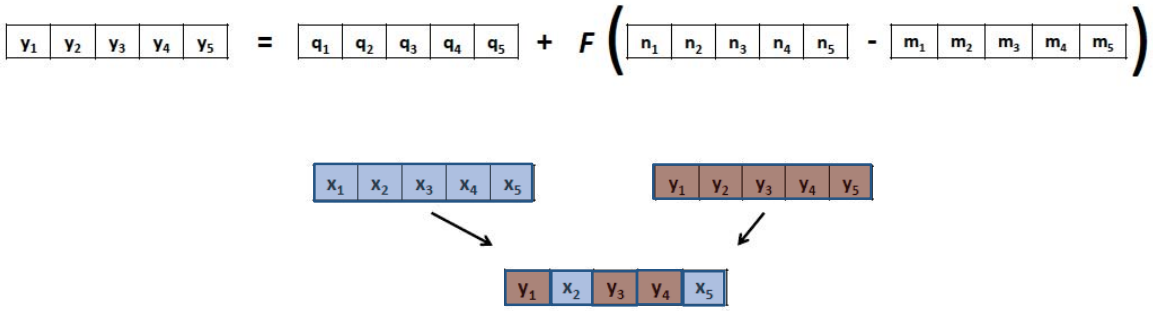

Figure 1.2: Illustration of Differential Evolution's main operator

The child solution is then compared with the parent from which it was created and if it is more fit, it replaces the parent in the population. This process of progressive improvement of the population is continued until some predefined stopping criterion is reached. Common choices for such criteria are runtime, number of generations of evolution, number of fitness evaluations, lack of improvement in fitness over a prescribed period, or some combination of these. Figure 1.2 illustrates the child solution creation process. For this example, the **x** vector is the parent solution. The creation of the cross-over partner **y** is shown as the weighted combination of three randomly drawn population members **q**, **n**, and **m** with scaling parameter **F**. From this and the parent solution, the child against whom the parent is compared is created by element-wise cross-over with some probability C_r which is called the cross-over rate. This cross-over allows for new solutions to maintain potentially beneficial elements from the population member from which they are made while still allowing for wholly new solutions. DE is often paired with a "mutation" operator which introduces the potential for entirely new genome elements to be made. A common type of mutation is the stochastic likelihood of applying random noise to each genome element of a new solution. This can provide a means of escaping local suboptima of the fitness function. This effect

does not replace the need for a sufficiently large initial population. If the population is too small, it may not contain the sufficient genetic diversity to eventually construct an adequate solution.

Chapter 2

Preliminary Work

Before applying DE to the MMS problem it was applied to five simpler single craft trajectories. For all problems, the DE would evolve initial velocities, with other parameters introduced as problems required, and numerically integrate the initial conditions forward in time in an attempt to reach a target point. The first four of these preliminary problems share the same launch and destination points. The launch point was set to $[6500, 0, 0]$ in a Cartesian coordinate system centered about the Earth where the x-y plane is the equatorial plane. In order do validate the results, the destination was chosen in such a way that the answer to the direct Lambert problem for a chosen time of flight could be easily expressed and recognized; as the answer will be the initial velocity belonging to the evolved trajectory, the destination point was made by choosing the time of flight as 30 minutes and numerically integrating the conditions forward in time. The known velocity that solves this direct Lambert problem is $[0, 5.6, 5.6]$km/s. The last preliminary problem is set in the rotating Earth-Moon coordinate system. The problems and the results are described in detail in the sections to follow. The DE implementation for problems $1 - 4$ terminated if any of the following three conditions was true:

- 20 minutes elapsed CPU time on an hp Pavillion g7 laptop with an intel i3 processor (60 for the problem 4 extension 4b)

- Maximum element-wise difference from known solution of 0.01
- Best fitness below 10^{-9}

The implementation of DE was a modification of Matlab code written by Storn and Price (14). Source recommended parameter values were used with some light testing to determine the used crossover rate. The crossover rate was set as 0.8, the scaling parameter was set to 0.85, and the population size was set to 5 times the length of the solution vector. The population was initialized with random real values unless otherwise noted. Due to problems with the numerical integrator (Matlab's *ode45*) stalling when set to narrow tolerances, the DE used a more lenient integration tolerance and passed the best found solution to Matlab's *fminsearch* which uses a simplex method for local optimization. Each of the first four problems was run 12 times so as to gain a better perspective on the methods average performance on the problem. The number of times problem five was run was not counted since the primary motivation for the problem was to determine if the method used in the first four problems could be applied to this more difficult problem in a rotating coordinate frame. Here "success" will be defined as achieving error within the tolerance of mission planning for the problem's domain. For the LEO environment of problems $1-4$, the required accuracy is on the order of a meter (Jacob Englander, personal communication). For problem 5 the only requirements are a position error and final velocity that allow for capture at L4.

2.1 Fitness Function for the Preliminary Problems

Equation 2.1 is the fitness function for the first four problems. Its terms allow for final positional error, time of flight variation from a chosen value, initial fuel expended (seen as proportional to the energy required, which in turn is proportional to the square of the

magnitude if the velocity change vector), and a crash penalty to be assessed.

$$f = w_1\|(\hat{P}_2 - P_2)\| + w_2\|(\hat{v} - v)\|^2 + w_3 C \tag{2.1}$$

where f is the fitness value, P_2 is the target location, $\hat{P}_2$ is point at which the trajectory terminates after numerical integration, v is the candidate solution's initial velocity vector, $\hat{v}$ is the velocity vector of the theoretical craft prior to the maneuver (this allows for the energy cost of adopting the new trajectory to be taken into account), C is a crash penalty to ensure that paths through the planet are not chosen (the value of C is the depth the craft traveled into the Earth), and w_i are weights balancing the importance of the terms.

Equation 2.2 shows the necessary changes required to adapt Equation 2.1 for the Earth-Moon frame. Here, the positional error is explicitly set for the target point L4. Since the arrival velocity is now a concern, the fuel required to counter it (again expressed and the square of the velocity's magnitude) serves to penalize the final velocity's magnitude so as to allow for capture at L4. The flight time focusing term from the prior equation has been altered to allow for conditioning the method to prefer longer flight times; this is to allow for a conditioning of evolution by the human knowledge that the low arrival velocity trajectories have long flight times. The last new term is an out-of-plane penalization which limits the computer's exploration of a known sub-optimal region.

$$f = w_1 * \|v_i\|^2 + w_2 * \frac{\|r_f - L4\|}{r_{12}} + w_3 * \|v_f\|^2 + w_4 * \frac{1}{\Delta t} + w_5 * (\|r_{i_z}\| + \|v_{i_z}\|)^2 + w_6 * C \tag{2.2}$$

where r_{i_z} and v_{i_z} are the out-of-plane components of initial position and velocity respectively, $L4$ is the L4 Lagrange point (which is one of two locations in the Earth-Moon system that is a stable equilibrium point), r_{12} is the distance between the centers of the Earth and Moon, and the remaining variables have definitions unchanged from Equation 2.1.

2.2 Lambert's Problem

Lambert's is a classic orbital mechanics problem. In this problem initial position, target position, and time of flight are specified and the answer is the initial velocity that completes the trajectory. There is an analytical means of finding the exact answer but it is restricted to simple Keplerian motion. With this problem, the method will be taxed with recovering a known solution as a benchmark test. As was explained earlier, by nature of the problems construction the answer will be the specified velocity used to choose the target point, $[0, 5.6, 5.6]$km/s. For this problem, the weighting vector w was set to $[10, 0, 0]$. The only specification for this problem is final target accuracy so the weights associated with the other terms are set to 0. It was not felt necessary to enable the crash penalty since it is computationally expensive to check for collision with such a low probability of occurrence; the consequence of this decision was seen in the results where one trajectory stochastically chose to travel through the planet.

2.3 Minimum Energy Lambert's Problem

This problem is a variation on the classical Lambert's problem where instead of specifying time of flight, minimization of the energy of the transfer ellipse is sought; time of flight is then added to the problem genome as a component of evolution. In the proper direction around Earth (not against spin) there is one such path. Initial velocity and time of flight are the answers to the problem but due to the uniqueness of the trajectory either suffices to specify the answer; here time of flight will be used as it is easier to understand. The correct answer for this problem is then 2413.58 seconds of fight time. Since here too there is a known analytical solution, this tests serves as a benchmark proving that the method can recover known result with more complicated considerations than simple target accuracy. For this problem w was set to $[1, 25, 0]$ so that initial velocity, which is proportional to ellipse energy,

would be minimized along with the target error. This weighting was found through trial and error. Again, the cost of crash avoidance checking outweighed the potential benefits.

2.4 Lambert's Problem with Oblateness

For this problem, the additional effect of the Earth's oblateness, explained in A.1.2, was added to the physics equations passed to the numerical integrator. It differs from the classical Lambert's problem in no other way. This problem demonstrates the extensibility if this solution model by allowing for complicated physical effects to be added to the problem description without altering the problem structure. For this problem the w vector was set to $[1, 0, 10^6]$. Since the perturbation to the gravity model was added the crash detection was enabled as a precaution even though since the solution should be reasonably close to the direct Lambert solution since there is not much time for the perturbation to move the end of the trajectory.

2.5 Multi-revolution Lambert's Problem

In spacecraft mission planning it may be advantageous to wait before arriving at a target location; waiting for an object/spacecraft to arrive at the target location for example. One means of accommodating this is to circle the planet, here Earth, multiple times before arrival. When considering only Keplerian motion this problem is trivial since one can orbit endlessly on the ellipse that connects initial position and target without the path changing; it will always return to target regardless of how many times one orbits the planet. Here oblateness effects are again added so as to produce a meaningful result. This means that the initial velocity must lead the target such that the precession of the orbit caused by the oblateness of the Earth moves the craft onto the target. This problem is split into two sub-problems. The first (4a) has a wait time of 5 revolution about Earth, the second (4b) has a

wait time of 20 revolutions about the Earth. Both of these are enforced by adding the proper number of periods to the direct Lambert solution and setting that to be the specified time of flight; this suffices since oblateness does not appreciably affect orbital radius. For both the sub-problems in this section, w was set to $[1, 0, 10^6]$. For this problem the crash detection is a must since the planet must be safely orbited numerous times. To accommodate the extra computational cost incurred by numerically integrating the trajectory for 20 orbits, problem 4b was run with the standard 20 minute CPU time limit and an additional run was conducted with the time limit raised to 60 minutes. Since this problem was considerably more difficult than the others, the initial population was seeded with Gaussian noise applied to the known direct Lambert's solution since they should be reasonably close. Testing was done with completely random initial populations but the results were notably worse and are not worth reporting here.

2.6 L4 Trajectory Problem

As mentioned in the beginning of this chapter, L4 is a stable gravitational equilibrium point. This type of location is ideal for long-duration missions (such as space stations or deep space habitats) since no fuel is needed for maintaining the orbit. For this problem no gravitational perturbations are considered and the problem is phrased inside a rotating coordinate frame in which the Earth and the Moon are static. The initial position is not fixed as it was with the other preliminary problems. Instead the distance from the center of the Earth is fixed (at 6578km) and the two angles that define the location on that spherical shell are components of the evolution. Time of flight too is a genome component. For a trajectory to L4 to be operationally viable, the initial fuel cost should be low and the arrival velocity must be sufficiently low to allow for the craft to be captured at L4; if the spacecraft is moving too fast it will pass through L4 or require additional fuel expenditure to slow itself. For this problem the w vector was set to $[1, 3000, 1, 0, 0, 1]$ to balance the target accuracy,

and velocity goals. The position error weight is high due to the normalization distance used; distances were divided by the separation distance between the Earth and the Moon. This test differs greatly from the others in both its CPU time limit and the hardware on which it was run. Since this problem is far more difficult and has longer times of flight considered, tests for this problem were given 10 hours CPU time. These tests were also not run on the aforementioned laptop but instead were run on the VACC (Vermont Advanced Computing Core). This ensured a greater likelihood of solutions being found.

2.7 Preliminary Results

The results from the first four problems are summarized in Table 2.1. For problem 2 where time is the deciding value, the successful trials had times of flight within seconds of the known correct time of flight. From the table it is clear that, when viewing the trials as restarts, the best returned trajectories are within the required tolerances of LEO mission planning.

Table 2.1: Number of successful trials (out of 12), average positional error, and best positional error of successful trials.

Test Problem	Successful Trials	Avg Pos Err (m)	Best Pos Err (m)
1	11	0.023	9.3E-3
2	11	0.071	6.7E-6
3	12	0.003	9.6E-4
4a	12	2.66E-3	9.63E-4
4b (20min)	5	3.04E-3	1.12E-3
4b (60min)	7	1.17E-3	9.43E-4

For the fifth problem, the final positional error was 35.4km and the velocity at target arrival was 0.859km/s which would allow for the craft to be captured at L4. Ideally the arrival velocity would be lower, reducing complications upon arrival (higher velocity means a more active path due to L4's stability), but attempts to favor lower final velocities during

evolution resulted missing the target entirely. That does not mean that there exists no such solutions, it simply means that the method presented here would have to be better tuned or perhaps altered to find them.

Chapter 3

Method

3.1 Numerical Integration vs. Analytical Orbit Equations

One thing common among many of the works discussed in Chapter 1 was the use of orbit relations during optimization. There are benefits to this approach as opposed to using numerical integration, the method here employed, but there are also limitations. Using analytical knowledge allows for instant detailed knowledge of the entirety of a potential trajectory. This reduces the computational time required for each fitness evaluation which ultimately allows for more generations of evolution. This also allows for the extraction of orbital elements (eccentricity, inclination, semi-major axis, etc.) that may be difficult or expensive to assess numerically. A major limitation is the restriction to orbits that can be expressed analytically. This means more complicated effects (such as atmospheric drag, solar radiation pressure, etc.), and combinations of effects, cannot be addressed with this method. Numerical integration allows for such effects to be taken into consideration during evolution; only the governing physical equations are needed rather than fully developed orbit formulas. By viewing the integration physics in a "black-box" manner solution methods

are completely independent of the physics considered. This ability to address a wider range of effects comes at the cost of computation time. This then stunts the total evolution by increasing the amount of allowed run-time spent on fitness evaluations instead of evolutionary progression, assuming that total run-time is limited as is often the case. This trade is a necessary one since no other method exists to address the inclusion of arbitrary collections of these gravitational perturbations.

3.2 Fitness Function

3.2.1 Final Form of the Fitness Function

The fitness function must contain elements that allow for every mission requirement to be met. As explained earlier, the MMS mission specifies requirements placed upon the size (average side-length) of the formation's tetrahedron as well as its quality (formerly referred to as QF but hereafter it may be referenced simply as "quality"); so these values should appear, in some form, in the fitness function. The balance of importance between quality and side-length could be achieved by weighting the considerations; this is commonly referred to as a penalty method when summing weighted quantifications of "unfitness" (as this is a minimization problem). For ease of use, the sum of weights on both parts should be 1, allowing for control of weighting to be done by specifying only a single weight. Minimizing the computational cost of fitness evaluations should also be a goal as lowering the amount of time spent on evaluating fitness allows for more time to be spent on the process of evolution when restricted to a constant time limit. With that in mind, it would then be irresponsible to have a fitness function that is evaluated continuously over the entire ROI. A simpler method that should achieve the same effect is to evaluate fitness at discrete points along the ROI. The exact number of evaluation points is not of great importance. The only requirement is that enough points are sampled to properly characterize the data; sampling a great

many points would not serve to improve accuracy – barring small yet drastic phenomena – and only slow fitness evaluation as adding points brings the process closer to the limit of continuous evaluation. Using Mathematica's "manipulate" function to test visualizations of possible functions with various parameter sets at a point of evaluation, Equation 3.1 was found to have the sought after global minimum and easy to follow contours. The tipping point for the weighting between quality and side-length also lies at neither extreme with no dramatic, sudden change; this means that capturing a suitable value should not require too precise a combing of the weighting space of $[0, 1]$.

$$\text{Fitness} = \sum_{i=1}^{p} (1 - w) \frac{|L_i - R|}{d} + \exp\left([10\, w(2 - Q_i)]^n\right) \tag{3.1}$$

where p is the number of discrete points of fitness evaluation, w is the tunable weight that balances quality and size, L_i is the average side length of the tetrahedron at a point of evaluation i, R is the formation's target size, d is a scaling parameter that when raised above 1 relaxes size penalties (set to 1 for current testing), Q_i is the quality of the formation at a point of evaluation i, and n controls the form of quality penalties which is set to 0.6 for the best results in current testing. For single orbit problems, the p is set to 50. For multiple orbit problems, p is set to $50 * r$ where r is the number of revolutions about the planet considered.

Figure 3.1 depicts the fitness function at a single point of evaluation plotted over a range of expected average side-length values; since population seeding (discussed in Section 3.5) is used extremely large values are unlikely. This function topology provides a clear and direct path that points to the desired formation quality and size from any initial point. A detail that is lost with this graphic is the fact that fitness is measured at many points that are linked together by progression through a gravitational field with extra physical considerations. This means that the fitness landscape as seen for a trial solution will not appear as simple as the function evaluated at a single point but the simplicity of the topology

shown here will help reduce the complexity of the complete fitness topology; if the function evaluated at a single point appeared very multi-modal or perhaps chaotic, this complexity would carry through to the aggregate of points making optimization more difficult.

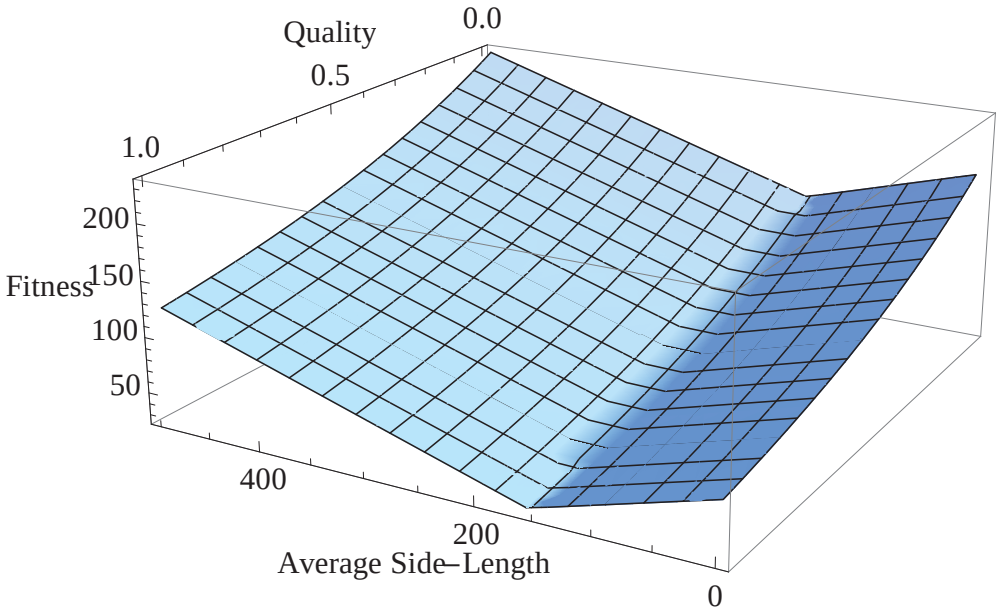

Figure 3.1: Plot of fitness function over expected range of values for target side-length of $160km$

3.2.2 Early Attempts at a Fitness Function

There was a completely different fitness function that was first used in experiments that did not feature any explicit mention of quality. Looking to works in multi-agent control, the concept of artificial potential functions (discussed in application here (15)) was seen as an attractive prospect for essentially scoring the formation on how regular, in terms of 3-D shape quality, it maintains itself about a fixed path. Artificial potential functions utilize environmental data as well as information pertaining to each agent and uses it to compute a potential that agents should seek to minimize by following the gradient. Fundamentally, it is a gradient-based scheme applied to a dynamic fitness landscape; it is dynamic in that

the unique (barring duplicates) fitness landscapes of each candidate solution change each time the solution evolves. To clarify, two distinct agents, satellites in this work, do not have topologically identical potential evaluations since each uses the other's position in determining the potential at their own location as well as the potential in their immediate vicinity. The potential must be carefully constructed so that mission specifications are met. The first component of the potential is a spherical minimum centered about the reference path. This minimum pulls all of the satellites along the path designated by the mission. The second and final component of the potential function is a repulsive, attenuating maximum placed at the location of every satellite aside from one's own location; as this is evaluated from the perspective of a satellite. The working mathematical formulation can be seen in Equation 3.2.

$$p = \sum_{i=1}^{4} \left[c_1 |(\mathbf{r_i} - \mathbf{R}) - L|^{e_1} + \sum_{j \in [1,4]-i} \frac{c_2}{|\mathbf{r_i} - \mathbf{r_j}|^{e_2}} \right] \tag{3.2}$$

where: $\mathbf{r_i}$ is the position of the i^{th} satellite, $\mathbf{R}$ is the position of the reference path, L is the radius of the spherical minimum, and c_1, c_2, e_1, e_2 are tunable parameters that control the relative strengths and profiles of attraction to the spherical minimum and repulsion from other satellites which were set as follows: $c_1 = 1$, $c_2 = 1$, $e_1 = 2$, $e_2 = 2$. The potential is valid at a single point in time and is summed over a discrete number of points along the ROI to give the fitness value much the same way as the final fitness definition. This method was abandoned as it was never able to settle upon a solution with sufficient quality. A hypothesis as to why this may be is that this function is a dynamic fitness landscape. The adjustment of a single satellite alters the local optima of all others. If each satellite were allowed time to find its own local optimum whilst the others were unchanged, taking turns as it were, then it may be possible for a solution that meets the mission criteria to be reached. This however is too inefficient a methodology as a faster means of achieving solutions of sufficient quality is readily available in the first fitness definition here presented.

3.3 MMS-Class Mission Specifications

For the purposes of this work, elements of the MMS mission were borrowed and modified to serve as guidelines. First, here only single impulse maneuvers were considered. While it is possible to setup the evolution to consider multiple propulsion firings, initial work in allowing two such firings appears to have expanded the solution search space too much given the computational time limits of the VACC. The perigee and apogee radii were not altered from their values in the MMS description; these points were placed on the x-axis of the Cartesian coordinate system used which means that they occur in the equatorial plane. The inclination has been changed from the 28.5° as noted in the mission description to 28°. The reason for this change was, simply put, an oversight; the initial description was read hastily and the decimal was omitted. The does not cause an issue since the inclination is close enough to the actual value that the oblateness effects that result are not dramatically different. Any inclination would serve for the purpose of demonstration as long as oblateness effects were present. The QF requirement was simplified. Instead of requiring QF to exceed 0.7 for 80% of the time spent in the ROI, the requirement is extended to the entire ROI. This would restrict the number of solutions found valid if only the full ±20° ROI was used since it is now a harder problem with the restriction to only a single impulsive maneuver but ROI is not held rigidly to the specification. Instead, reaching the full ROI for a test configuration is the goal. The ROI was "staged" from a computationally manageable size up to where the other requirements were no longer met. The staging process is explained in Section 3.4. The bounds of allowable side-length were made symmetric so as to simplify the staging of results. The furthest bound from target was applied symmetrically in determining permissible formation sizes. This means that when the target of a test is 10km, the allowable range is ±8km. When the target is 160km, the allowable range is ±30km.

3.4 Staging Procedure in Testing

When optimizing according to the here described fitness function, larger ROI windows increase the amount of time required for algorithm termination according to the preferred condition of stagnating improvement. For the MMS orbit the time window corresponding to $\pm 20^\circ$ is approximately $\pm 23,500$ seconds about apogee. Given the time required, directly optimizing for a time window of even $\pm 10,000$ seconds is not possible; there is little doubt that some trials would find marginally acceptable solutions but none would finish execution by the preferred conditions (not elapsed time). To address this issue, the problem is run through a *staging process* of increasing window size, feeding the previous solutions as the population seeds for the later runs. Time windows are started at $\pm 1,000$ seconds and then transition to $\pm 5,000$ seconds. From there, the staging follows increments of $5,000$ seconds until either results no longer satisfy the mission requirements or the full $\pm 20^\circ$ window is met. This chosen staging increment was settled upon through trial. Using these increments, tests most often conclude by the preferred termination conditions. This method is used since solutions for larger windows should locally be close to optimal within a smaller window. In essence, later stages shape the heretofore untamed edges of earlier stages.

When considering multiple revolutions, the same approach is used but due to a different concern. The time required to numerically integrate paths through multiple revolutions greatly increases the time spent on a single fitness evaluation. The concern now is that the population within a trial will not be given sufficient time to evolve through many generations. This concern is also why all multiple revolution tests were given higher time allowances. The staging follows much the same procedure as it did with the window staging. A result from a single revolution test is used to seed a test that considers the effects of 5 revolutions. This is continued in increments of 5 revolutions until the physical constraints of being bound to a single impulse are observed; i.e. that initial and final orbits fall below

mission requirements. Originally it was thought to be wiser to stage window before staging revolution count but it would seem that the per revolution effect of oblateness is greater than that approach allows. Subsequently the reverse is used, staging revolutions using the $\pm 1,000$ seconds results then, if seen worthwhile, staging the ROI window.

3.5 Experiment Details

For this problem initial velocities are to be evolved. The genome for this problem was set to be a listing of the Cartesian velocity vector elements of all satellites participating in evolution in a given trial solution. For all of the tests conducted, one satellite of the formation is constrained to follow the reference path which ensures that the formation will pass through the appropriate space for scientific measurement if the formation goals are met. This satellite's initial conditions thus do not undergo evolution. In many implementations of DE, the initial population is random so as to cover the search space. For this application, with the scale of the orbits involved, the approach of seeding the initial population was adopted. Since the final trajectories of all formation members must not vary too greatly from the fixed reference in order for the formation to meet the mission requirements, Gaussian noise was applied to the reference path to provide the initial population of formation trajectories for each test. The standard deviation for the Normal distribution was set to 0.1km/s for test Cases $1-3$ and to 0.01km/s for test Cases 4 and 5; these values were found through trial. These low standard deviations use human knowledge of the problem, namely that that trajectories too different from the fettered reference cannot meet the mission requirements due to workings of Keplerian motion, to restrict the search space to primarily (a reasonable judgment) useful solutions. This enables the relative tolerance of the numerical integrator to be set to greater accuracy (0.00001) since solutions made of dynamical "garbage" values too greatly slow the integrator; although accuracy here is not of the primary concern as the method is the focus of the work.

The numerical studies have been divided into a set of five test Cases, described below. The additional physical effect of the Earth's oblateness is also present in all Cases. For every test, the DE was set with a scaling parameter $F = 0.85$, a crossover rate $C_r = 0.8$, and a population size of 45 which is five times the number of independent variables (three 3-dimensional velocity vectors). Each test set has 51 independent trials where the only thing differentiating the trials is the balancing weight w. For the 51 trials, w is set to values of the range $[0-1]$ in increments of 0.02. Prior to finalizing test Cases for investigation, preliminary investigations were performed on reference orbits in order to determine the proper scalings for the fitness function (Eq. 3.1). While the results were relevant for the internal purpose of constructing a proper definition of fitness, they do not lend any understanding to the more focused task of simulated MMS mission planning.

3.5.1 Case 1: MMS orbit launching from a linear configuration at -90° anomaly

In this case, the four satellites started their numerical simulation from a radial line at -90° anomaly separated by 100km. The merit of this configuration is that it is quite akin to the actual launch of the MMS mission. A key difference here though is that these experiments are restricted to a single impulse whereas the MMS mission allows two maneuvers initially. Starting at -90° anomaly is not an arbitrary choice. While perigee would appear to be the most fuel-efficient location for the impulsive maneuvers due to the Oberth effect, in practice, the satellites are moving too fast through perigee to effectively communicate corrective maneuvers to ground control. Corrections are therefore made at $\pm 90^\circ$ true anomaly. The -90° scenario was included to permit a more significant impact of perturbations to be realized during the orbit so as to better demonstrate the robustness of the computational approach in incorporating such effects. Tests within this Case were restricted to a CPU-time

limit of 10 hours due to available computing resources.

3.5.2 Case 2: MMS orbit launching from a regular tetrahedron at -90° anomaly

This Case differs from Case 1 only in how the satellites are initially arranged. In an attempt to lessen the deleterious effects of being restricted to a single impulse, satellites are launched from an initial perfect tetrahedron. Thus when the formation must return to a rough approximation of its initial configuration after one revolution, it returns to something of better quality at a smaller size than the target side-length so that the end of the ROI is not as greatly affected as in Case 1. Since the two target side-lengths are an order of magnitude apart, different initial side-lengths were chosen for 10km target test and the 160km target test. For the 10km target an initial side-length of 6km was chosen as it was a reasonable lower bound; this may deviate from the previously stated symmetric simplification but starting the configuration as 2km separation would be unsafe. For the 160km target an initial side-length of 130km was used as it is the specified lower bound of acceptable side-lengths for that target. The reason as to why the initial tetrahedra are smaller than their respective test target sizes is an observation of the relative motion to two entities in orbit. If two objects lying on the same line drawn from the center of the planet have the same velocity and are separated by some distance at periapsis, the relative distance between them will be greater at apoapsis. Thus it was thought reasonable to start the satellites with a relative separation that was less than their target side-length. The exact choice of size is not critical since sufficient orbit space is given from launch to ROI to compensate.

3.5.3 Case 3: MMS orbit launching from a regular tetrahedron at apogee

If launch considerations are abandoned, then the problem is reduced to a search for ellipses in space that fit the requirements of the mission. However, this search is not directly possible when simulating satellites numerically without adding the evolution of initial position which would too greatly expand the search space for this application. The interesting condition of placing perfect tetrahedra at apogee was chosen as a starting point for such a search. The difficulty this condition imposes is the fact that satellites are initially halfway through the ROI by description. To address this, the initial conditions at apogee were numerically integrated without the effects of oblateness so as to place them at the start of the ROI. Those ending conditions were then numerically integrated throughout the ROI with oblateness effects re-applied. To account for the additional step these initial conditions added to implementation, tests of this case were given a CPU time limit of 20 hours. One consequence of this approach is that the perfect initial tetrahedron that was the interest in this deployment is no longer perfect and now it does not occur exactly at apogee as that point has shifted in time due to perturbations. Nonetheless this Case is held as an interesting condition to explore. In this condition is the strong assumption that trajectories meeting mission requirements peak in quality in the center of the ROI which may not hold true for the globally optimal solution but this should be true of some trajectories as one would expect.

3.5.4 Cases 4 & 5: Extension of Cases 2 & 3 to Multiple Revolutions

Here the results of Cases 2 and 3 were used to seed an evolution population that would have the fitness function expanded to include multiple revolutions for Cases 4 & 5 respectively.

3.5. EXPERIMENT DETAILS

As mentioned earlier, staging the number of revolutions was done using a ROI window of $\pm 1,000$ seconds. The best suited results from the $\pm 1,000$ second ROI single revolution tests (Cases 2 & 3) were used to seed a 5 revolution expansion test of the same balancing weight and ROI. From there testing bifurcated. One line of tests was conducted expanding only the ROI window within those 5 revolutions. The other line of testing used only the $\pm 1,000$ second ROI (in each revolution) and expanded the revolution count of the trial; 15 revolutions was used as the stopping point, this was chosen because the ability of trials to meet requirements beyond this point was rare in some initial testing. These tests more quickly met with the limitations of using a single impulse model but testing along revolution and ROI window expansions was conducted in a more general manner than the previous cases; the belief is held that the method is sufficiently demonstrated here to be extended to less restrictive conditions.

Chapter 4

Results

4.1 Case 1

In this first Case, the $L = 160$ km target tests were found to meet the mission requirements through the second stage of $\pm 10,000$ seconds, as evidenced by the tetrahedral quality and average side length metrics in Figures 4.1 and 4.2. Visualizations of the corresponding tetrahedral topology entering the ROI, at apogee, and exiting the ROI are shown in Figure 4.3; such depictions of formation will hereafter follow the single revolution result graphs for clarity. The highest average quality of any single trial was 0.957 with that trial having a peak quality of 0.999. The standard deviation of side-length of that trial was $7.650km$. The balance parameter of this trial was 0.8. The quality and side-length profiles take shapes one would expect; even though they appear reasonable, this does not imply they are globally optimal. Both are roughly symmetric about their centers which follows the reasoning that is if one wishes to maximize/minimize a quantity over a region, the optimum would lie in the center with the edges straying from the best value. Although mostly symmetrical, a shifted center of the profiles with respect to the center of the ROI is apparent for some trials. One explanation for this is the inherent asymmetry of the launch condition. Since this test launched from $-90°$ anomaly, the satellites must return to a rough approximation of their

initial formation; if only Keplerian motion were considered it would be a return to the exact initial formation but oblateness effects slightly skew the formation during the course of an orbit. A linear formation is of 0 quality due to a lack of volume so the formation returning to a line is not desirable from a quality standpoint pragmatic for launch though it may be.

The 10km target tests produced no results at the smallest ROI that met the stated requirements. The distinction here between the test that was capable of staging and the one that was not able to stage is the length-scales involved. Just by inspection of the length plot for the 160km target one sees an overshoot at apogee so that length requirements may be met within the window. If we assume that the overshoot is proportional to the difficulty imposed by the initial conditions, then it seems sensible that the 10km test would be unable to meet the requirements as there is a finite possible overshoot at the 10km target scale; it would also be reasonable to believe that approaching 0km average side-length would be met with exponential (in a qualitative, not strictly mathematical sense) resistance as it is a physical limit (distance is positive definite). At the very least, this may mean that smaller length scale formations may be more affected by choices of initial conditions when restricted to only single impulse trajectories. This assertion will be investigated in the later trials which use initial formations that would make meeting mission requirements easier; this statement is based on human intuition, starting at something much closer to ideal should translate to less effort expended in the transition to an improvement.

4.2 Case 2

The 160 km experiments of this Case fared one stage better than those of Case 1; meeting mission requirements for the ROI of $\pm 15,000$ seconds (Figures 4.4 and 4.5). While this initial condition may be logistically more difficult to implement in a real-world launch scenario, it is still a valid configuration for testing. The highest average quality for this test was 0.936 with a peak quality of 0.988. The standard deviation of side-length of that

trial was 10.499km. For this test, the balance parameter of the best trial was 0.66. The asymmetry observed in the quality graph of Case 1 is even more apparent here. The true anomalies shown are not symmetric about 180° due to the discretization of the ROI in the time domain during fitness evaluation; this potentially could have affected the graph by shifting the mean time of the points of evaluation further along the path. At cursory inspection of the presented results for Cases 1 & 2, it appears that more trials appear in the graphs for Case 1 which would indicate that the problem was better solved by a wider range of balancing parameters which implies the initial positions of Case 1 were better suited to the problem. This overlooks the fact that the results for Case 2 proceeded further in the staging process which means the ROI considered is larger. In fact Case 2 had more 160km trials proceed to the stage past which Case 1's 160km trials could not proceed.

Similar to the 160km test, the 10km test surpassed its Case 1 counterpart and produced results that met mission standards up to an ROI of $\pm 10,000$ seconds (Figures 4.7 and 4.8). Only a single test from this group proceeded for the duration of testing. The average quality is this test was 0.903, peaking at 0.935. The standard deviation of side-length of this trial was 0.571km. The balance parameter was 0.06 which explains the small standard deviation of side-length as compared to the other trials since the magnitude of the parameter can be viewed as the percentage weight of quality relative to fitness; thus the compliment values formation size. Only speculation can be given as to why the side-length profile is so asymmetric. Since evolution is a stochastic process, complete rationalization of the solution is impossible. All that can be said for certain is plainly obvious, that of all the trial solutions surveyed, this fared the best during this run. If the concern of this work was more performance focused instead of demonstrative and application-based conducting multiple runs of the same problem would allow for some investigation into this odd result.

One thing to be learned in comparing Cases 1 and 2 is that the initial configuration greatly influences the allowable width of the ROI. This is undoubtedly exacerbated by the

imposed restriction of allowing only a single impulse maneuver.

4.3 Case 3

For the target of 10km, the staging procedure was able to produce results that met the mission design constraints through the semi-final stage (Figures 4.10 and 4.11); which means the true maximum ROI that met mission requirements lies between the ROIs of ±20000 and ±23500 seconds. The best trial had an average quality of 0.946 and a peak quality of 0.998. The standard deviation of side-length of this trial was 1.145km. The balancing parameter for that test was 0.8, as it was for the 160km trial in Case 1. The full ±20° was not met, this is attributable to the initial configuration. Unlike before where gravity would return the formation to a rough approximation of the initial shape outside of the ROI, effectively pinning a high quality tetrahedron apogee may have made better trajectories physically unattainable. A thought to consider is the possibility that orbits meeting the requirements through the full ROI may have lower peak quality or perhaps non-centered, multiple peaks. Unfortunately qualities in other works have not been reported in such a way as to directly compare them. Something seen here that has yet to appear in prior reported results is this extended apex structure. While not intuitive, this shape extends the dwell-time at higher qualities. Despite this anomalous quality profile, the side-length profile does not appear qualitatively different from others here presented. This would imply that the relation between quality and side-length along the trajectory as demanded by gravity is not simple.

The 160km target experiments of this Case unfortunately fell one stage shorter than the smaller target; meeting the requirements only for the staged ROI of ±15000 seconds (Figures 4.13 and 4.14). The highest average quality of any trial was 0.953 with a maximum of 0.994. The standard deviation of side-length of this trial was 9.285km. The balancing parameter for that trial was 0.66, as it was for the same target length in Case 2. Ultimately

this demonstrates that the initial premise of "perfection at apogee" is not accurate when searching for ellipses that meet the MMS mission requirements for the full $\pm 20^{\circ}$ ROI as outlined; at least within a single-impulse framework.

An interesting repetition of balance weights is observed with these shown results. Only two appear to be linked by formation size. This is likely coincidental as only single test batches were run and balancing parameters were only tested in increments of 0.02.

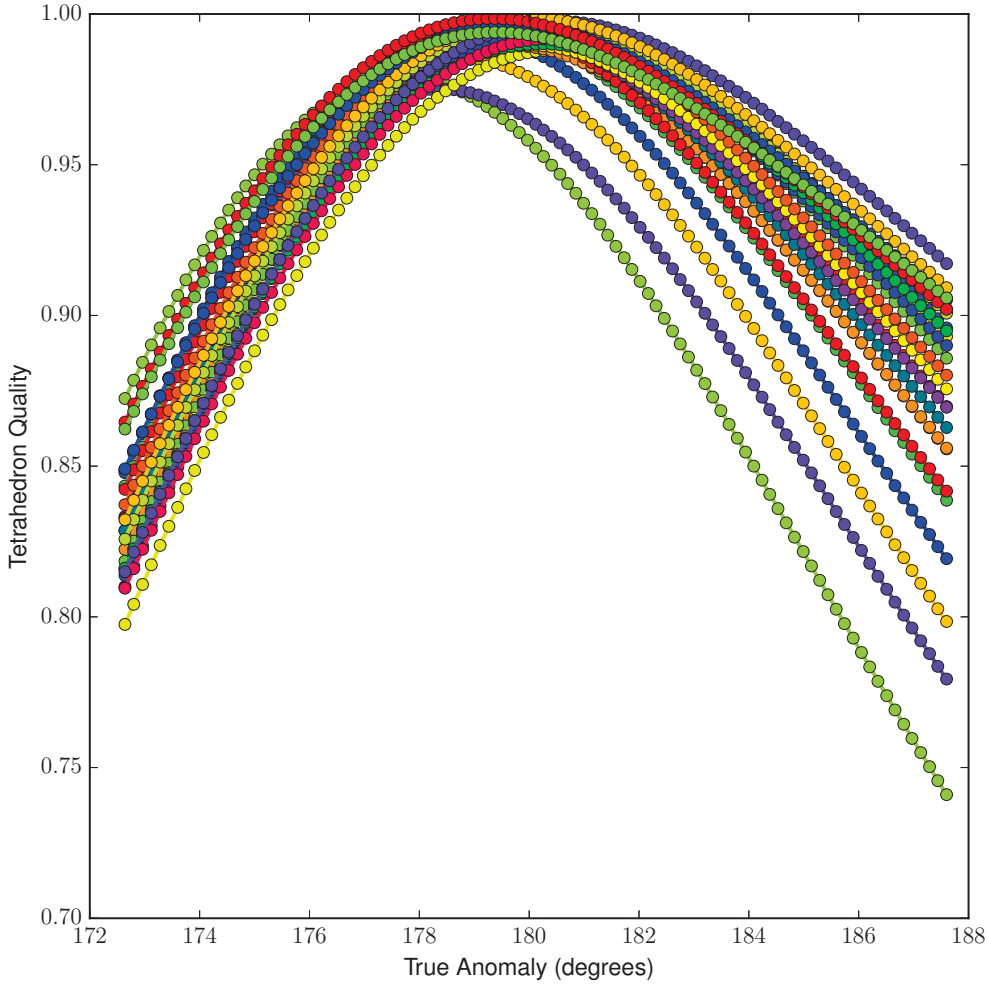

Figure 4.1: Case 1 : $L = 160$ km target test ; $\pm 10,000$ second ROI, Quality Graph

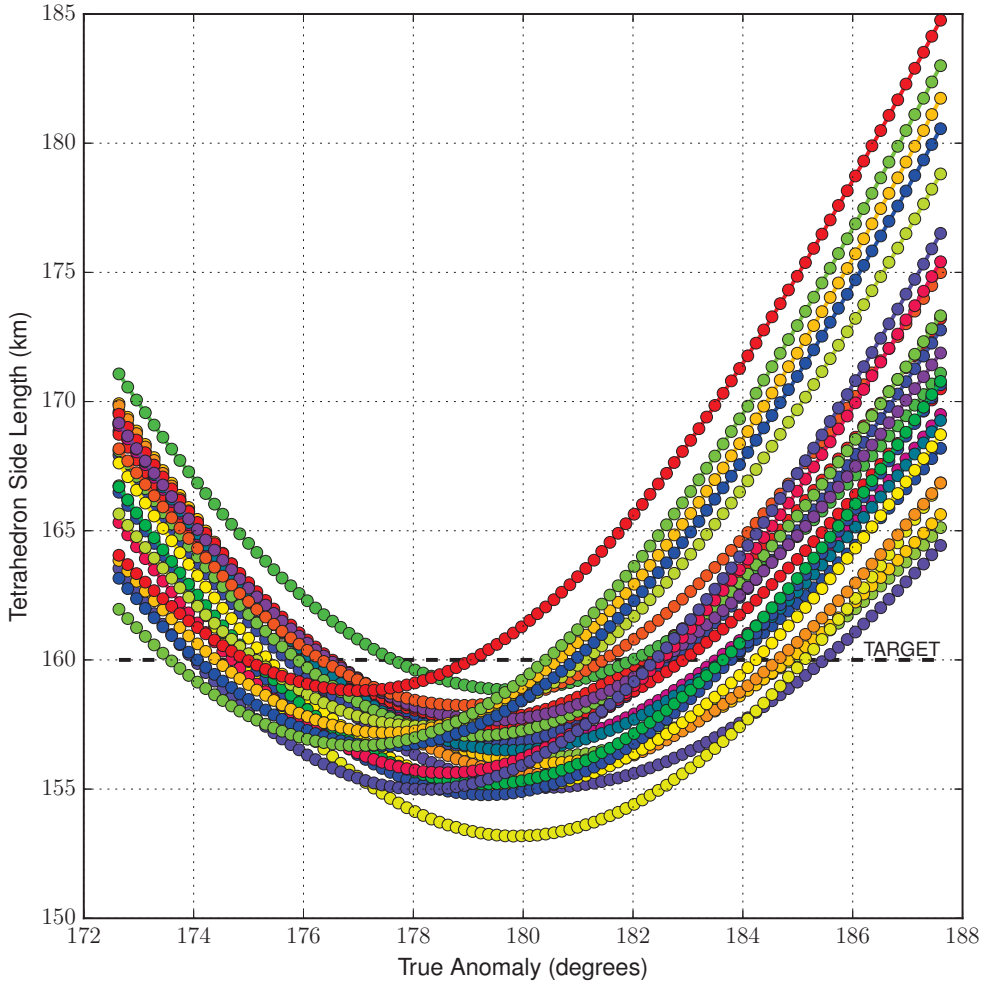

Figure 4.2: Case 1 : $L = 160$ km target test ; $\pm 10,000$ second ROI, Side-Length Graph

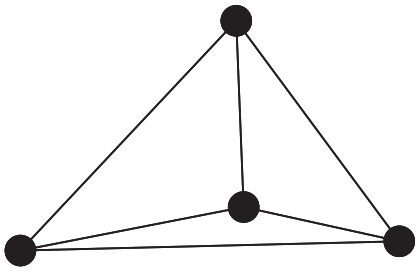

(a) Formation Entering ROI

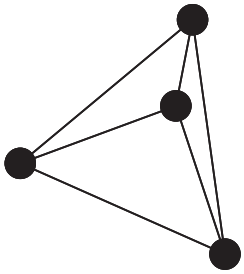

(b) Formation at Apogee

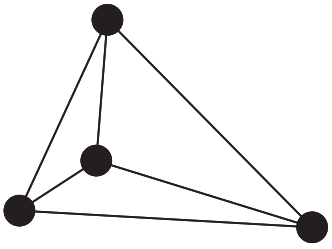

(c) Formation Exiting ROI

Figure 4.3: Tetrahedral configurations for Case 1 within the region of interest

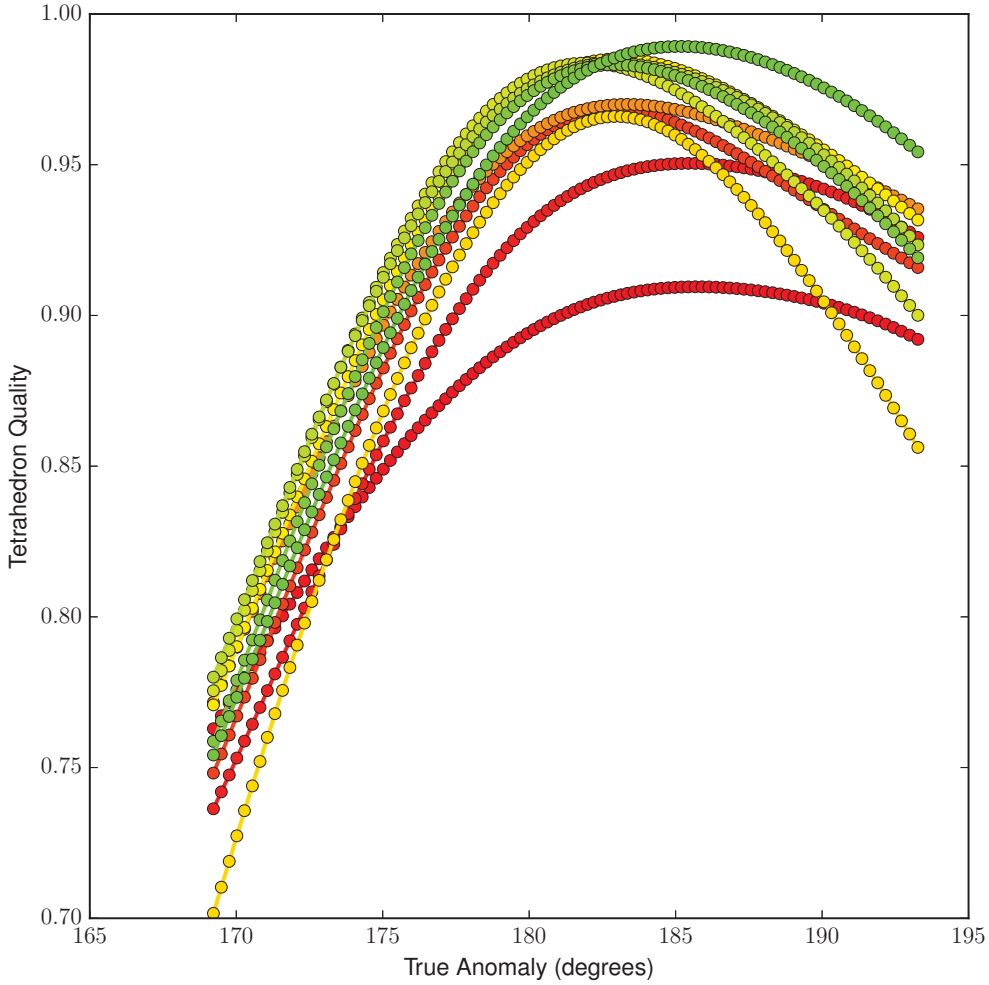

Figure 4.4: Case 2 : $L = 160$ km target test ; $\pm 15,000$ second ROI, Quality Graph

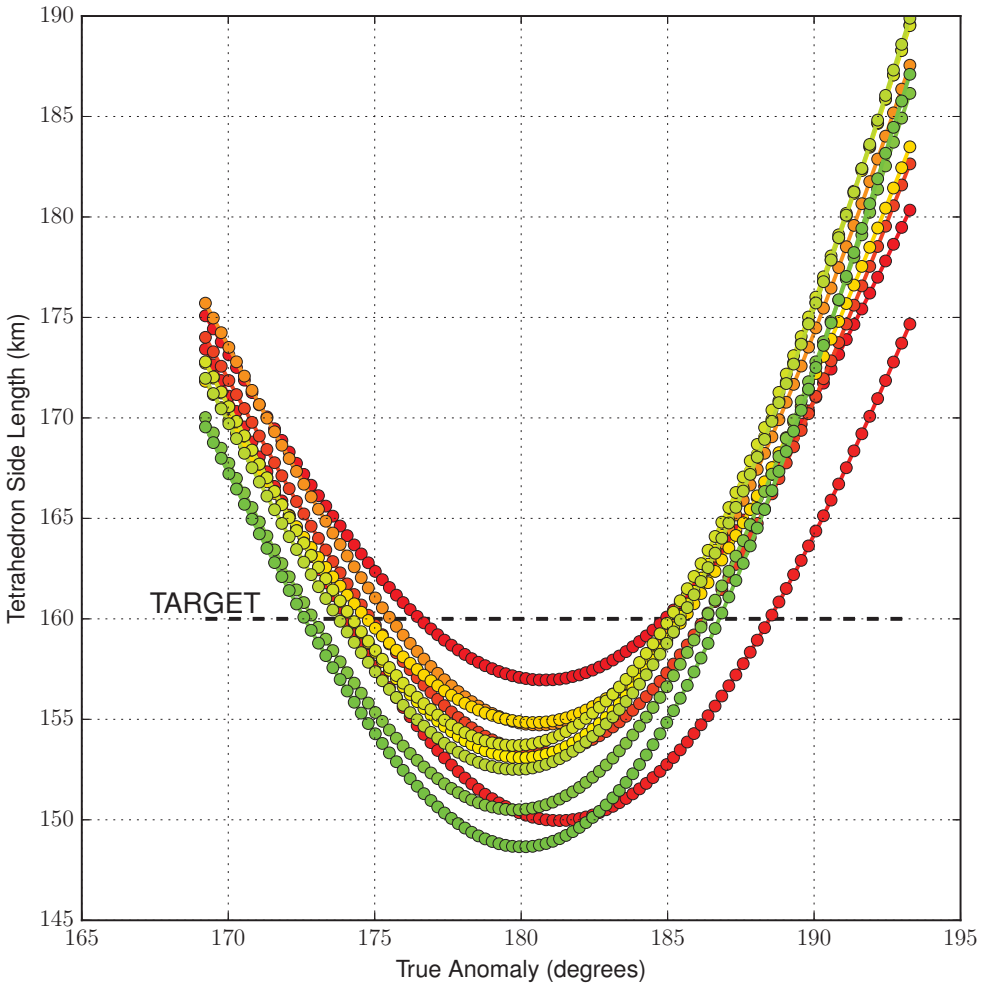

Figure 4.5: Case 2 : $L = 160$ km target test ; $\pm 15,000$ second ROI, Side-Length Graph

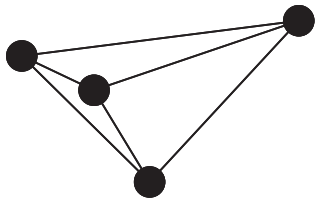

(a) Formation Entering ROI

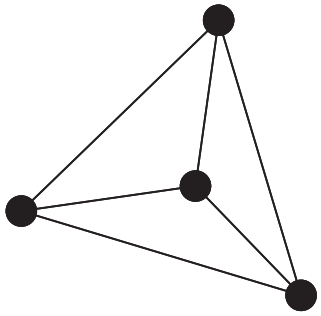

(b) Formation at Apogee

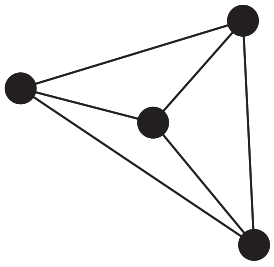

(c) Formation Exiting ROI

Figure 4.6: Tetrahedral configurations for Case 2 $L = 160km$ target test within the region of interest

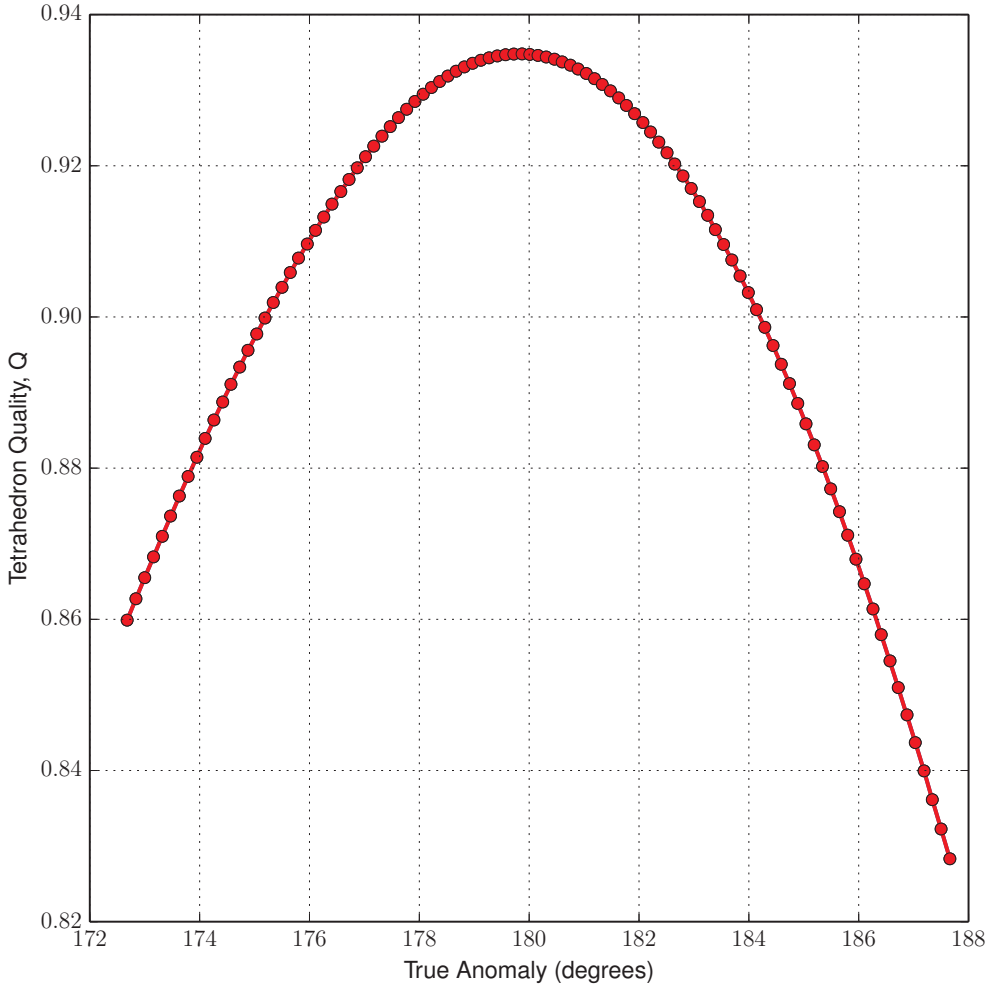

Figure 4.7: Case 2 : $L = 10$ km target test ; $\pm 10,000$ second ROI, Quality Graph

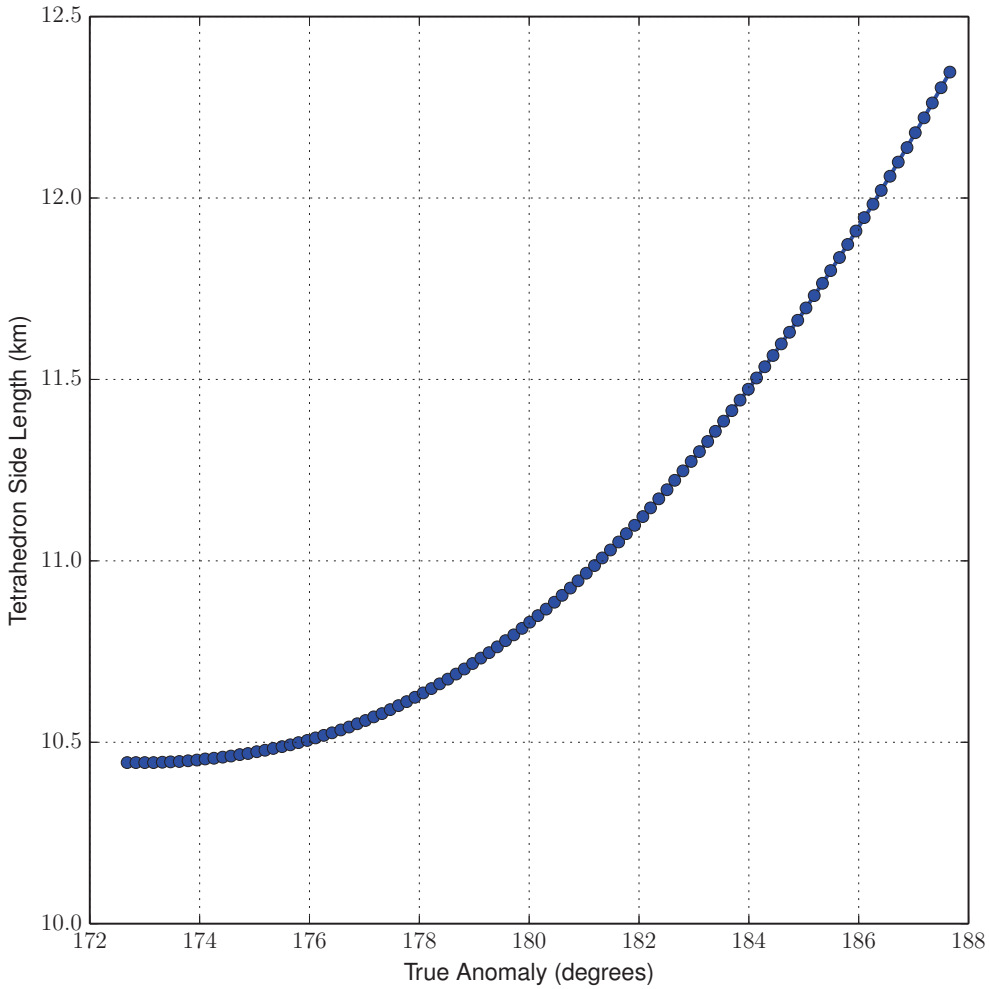

Figure 4.8: Case 2 : $L = 10$ km target test ; $\pm 10,000$ second ROI, Side-Length Graph

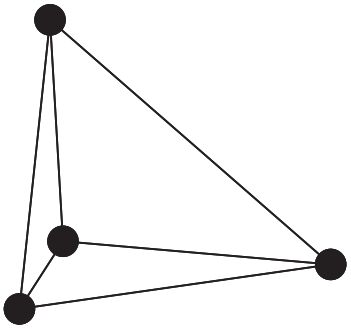

(a) Formation Entering ROI

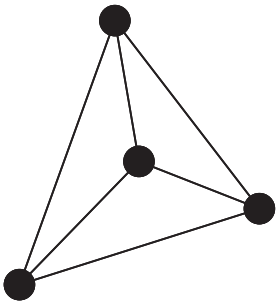

(b) Formation at Apogee

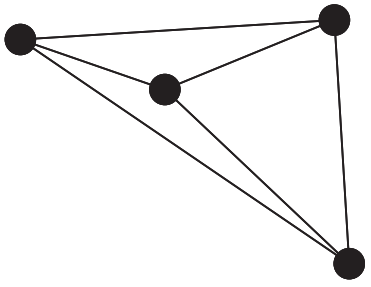

(c) Formation Exiting ROI

Figure 4.9: Tetrahedral configurations for Case 2 $L = 10km$ target test within the region of interest

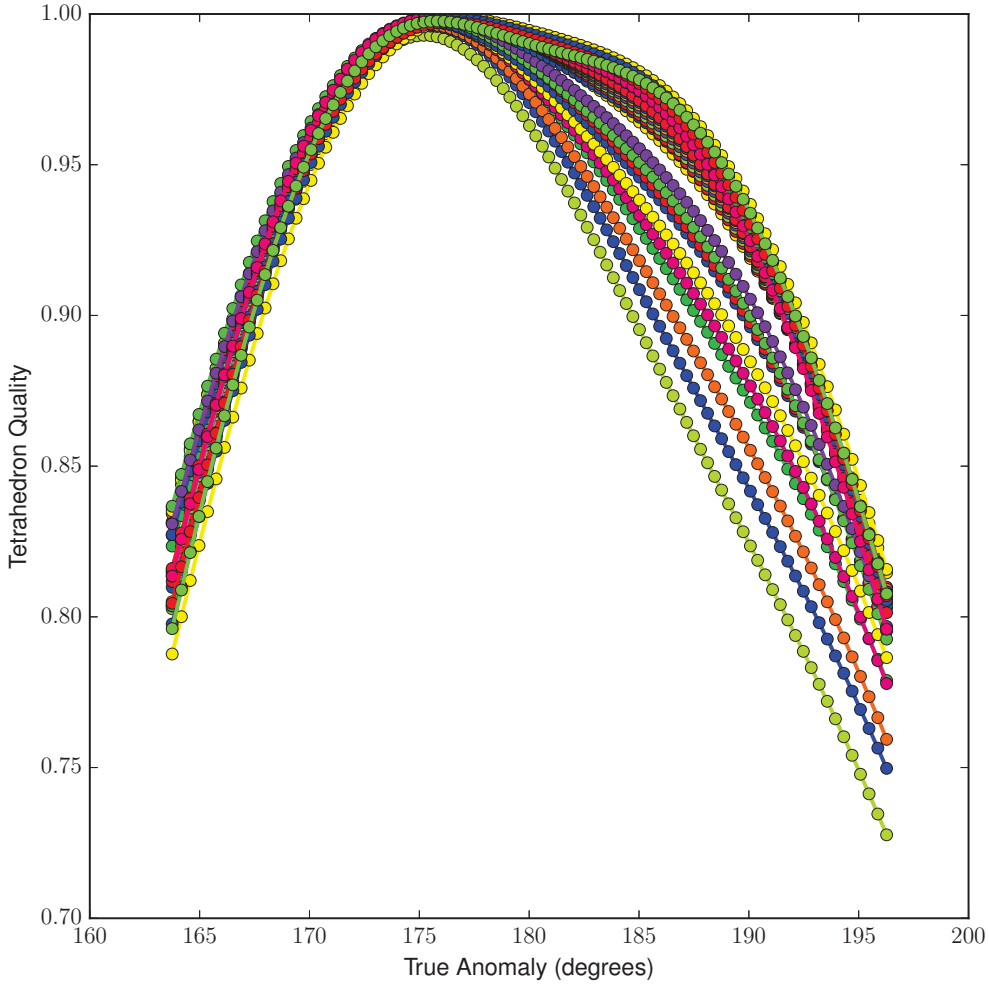

Figure 4.10: Case 3 : $L = 10$ km target test ; $\pm 20,000$ second ROI, Quality Graph

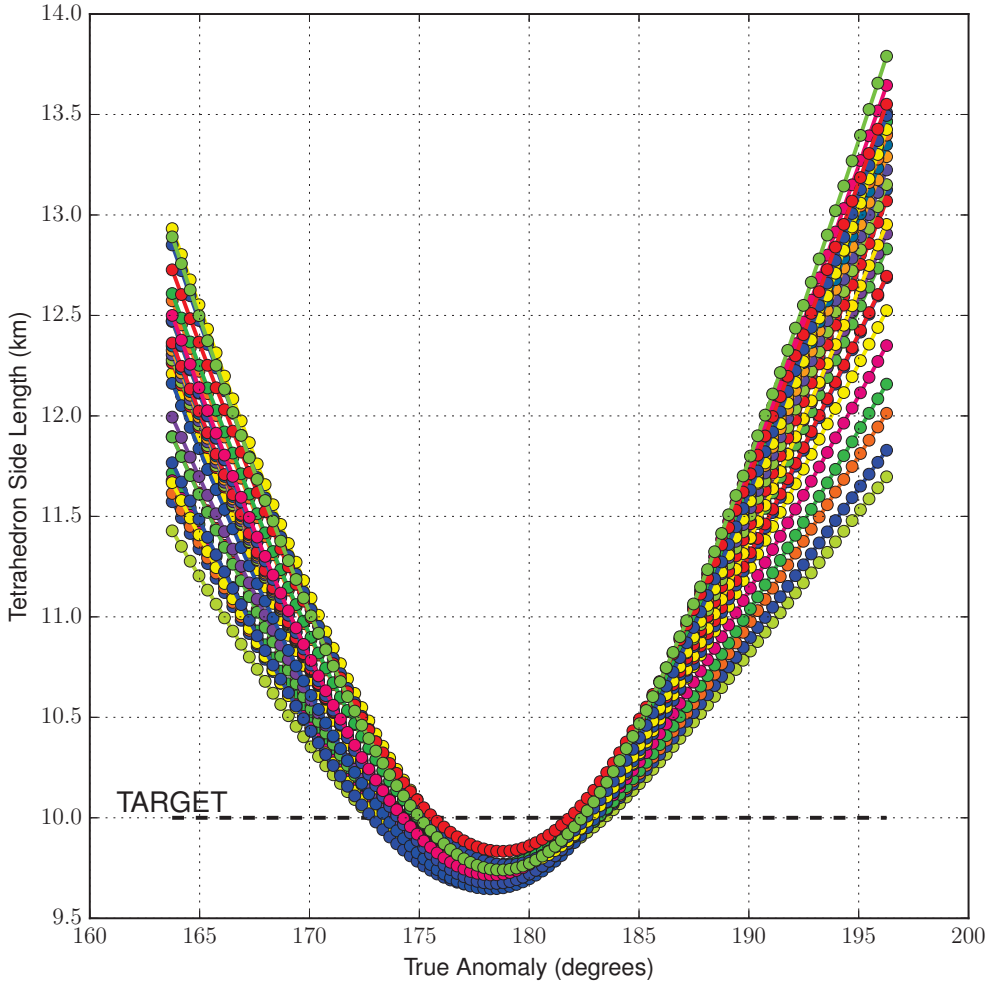

Figure 4.11: Case 3 : $L = 10$ km target test ; $\pm 20,000$ second ROI, Side-Length Graph

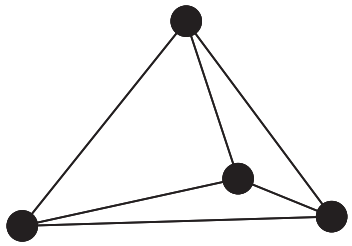

(a) Formation Entering ROI

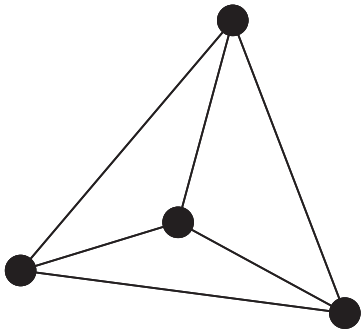

(b) Formation at Apogee

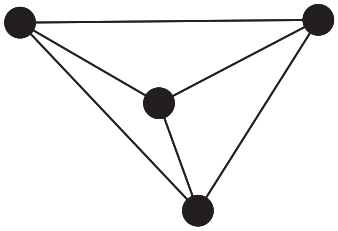

(c) Formation Exiting ROI

Figure 4.12: Tetrahedral configurations for Case 3 $L = 10km$ target test within the region of interest

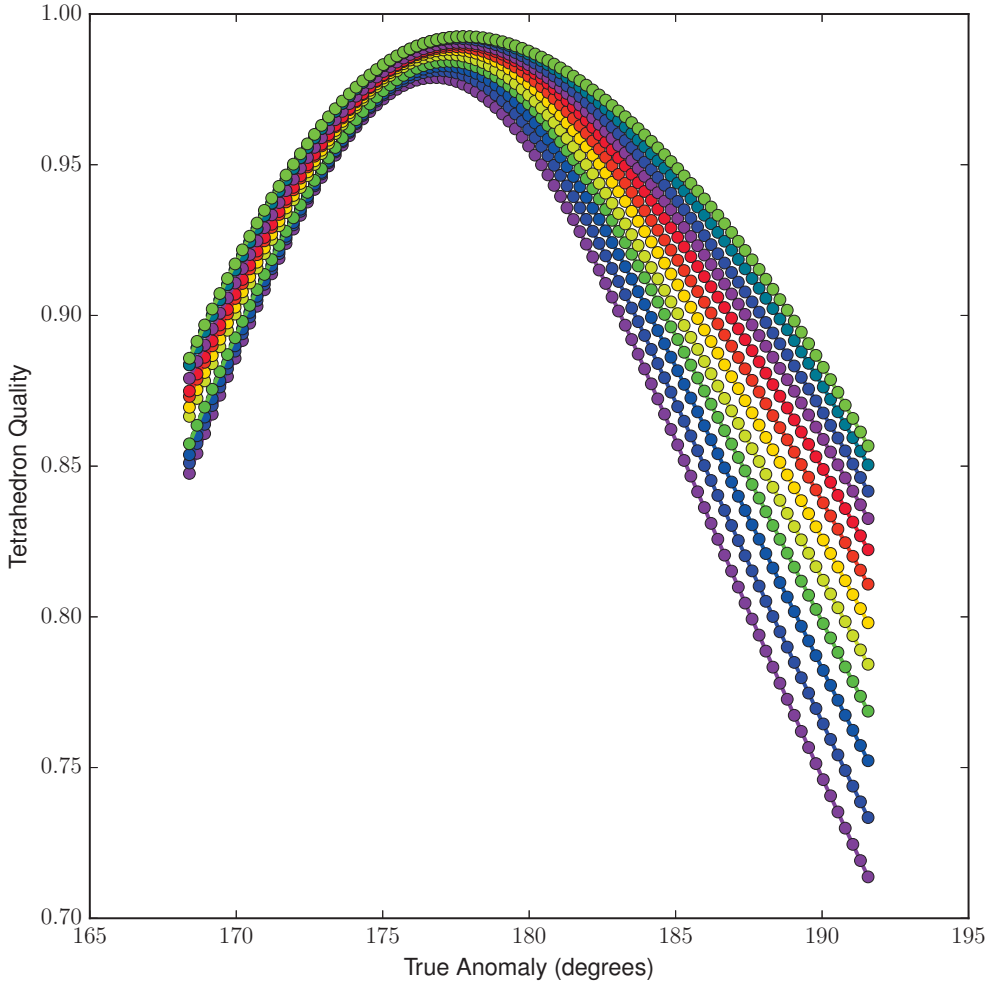

Figure 4.13: Case 3 : $L = 160$ km target test ; $\pm 15,000$ second ROI, Quality Graph

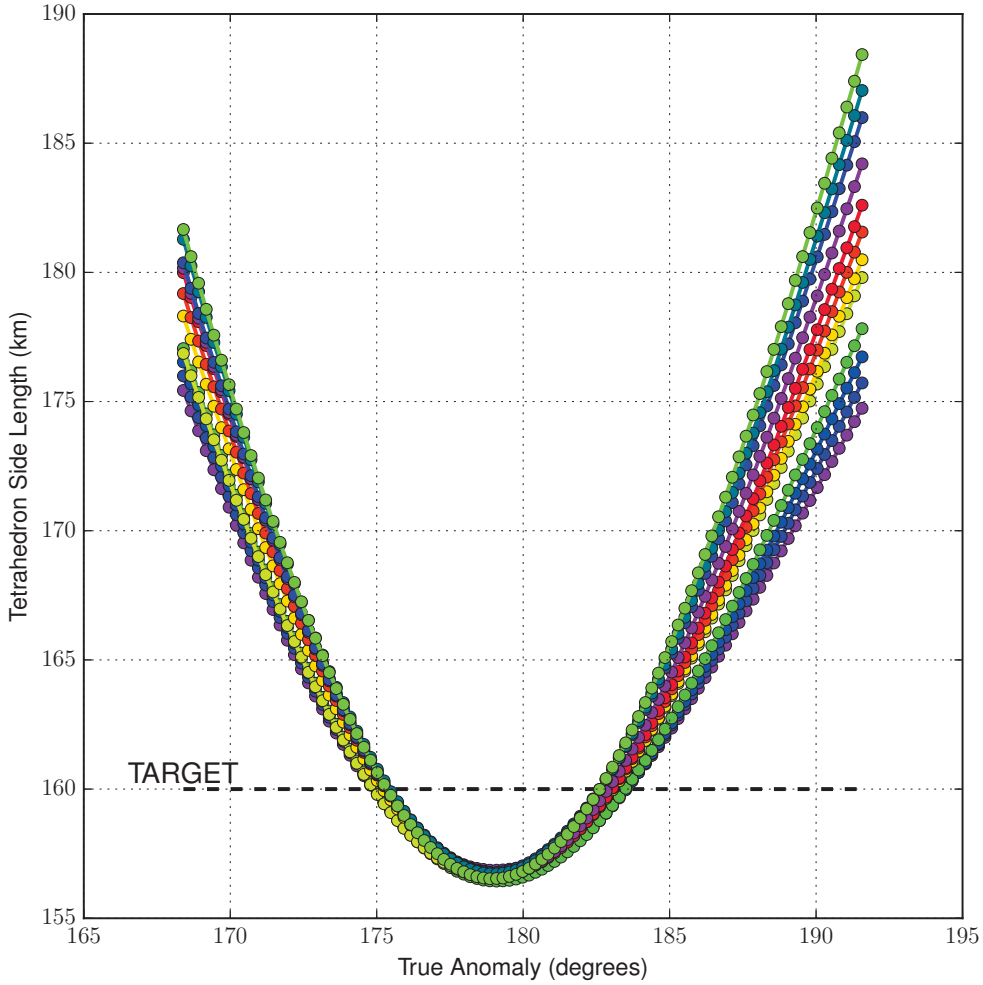

Figure 4.14: Case 3 : $L = 160$ km target test ; $\pm 15,000$ second ROI, Side-Length Graph

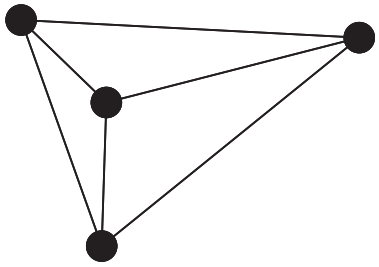

(a) Formation Entering ROI

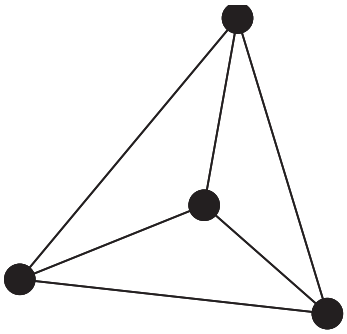

(b) Formation at Apogee

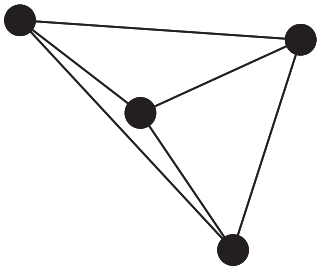

(c) Formation Exiting ROI

Figure 4.15: Tetrahedral configurations for Case 3 $L = 160km$ target test within the region of interest

4.4 Case 4

This Case serves more to demonstrate the ability of increasing the number of revolutions considered as part of the ROI than to show for how long mission requirements are met. This is due to the fact that increasing the revolution count with the here employed single impulse design too greatly limits the revolutions that can be added. Unfortunately the initial configuration of Case 2 did not lead to any notable revolution expansion results for the 10km target but sufficient results were obtained for the 160km target hereafter discussed. In Figures 4.16 and 4.18 a $\pm 1,000$ second ROI is expanded to consider 15 orbits about Earth. To help clarify the these plots, all multi-revolution results shown will be followed by a plot of the center revolution so as to alleviate the issue of scale inherent in the multi-plot structure of these multi-revolution results. While this shown result does not meet the mission requirements throughout every revolution, it shows that results can be extended as this result was generated by extending a test that originally considered only a single revolution. Only one trial of the test batch proceeded to this level of staging which shows the difficulty of the requirements with the placed limitations.

The revolution staging process functions in a predictable manner. If one wishes to meet a requirement over a region, the peak would reasonably be around the center of that region. When the ROI is extended to multiple revolutions, the seeded solution that focused on a single revolution sees its peek move toward the middle revolution; thus a rough symmetry is seen throughout ROIs of both single and multiple revolutions. Here it appears that the later revolutions trail off thus deviating from that which would be symmetric. Again, due to the stochastic nature of evolution, explanations are not concrete since omniscience is impossible. One explanation which withstands scrutiny is that control of the immediate future of the trajectory is far easier than controlling the distant future given the introduction of the non-Keplerian element. The gravitational perturbations that make this multiple revolution

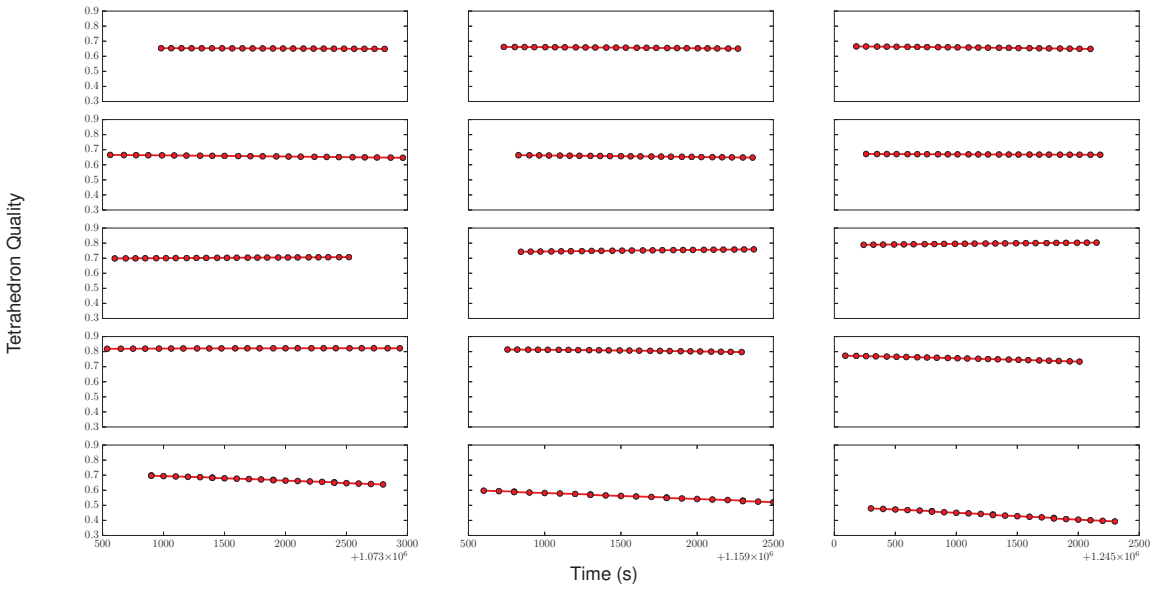

Figure 4.16: Case 4 : $L = 160$ km target test ; 15 revolutions about Earth ; $\pm 1,000$ second ROI. Horizontal axis is time in seconds. Quality Graph

analysis meaningful also make distant events more difficult to control. Thus correlations between changes in the initial velocity of a solution and the quality (or side-length) are more direct for earlier revolutions as the effects of the oblateness perturbation (or any considered non-Keplerian effect) have not yet compounded.

As mentioned before, the ROI window must be staged after the number of revolutions. Figures 4.20 and 4.22 show a 5 revolution result that was further extended to a ROI of $\pm 15,000$ seconds. The results do not meet the mission requirements but considering the limitation of the single impulse restriction, how well quality and side-length are maintained demonstrates that the here outlined staging procedure works as intended. Similar to Case 2's 10km result, a leveling off of the peak in quality is observed but there does not appear to be any strong commonality between the tests; this is then just further evidence of non-intuitive optima.

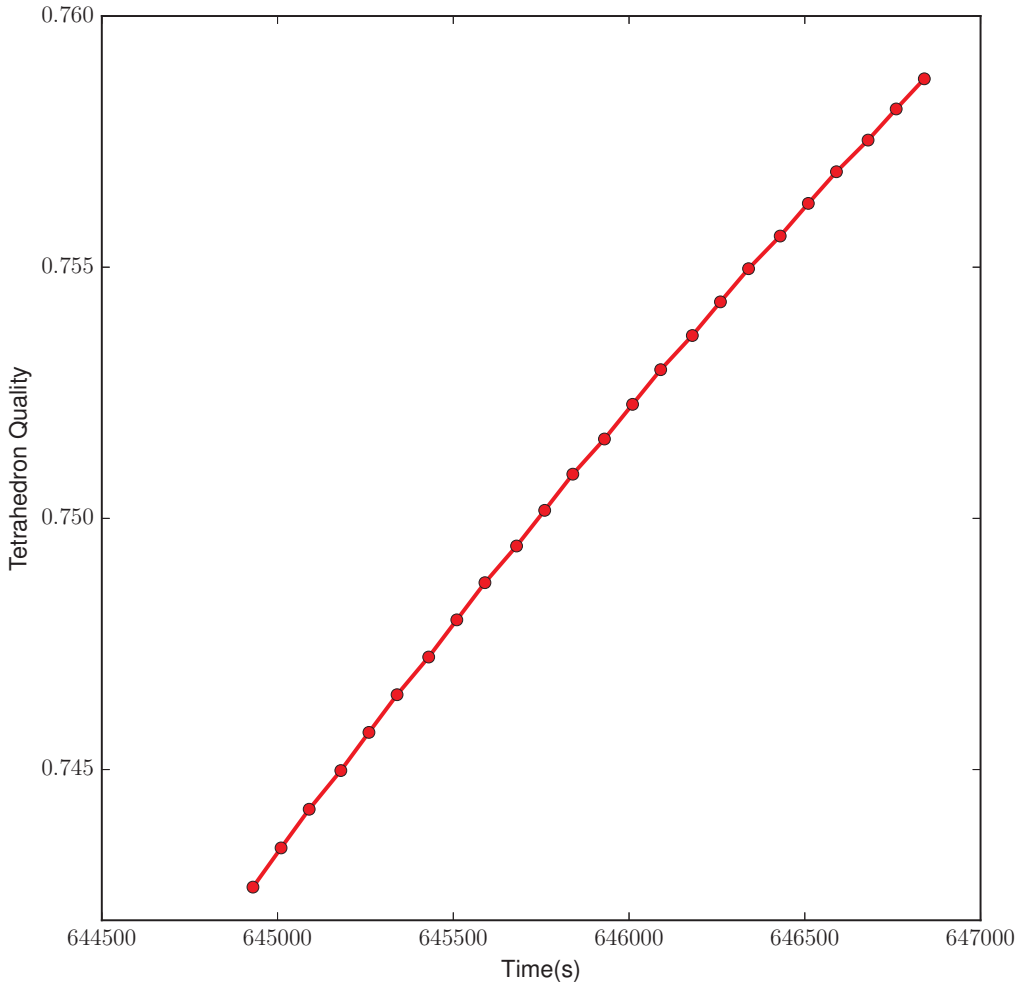

Figure 4.17: Quality graph focused on the center revolution in Figure 4.16

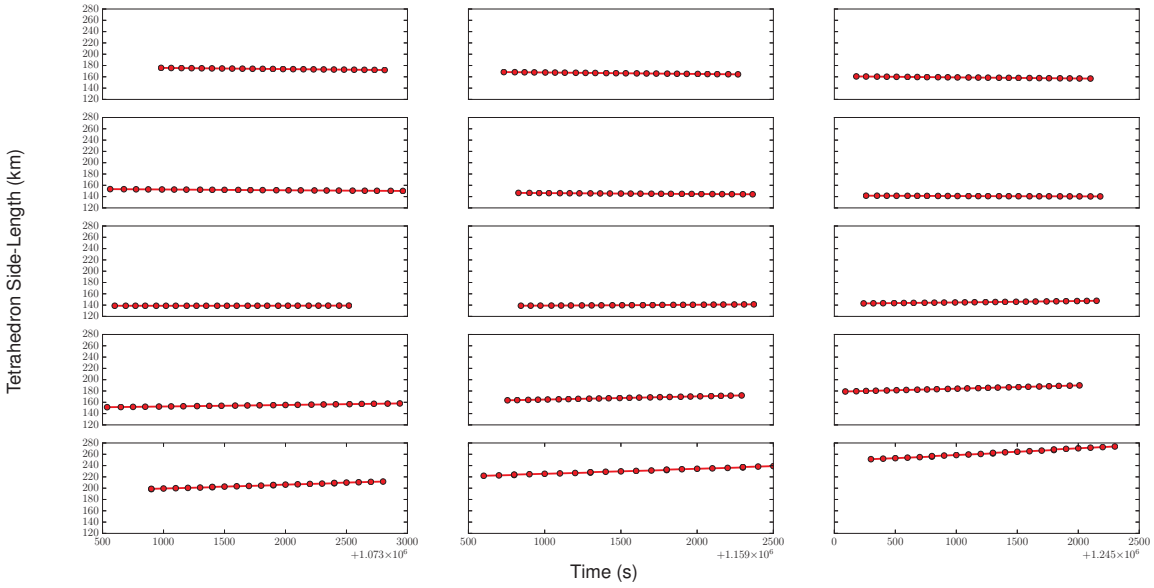

Figure 4.18: Case 4 : $L = 160$ km target test ; 15 revolutions about Earth ; $\pm 1,000$ second ROI. Horizontal axis is time in seconds. Side-Length Graph

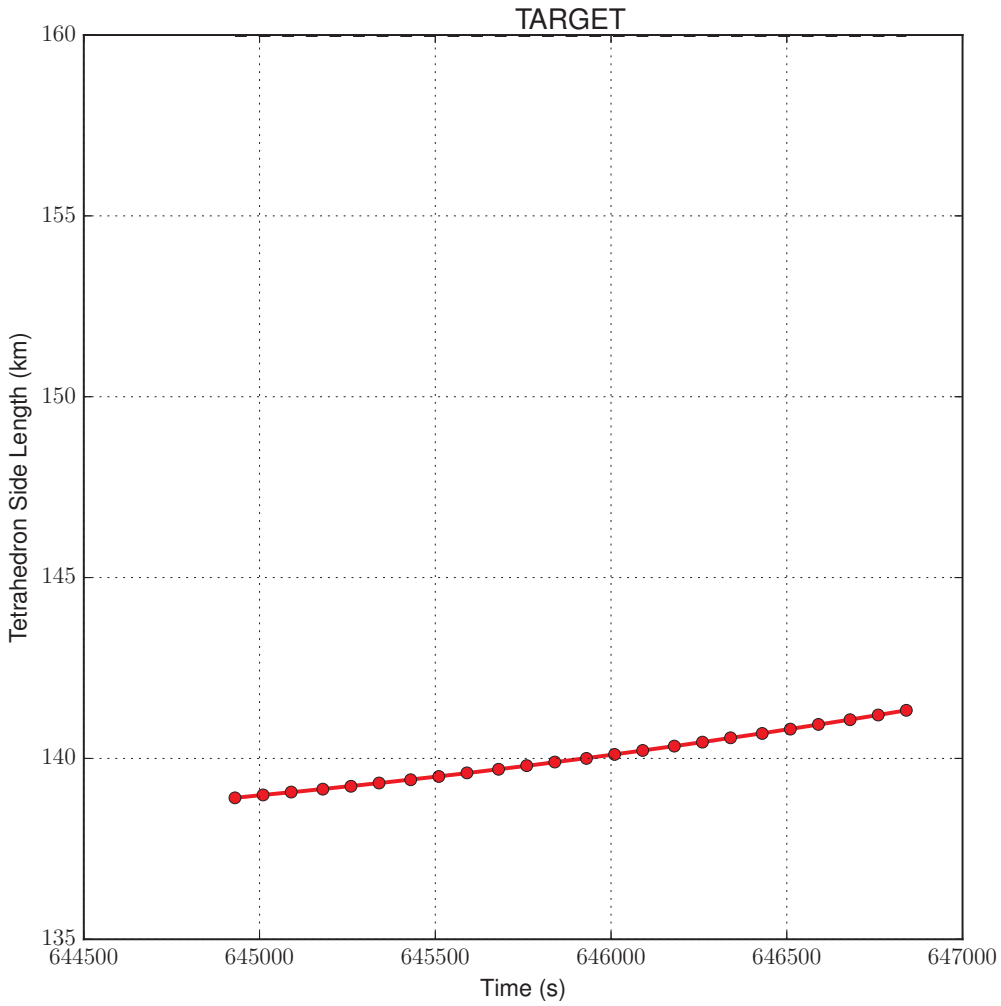

Figure 4.19: Side-Length graph focused on the center revolution in Figure 4.18

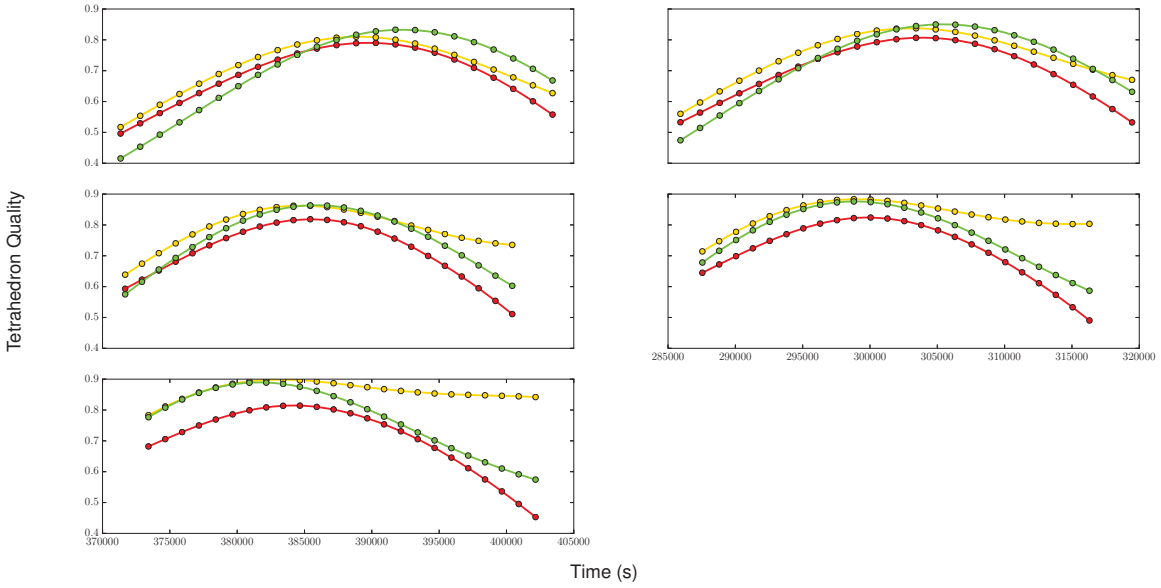

Figure 4.20: Case 4 : $L = 160$ km target test ; 5 revolutions about Earth ; $\pm 15,000$ second ROI. Horizontal axis is time in seconds. Quality Graph

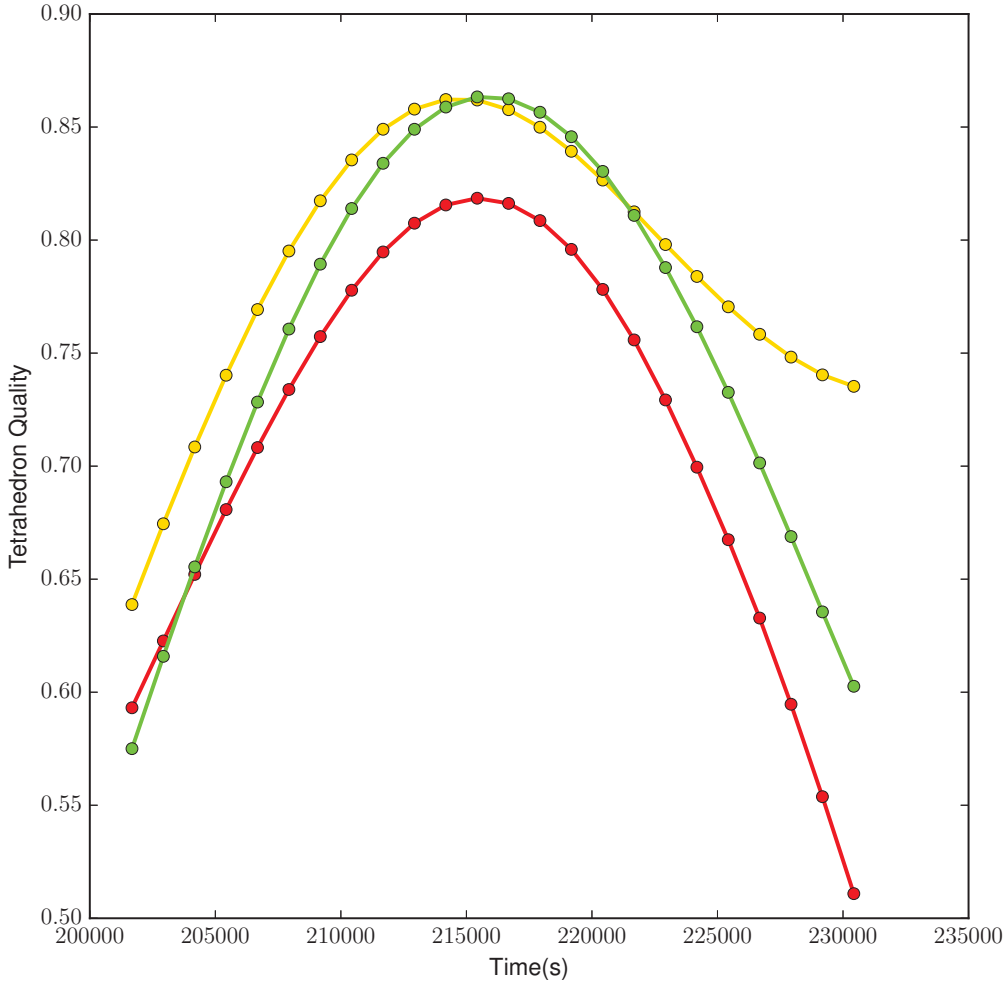

Figure 4.21: Quality graph focused on the center revolution in Figure 4.20

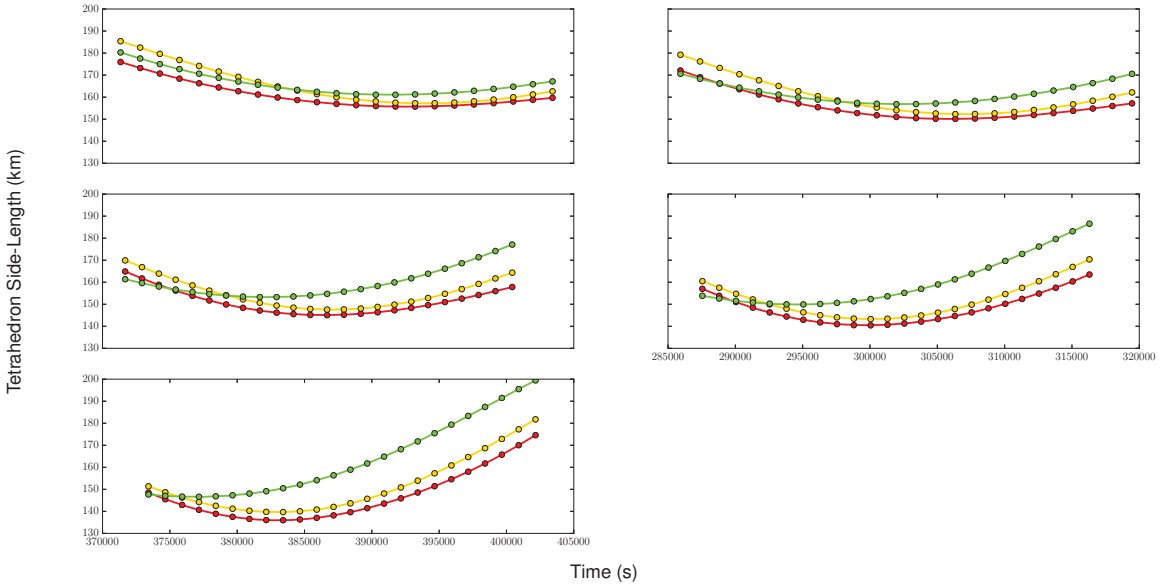

Figure 4.22: Case 4 : $L = 160$ km target test ; 5 revolutions about Earth ; $\pm 15,000$ second ROI. Horizontal axis is time in seconds. Side-Length Graph

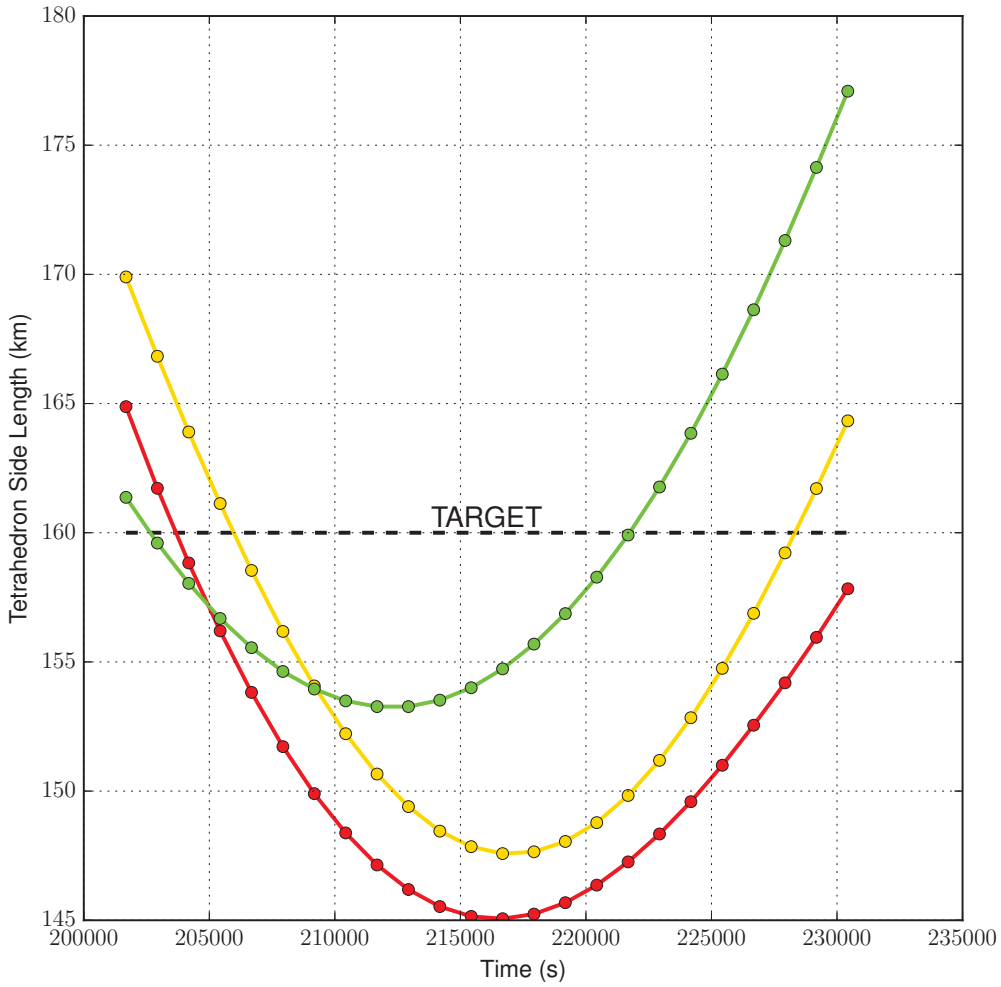

Figure 4.23: Side-Length graph focused on the center revolution in Figure 4.22

4.5 Case 5

As could have been expected when comparing the results of Cases 2 & 3, the extension to multiple revolution of the initial conditions from Case 3 fared better in terms of extent of expansion. Here, unlike in Case 4, the 10km target produced staged revolution results. The 160km target tests also provided better profiles than those seen in Case 4. Figures 4.24 and 4.26 are from a test that mirrors the 160km, 15,000 second ROI of Case 4. Here, it is clear that this test has more profiles at this level of staging but what may not be easily observed is that some trials within this test still meet the mission requirements whereas its Case 4 counterpart did not have any such trials. Allowing this test to continue along the staging process, we have the results shown in Figures 4.28 and 4.30 which, although no longer strictly meeting the mission goals, show that this set of trajectories only barely exceeds the side-length bounds. Another promising aspect of these results is the uniformity of the profiles which implies that, for this initial configuration, the method is not extremely sensitive to the balancing weight which would make use of this method in practical application much easier; if unable to run large batch runs of this type there is less issue in finding weights that produce good initial trajectories.

In terms of the expansion in the number of revolutions considered in the ROI, the results for Case 5 far exceed the result of Case 4. In Figures 4.32 and 4.34 it is clear that more than one trial proceeded through the staging process to 15 revolutions. One may also note that the quality across all revolutions is much higher and the adherence to the side-length target is such that this test still meets the mission requirements; the attempt was made to further stage these results but profiles fell far short of the requirements.

In comparison of Case 4 and Case 5's 160km results, it shows that the initial conditions of Case 3 that produced better results than Case 2 during a single orbit also better allow for ROI expansion beyond a single revolution. Regardless of how result Cases compare, all

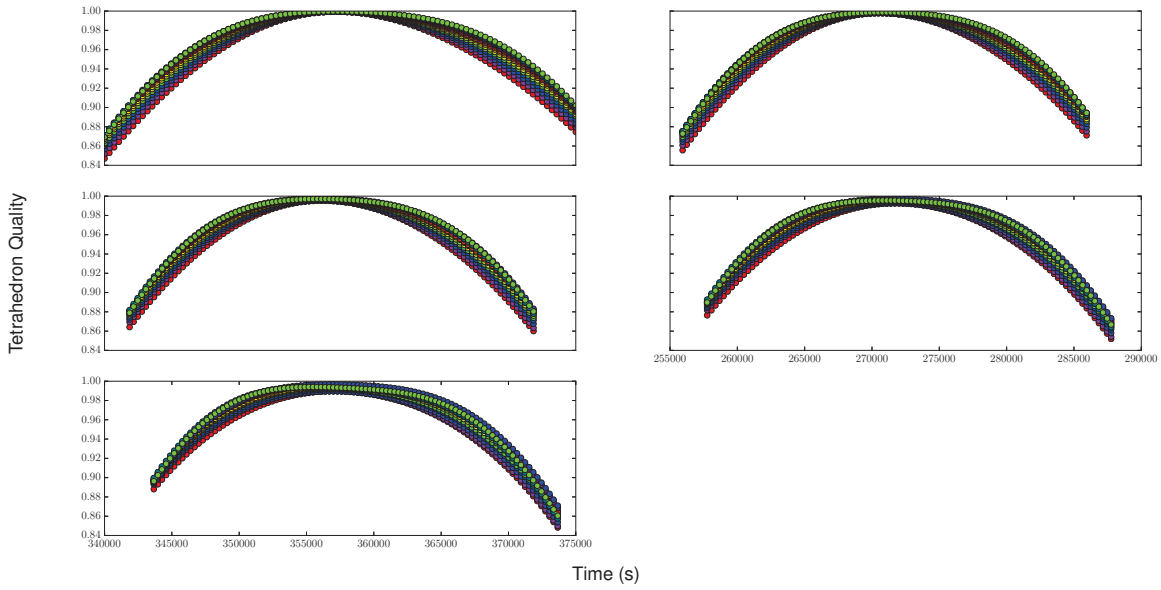

Figure 4.24: Case 5 : $L = 160$ km target test ; 5 revolutions about Earth ; $\pm 15,000$ second ROI. Horizontal axis is time in seconds. Quality Graph

of these results show that DE is capable of finding valid mission trajectories for differing initial configurations but how well these results scale during staging is dependent on the choice of initial configuration.

Since Case 4 did not produce any results for the 10km target scale, comparisons between the Cases cannot be made. For this target scale, although the results fall just short of the quality requirement, trajectories were found for a test that evaluated across the entire MMS ROI. In Figures 4.36 and 4.38 are the results from a test that met the semi-final stage requirements but fell just shy of a complete ROI result; as could have been anticipated since the result from which it was seeded also could not stage to the complete MMS ROI. The profiles exhibit similar symmetry to the earlier trials. There is a rough symmetry of the profiles within a single orbit but also a greater symmetry when viewing all revolutions at once; the profiles for the non-central revolution have trailing edges on the expected sides.

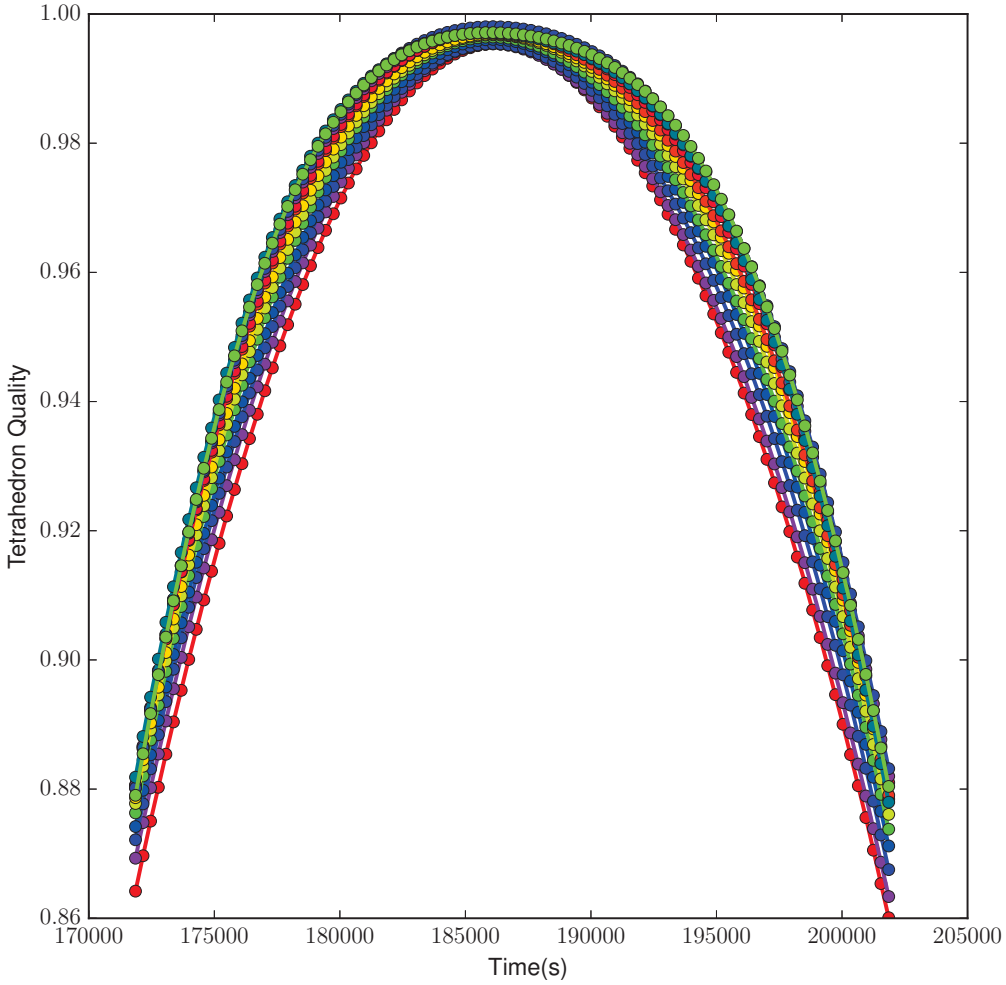

Figure 4.25: Quality graph focused on the center revolution in Figure 4.24

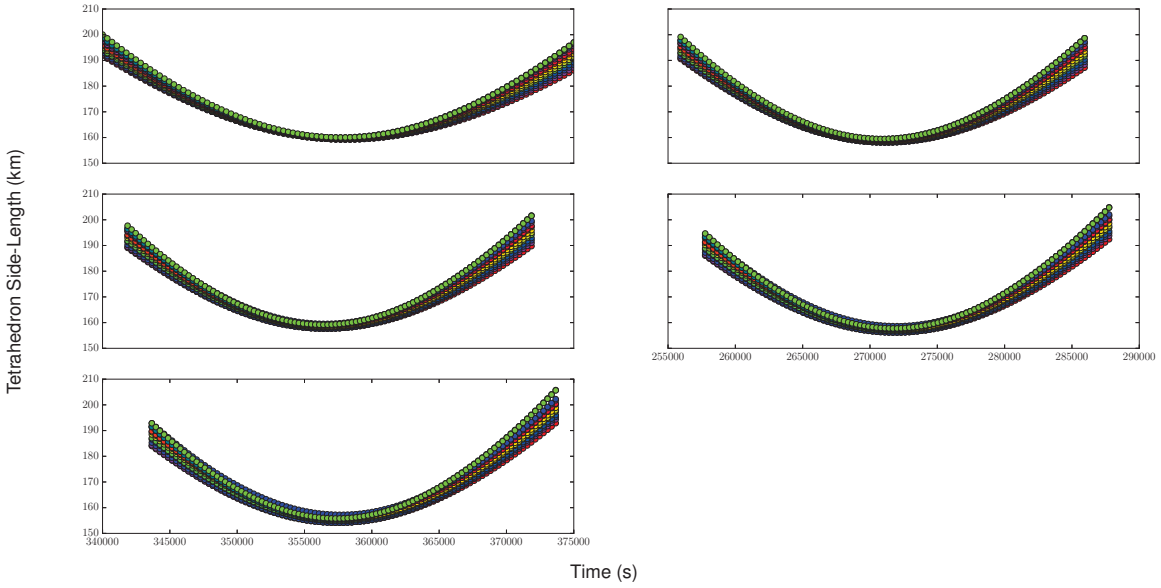

Figure 4.26: Case 5 : $L = 160$ km target test ; 5 revolutions about Earth ; $\pm 15,000$ second ROI. Horizontal axis is time in seconds. Side-Length Graph

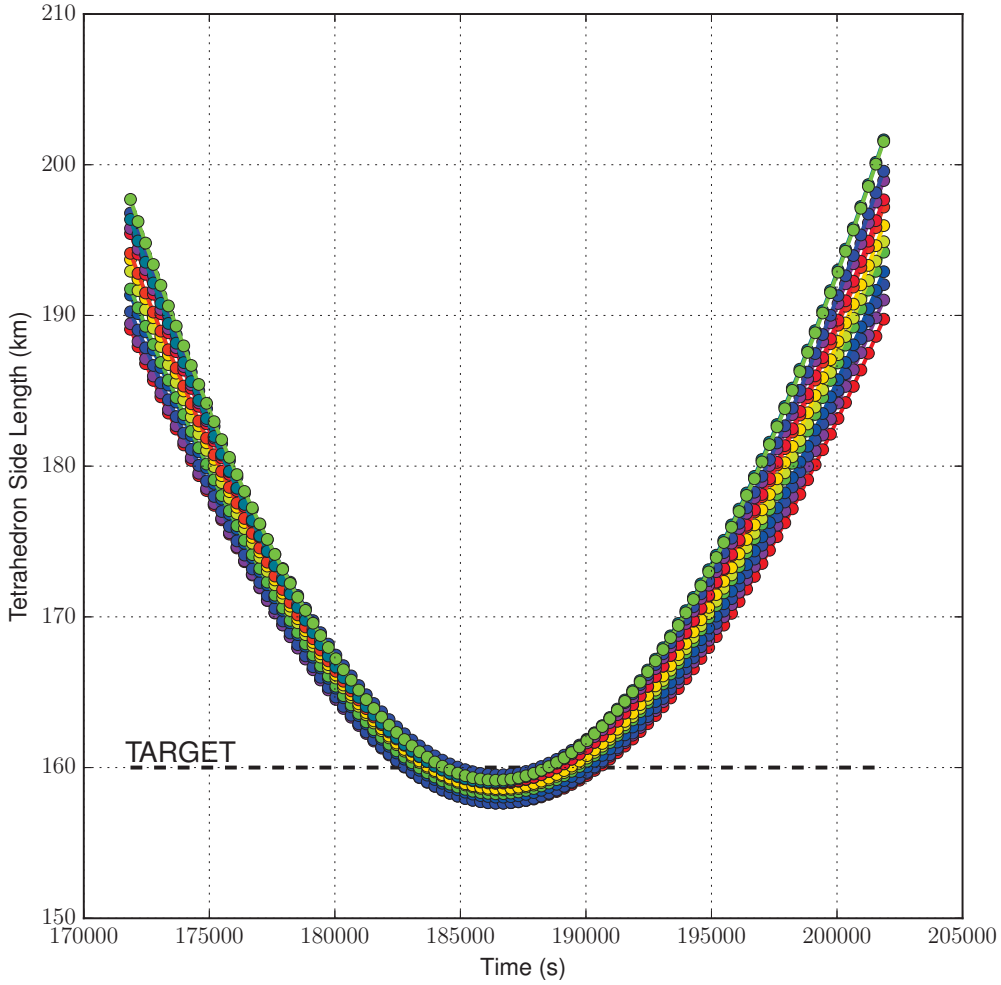

Figure 4.27: Side-Length graph focused on the center revolution in Figure 4.26

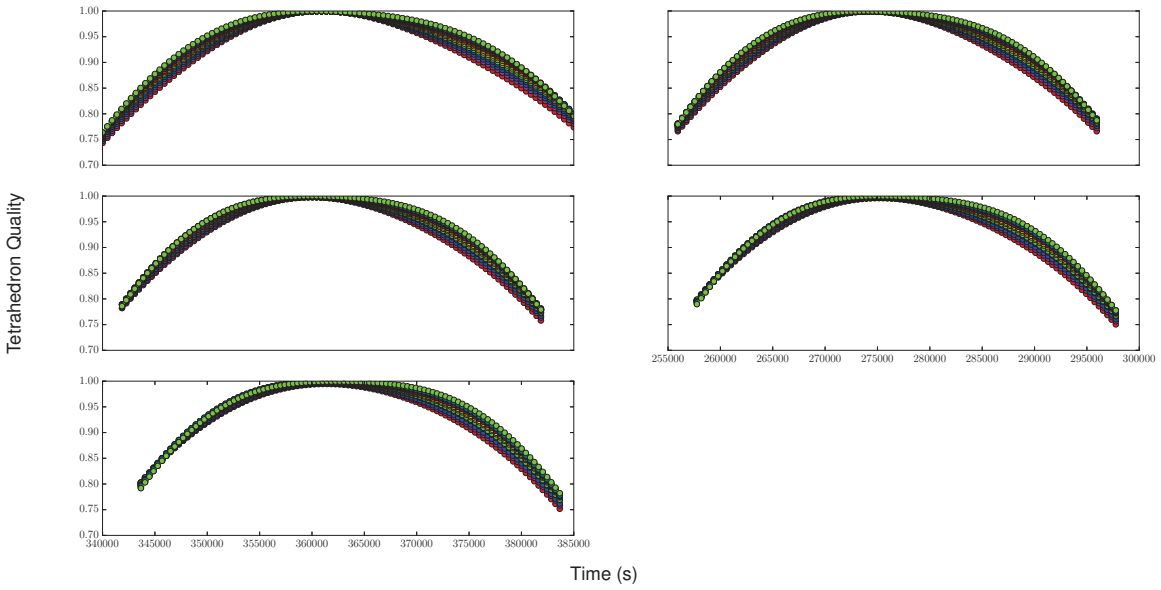

Figure 4.28: Case 5 : $L = 160$ km target test ; 5 revolutions about Earth ; $\pm 20,000$ second ROI. Horizontal axis is time in seconds. Quality Graph

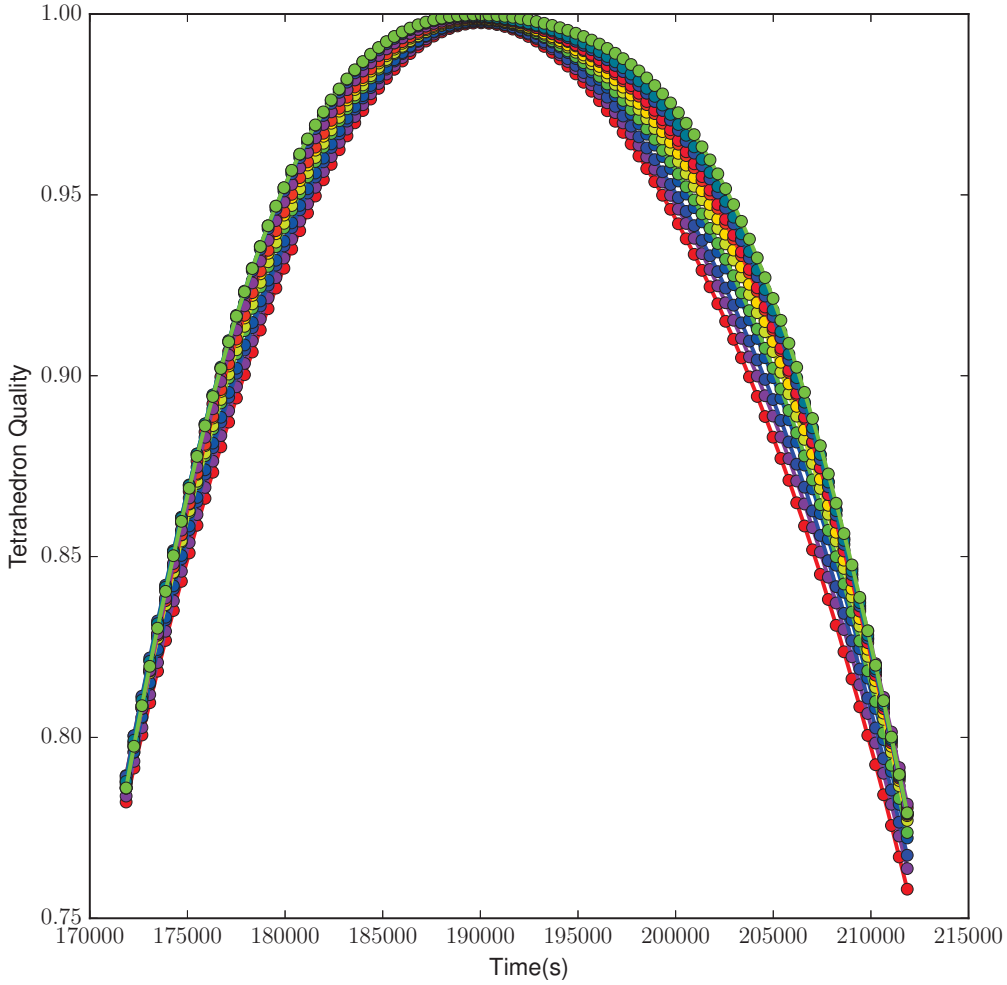

Figure 4.29: Quality graph focused on the center revolution in Figure 4.28

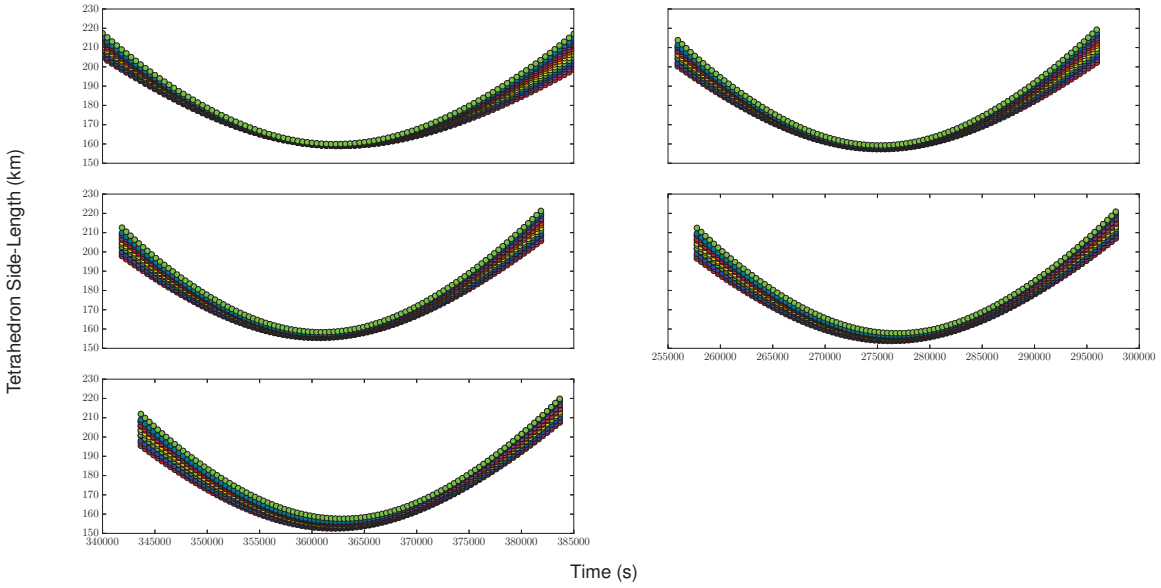

Figure 4.30: Case 5 : $L = 160$ km target test ; 5 revolutions about Earth ; $\pm 20,000$ second ROI. Horizontal axis is time in seconds. Side-Length Graph

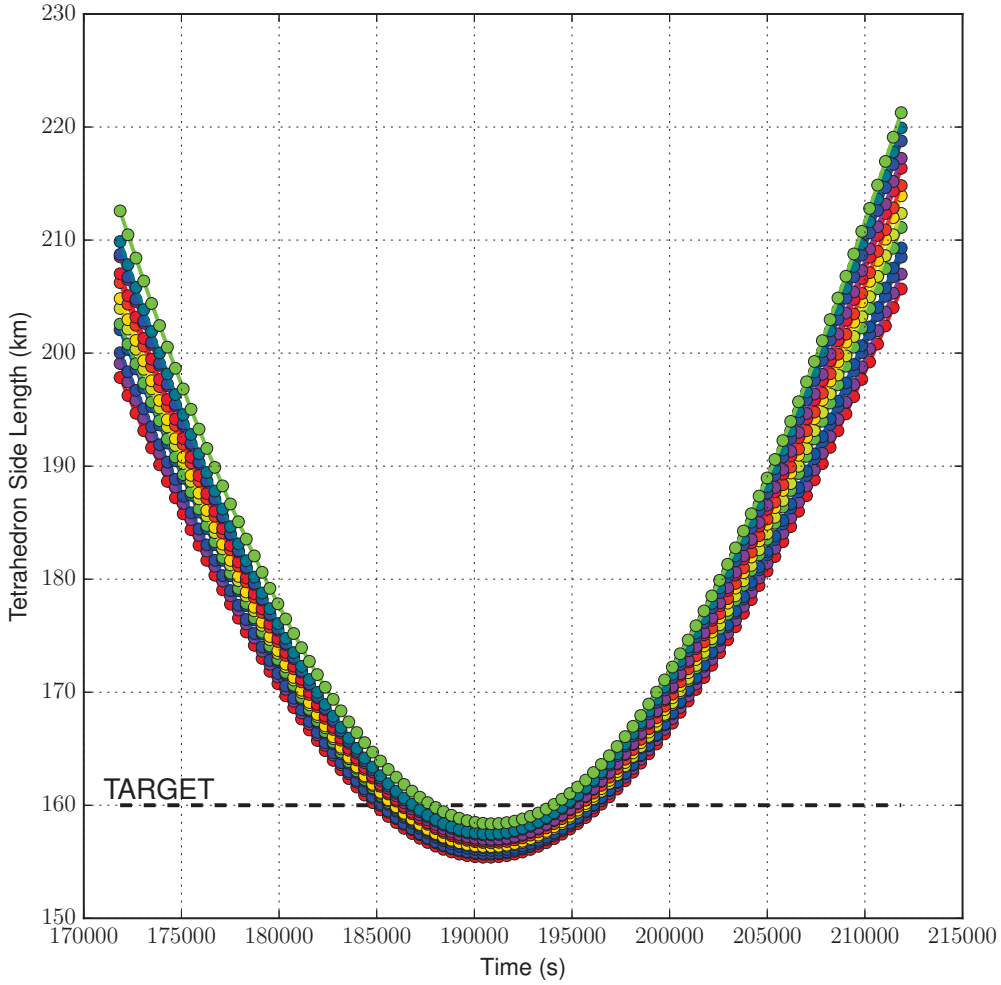

Figure 4.31: Side-Length graph focused on the center revolution in Figure 4.30

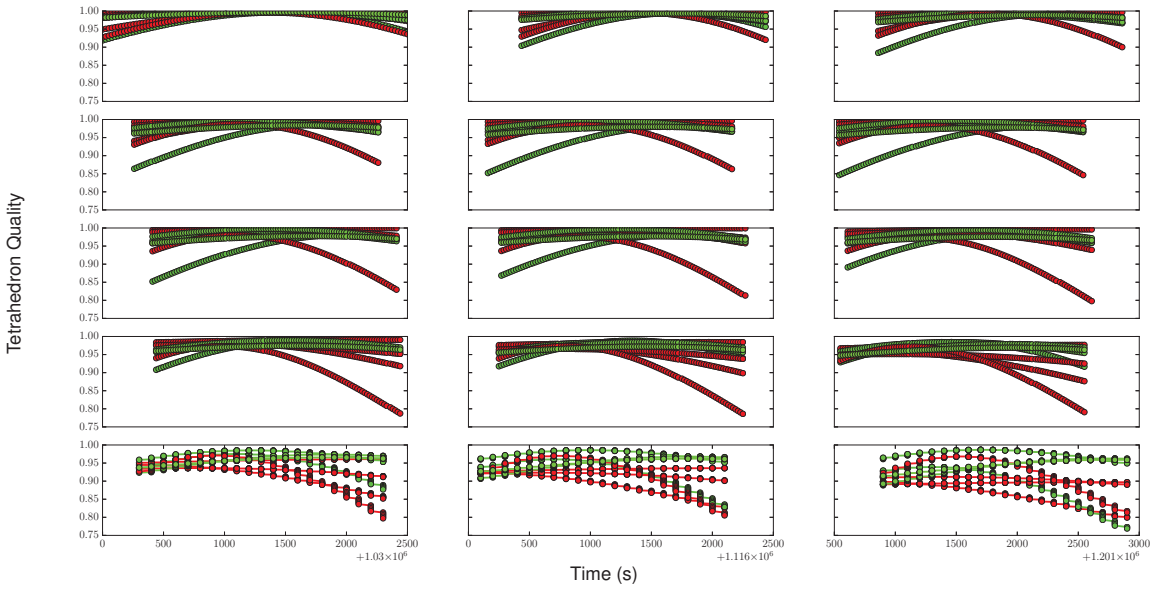

Figure 4.32: Case 5 : $L = 160$ km target test ; 15 revolutions about Earth ; $\pm 1,000$ second ROI. Horizontal axis is time in seconds. Quality Graph

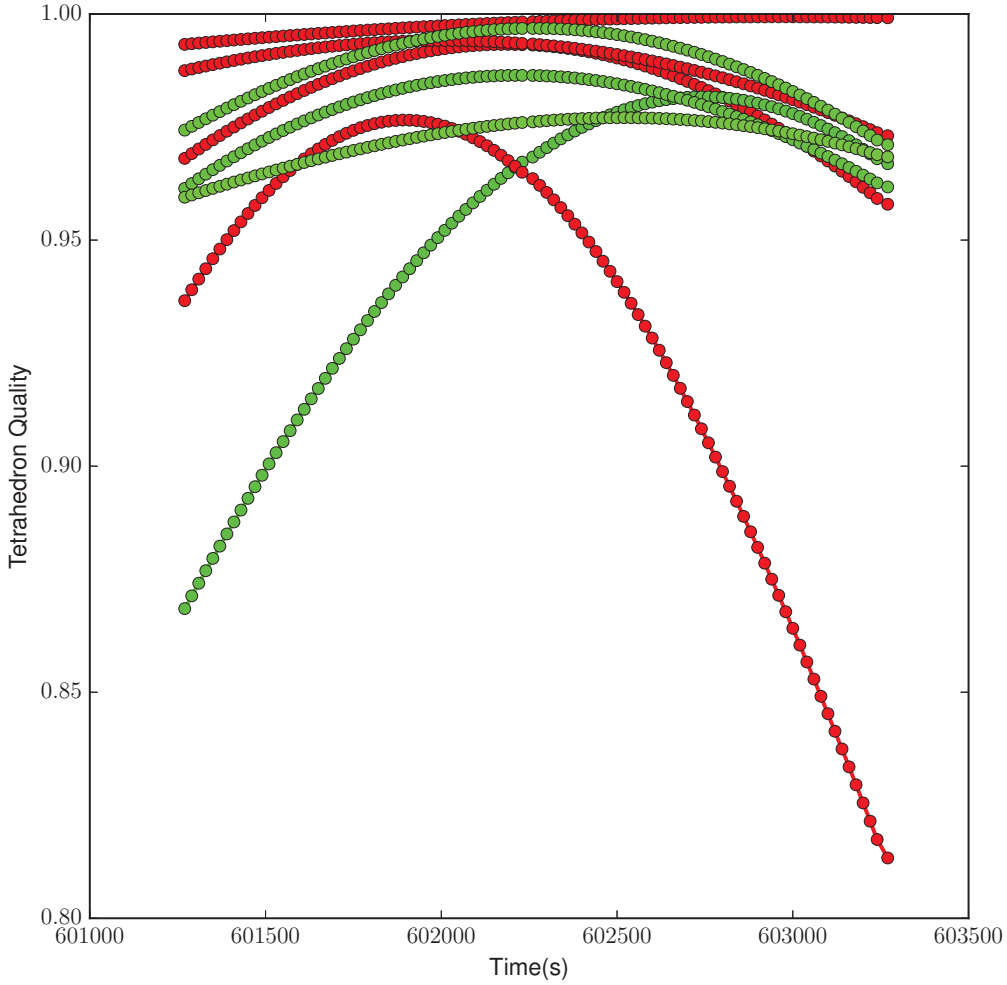

Figure 4.33: Quality graph focused on the center revolution in Figure 4.32

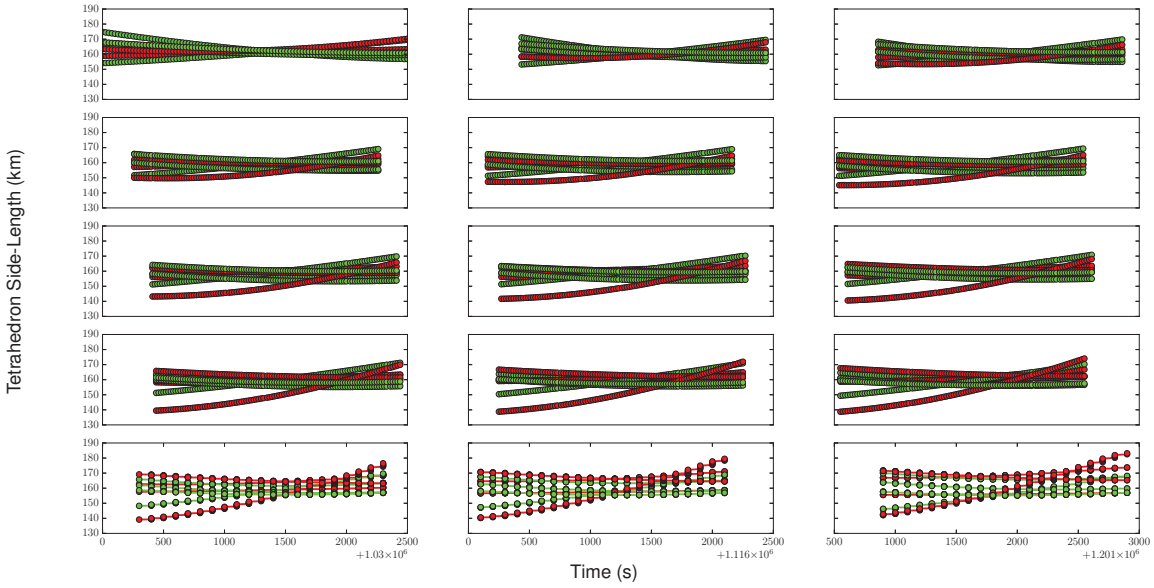

Figure 4.34: Case 5 : $L = 160$ km target test ; 15 revolutions about Earth ; $\pm 1,000$ second ROI. Horizontal axis is time in seconds. Side-Length Graph

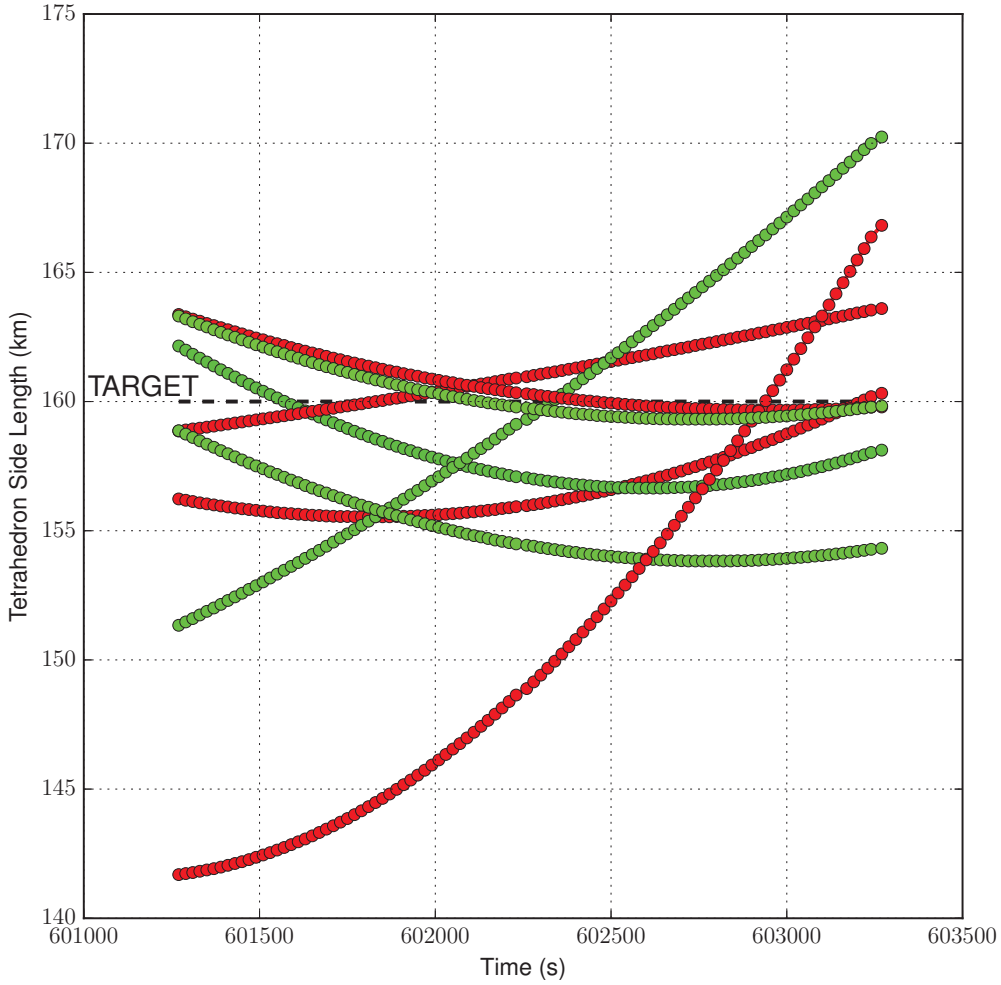

Figure 4.35: Side-Length graph focused on the center revolution in Figure 4.34

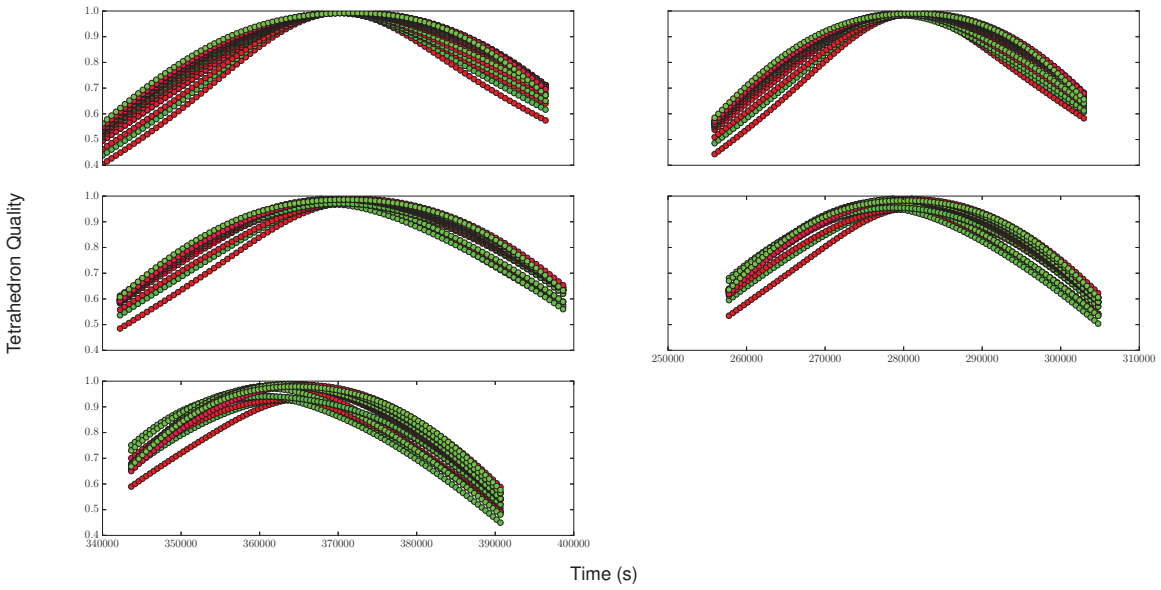

Figure 4.36: Case 5 : $L = 10$ km target test ; 5 revolutions about Earth ; $\pm 23,500$ second ROI. Horizontal axis is time in seconds. Quality Graph

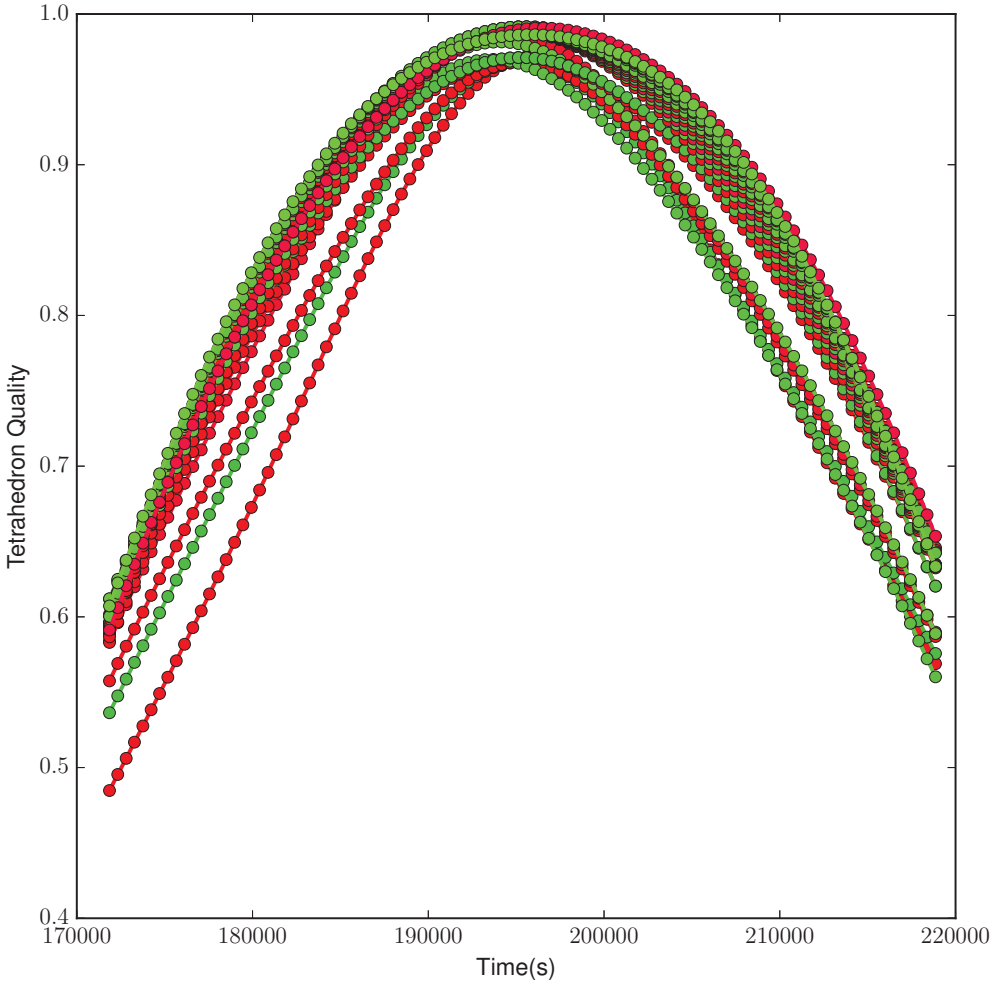

Figure 4.37: Quality graph focused on the center revolution in Figure 4.36

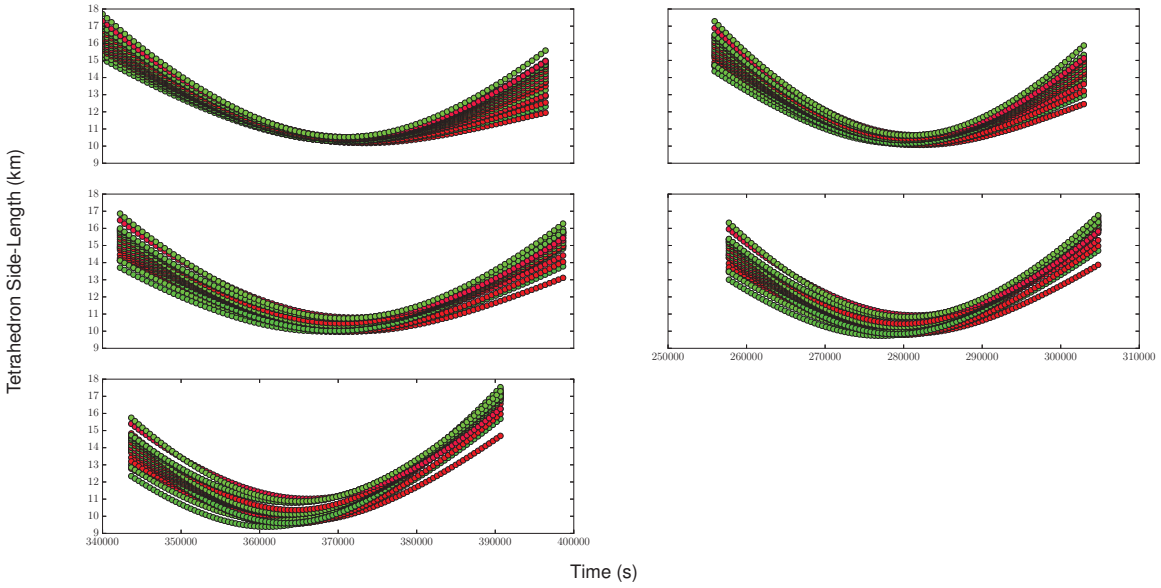

Figure 4.38: Case 5 : $L = 10$ km target test ; 5 revolutions about Earth ; $\pm 23,500$ second ROI. Horizontal axis is time in seconds. Side-Length Graph

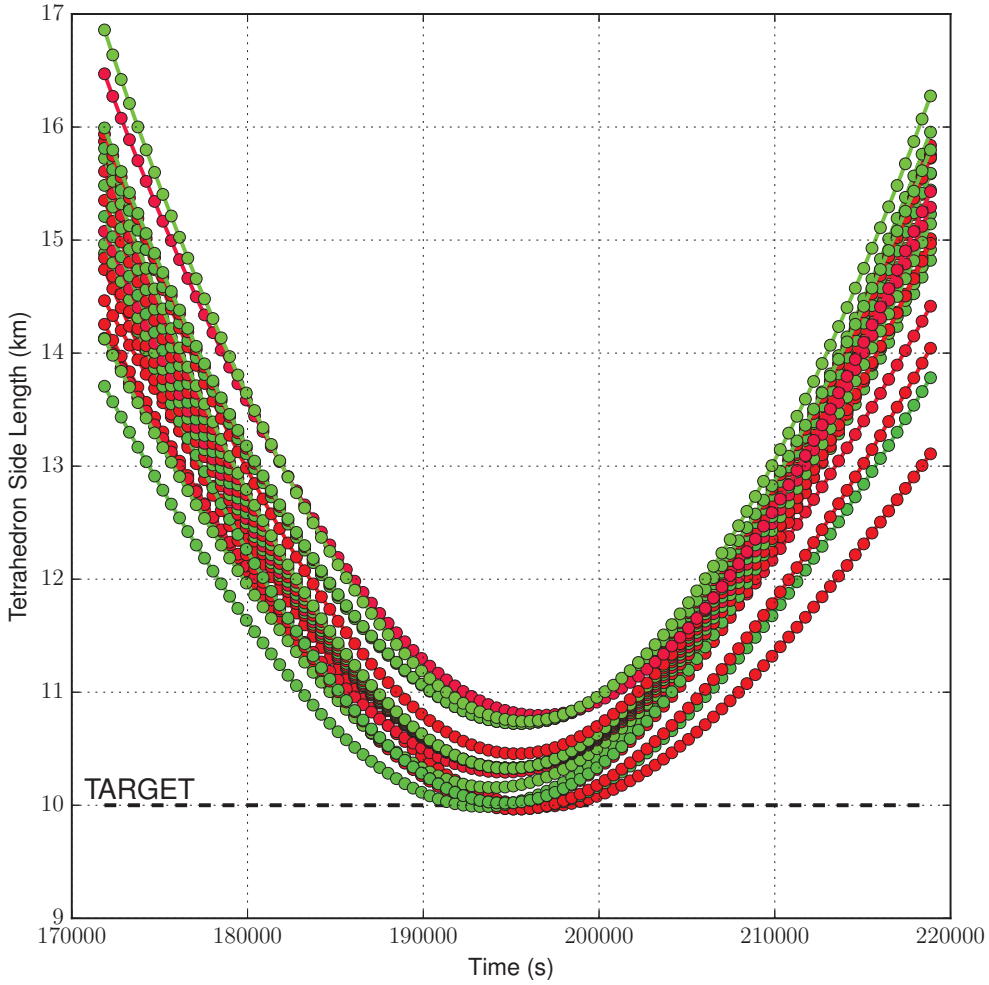

Figure 4.39: Side-Length graph focused on the center revolution in Figure 4.38

When extending the 10km results by revolution an interesting phenomenon is observed. In Figures 4.40 and 4.42 is an expansion of 10 revolutions where near linear profiles are observed with only minor deviation in the later revolutions; this is not too surprising since the ROI is only $\pm 1,000$ seconds. If this result is extended by another 5 revolutions however, it appears that physical constraints force the adoption of an unexpected optima. Figures 4.44 and 4.46 show this unfortunate transition. Fitness only aims to optimize the two formation quantities without explicit responses, such as an additional penalty, for not meeting the quality and size goals; the requirements' bounds do not appear in fitness. This was done in the belief that if such measures ever came into play during evolution, it would mean that the method was already unable to find trajectories that met the requirements; whether or not solutions would exist for such problems could not be known *a priori*. It would seem that since changes in position are closer to the order of the scale of the formation for 10km targets as opposed to 160km targets, that a finer line is walked when optimizing for smaller scale formations. This is reinforced by the fact that the 10km revolution expansion results shown in Figure 4.46 do not exhibit the same symmetry across revolutions as seen in the 160km tests. Trajectories cannot lead the perturbative effects to transition symmetrically through a peak value since there may not be sufficient allowance to do so; the necessary change needed to accomplish such a leading of the peak may if fact cause the observed transition to profiles that are less optimal.

4.6 Comparison with Non-Evolutionary Optimization Methods

Given that the purpose of the presented definition of fitness is to facilitate DE's evolutionary progression, whether or not a non-evolutionary optimization scheme can make use of this fitness definition to solve the problem is of interest. To answer this, trials were run using

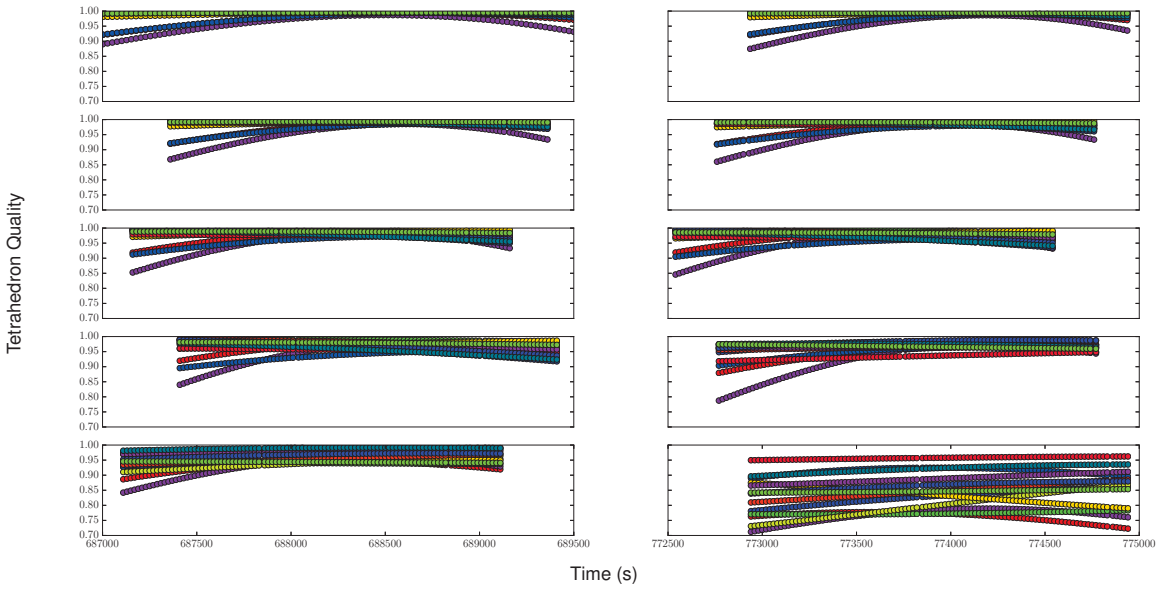

Figure 4.40: Case 5 : $L = 10$ km target test ; 10 revolutions about Earth ; $\pm 1,000$ second ROI. Horizontal axis is time in seconds. Quality Graph

matlab's *fmincon* allowing the same amount of time as was allotted for the DE trials. *fmincon* is not itself a local optimization method; it contains four separate local optimization algorithms the choice of which is a user controlled input parameter. The available algorithms are an interior point method, a trust-region based method, a sequential quadratic programming (SQP) method, and an active set method. Of these, only the SQP and active set methods could be used on the problem due to how it was posed. The active set method stalled and was unable to recover. The SQP algorithm was able to solve the problems to which it was applied.

Matlab's *fmincon* using SQP was applied to both side-length targets of the MMS design problem using Case 2's initial configuration. The trials were set to allow the local solver to terminate under either lack of improvement or 10 hours elapsed time. Figures 4.48 and 4.49 show the 160km target results obtained through SQP; the same set of 51 trials was run since the unique balancing weights constitute distinct definitions of fitness. This

optimizer was able to proceed to, but not past, the same level of staging as was DE. The highest average quality was 0.928 with a peak of 0.979. The standard deviation of side-length was 8.964. The balancing parameter for the trial associated with these values was 0.52. Figures 4.50 and 4.51 show the 10km target results. Here the highest average quality was 0.950 with a maximum value of 0.966. The standard deviation of the side-length of that trial was 1.824 and the balancing parameter was 0.80. Comparing these results against their Case 2 counterparts (figures 4.4 and 4.5 for the 160km target and figures 4.7 and 4.8 for the 10km target) in a strict quantitative sense would be improper as a statistically significant number of tests was not conducted but in a broader sense it appears that both are capable of approaching the problem. While SQP was faster in finding solution, the quadratic approximations inherent in the algorithm become less valid as problem complexity increases. While it is true the DE would also find such problems more difficult than the current problem, as a "global" scheme DE would likely be better equipped for scaling complexity. Beyond this speculation no further conclusions can be reached as the application of DE, and not a performance comparison of it to other schemes, was the focus of this work.

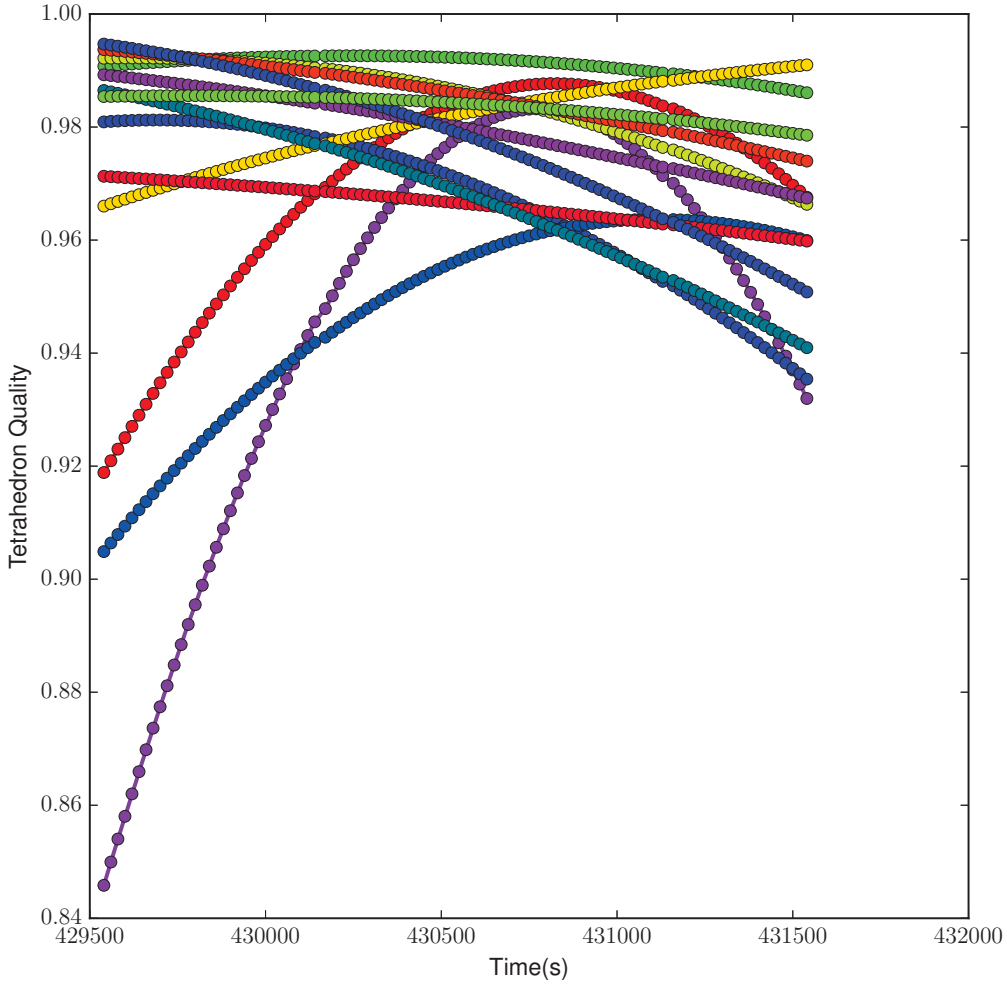

Figure 4.41: Quality graph focused on the center revolution in Figure 4.40

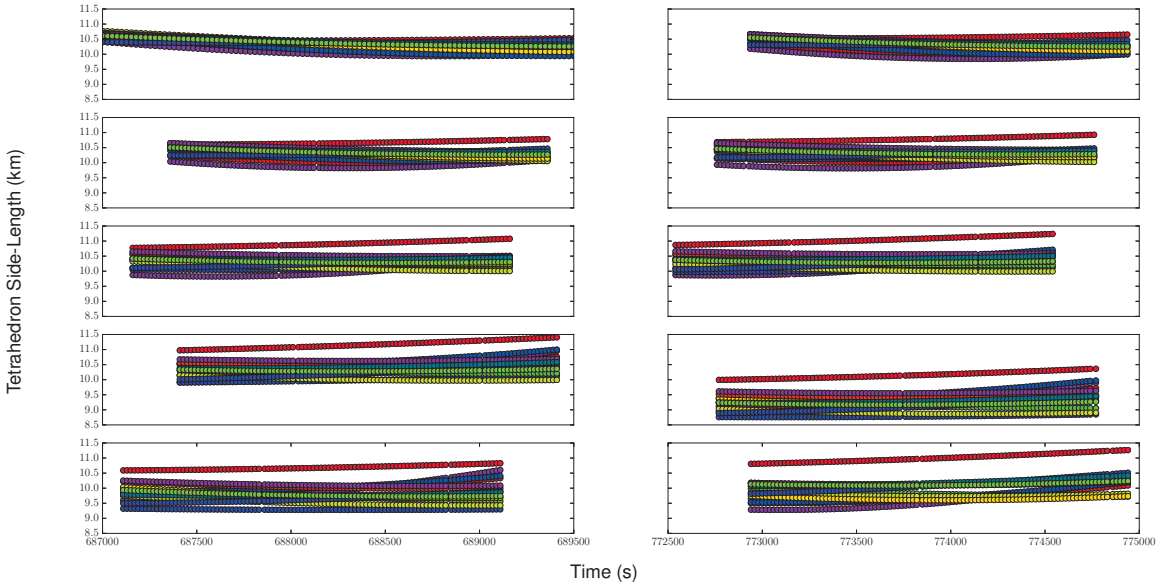

Figure 4.42: Case 5 : $L = 10$ km target test ; 10 revolutions about Earth ; $\pm 1,000$ second ROI. Horizontal axis is time in seconds. Side-Length Graph

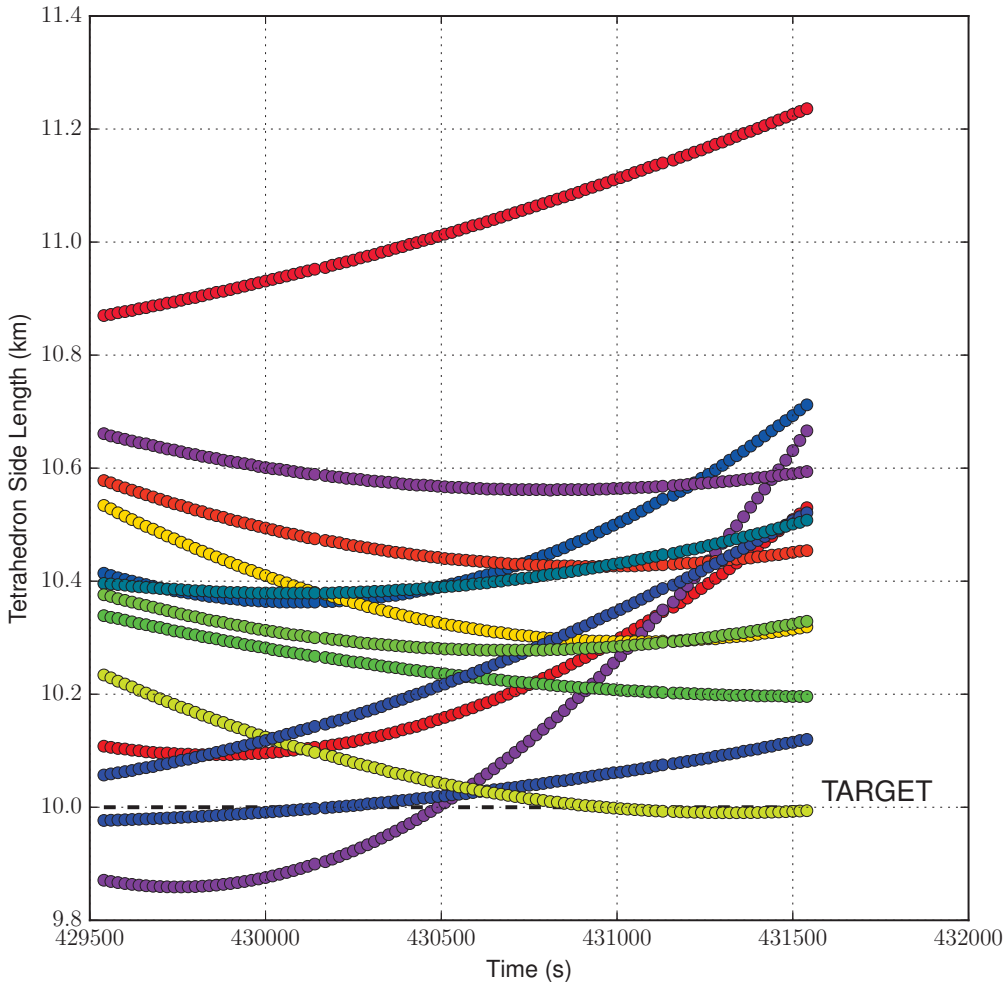

Figure 4.43: Side-Length graph focused on the center revolution in Figure 4.42

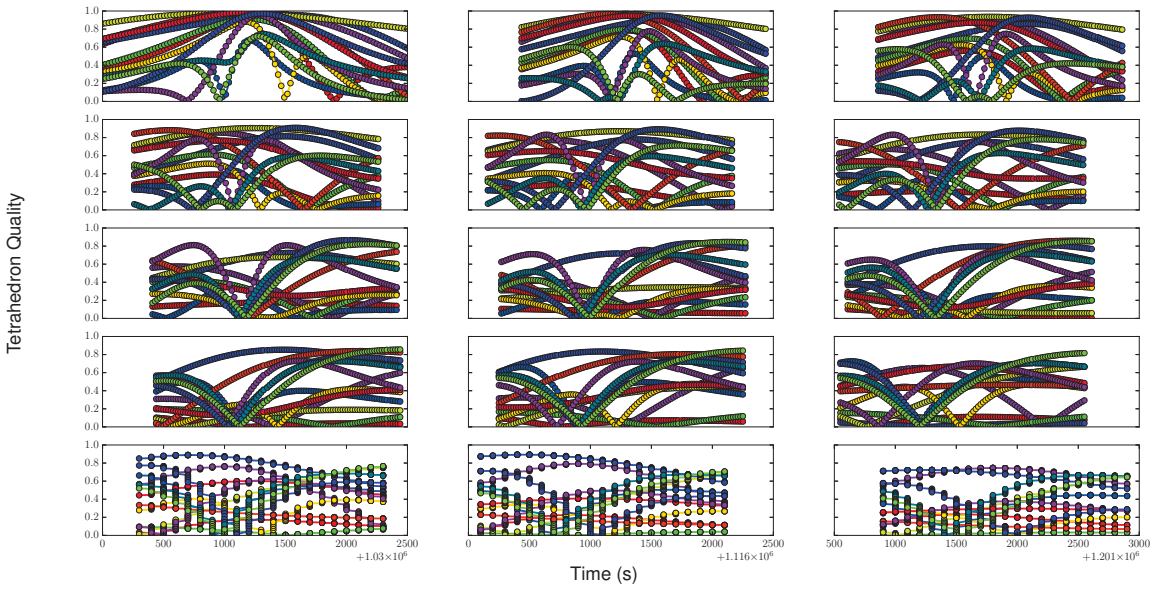

Figure 4.44: Case 5 : $L = 10$ km target test ; 15 revolutions about Earth ; $\pm 1,000$ second ROI. Horizontal axis is time in seconds. Quality Graph

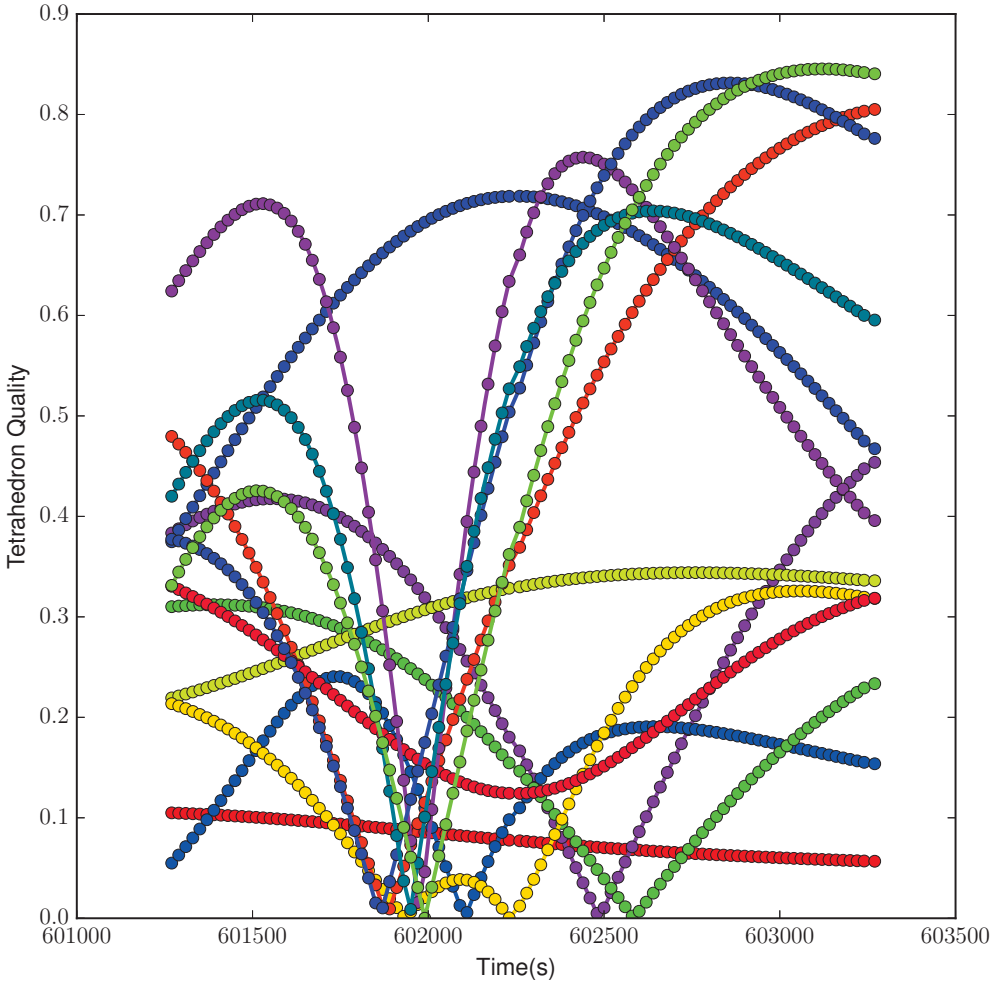

Figure 4.45: Quality graph focused on the center revolution in Figure 4.44

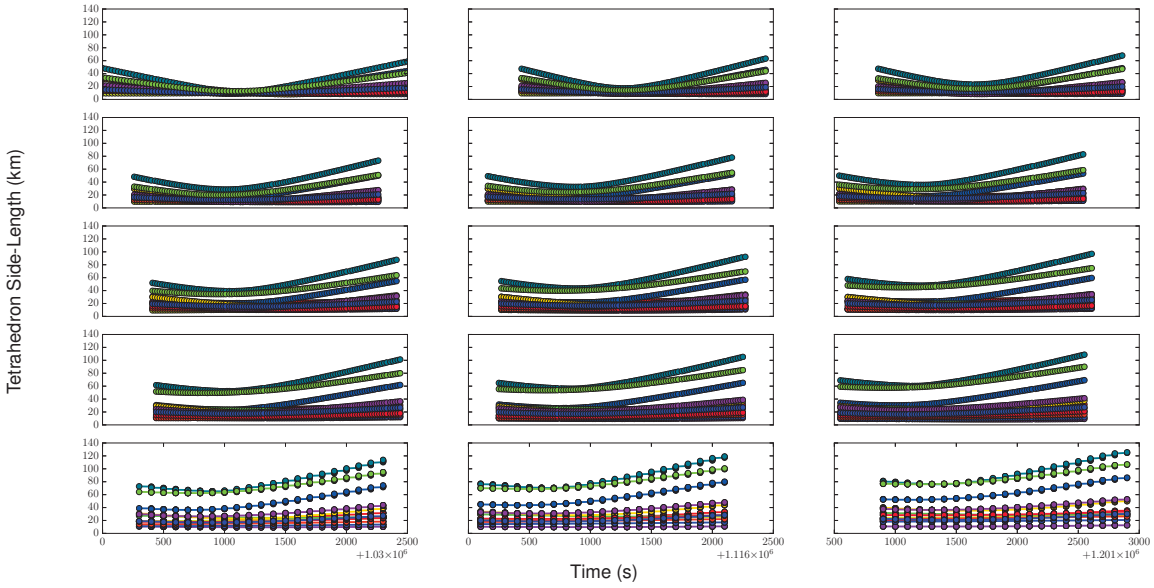

Figure 4.46: Case 5 : $L = 10$ km target test ; 15 revolutions about Earth ; $\pm 1,000$ second ROI. Horizontal axis is time in seconds. Side-Length Graph

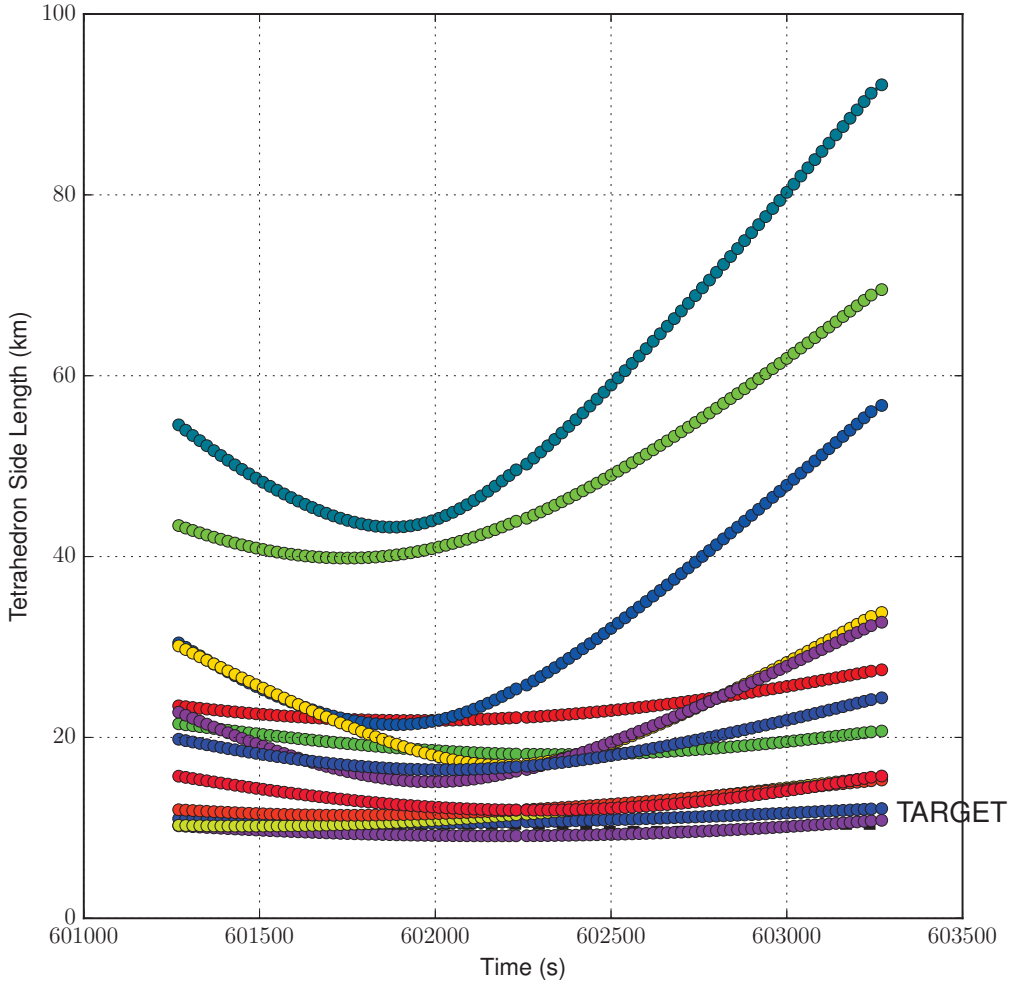

Figure 4.47: Side-Length graph focused on the center revolution in Figure 4.46

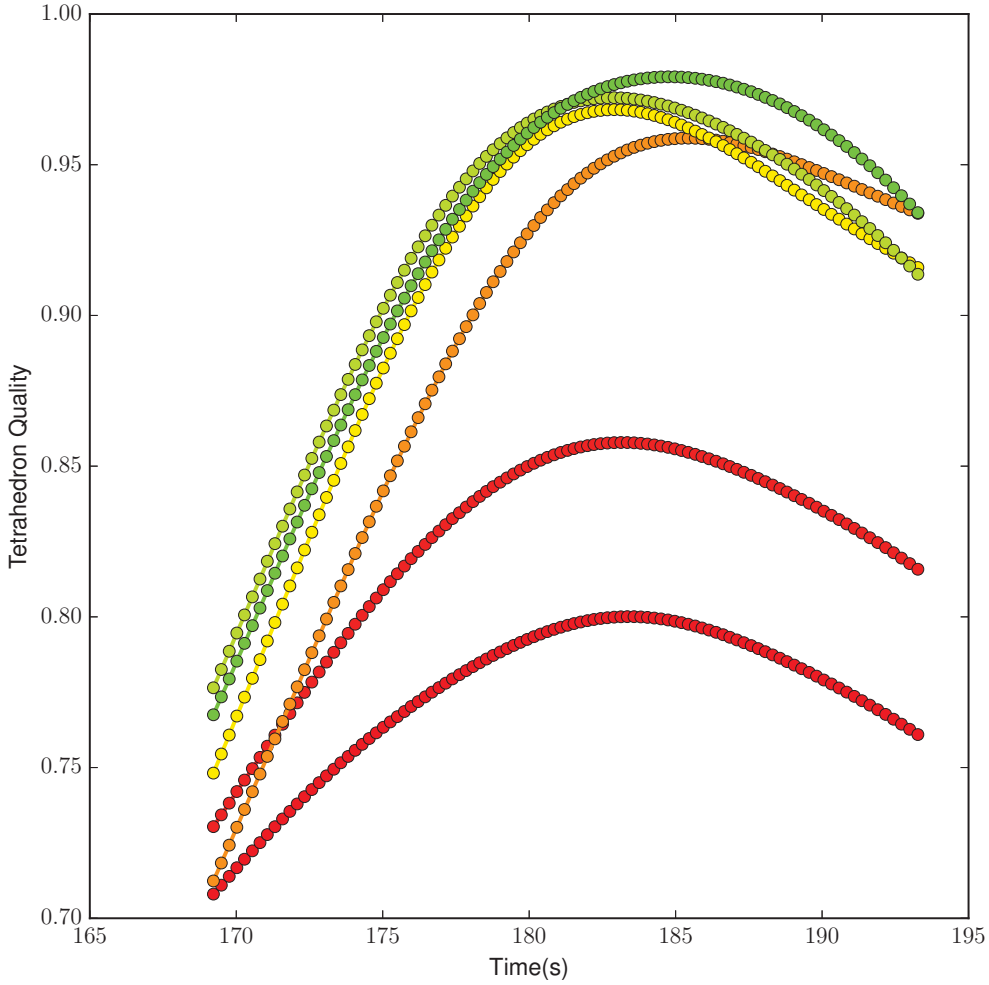

Figure 4.48: Local Optimizer : $L = 160$ km target test ; $\pm 15,000$ second ROI, Quality Graph

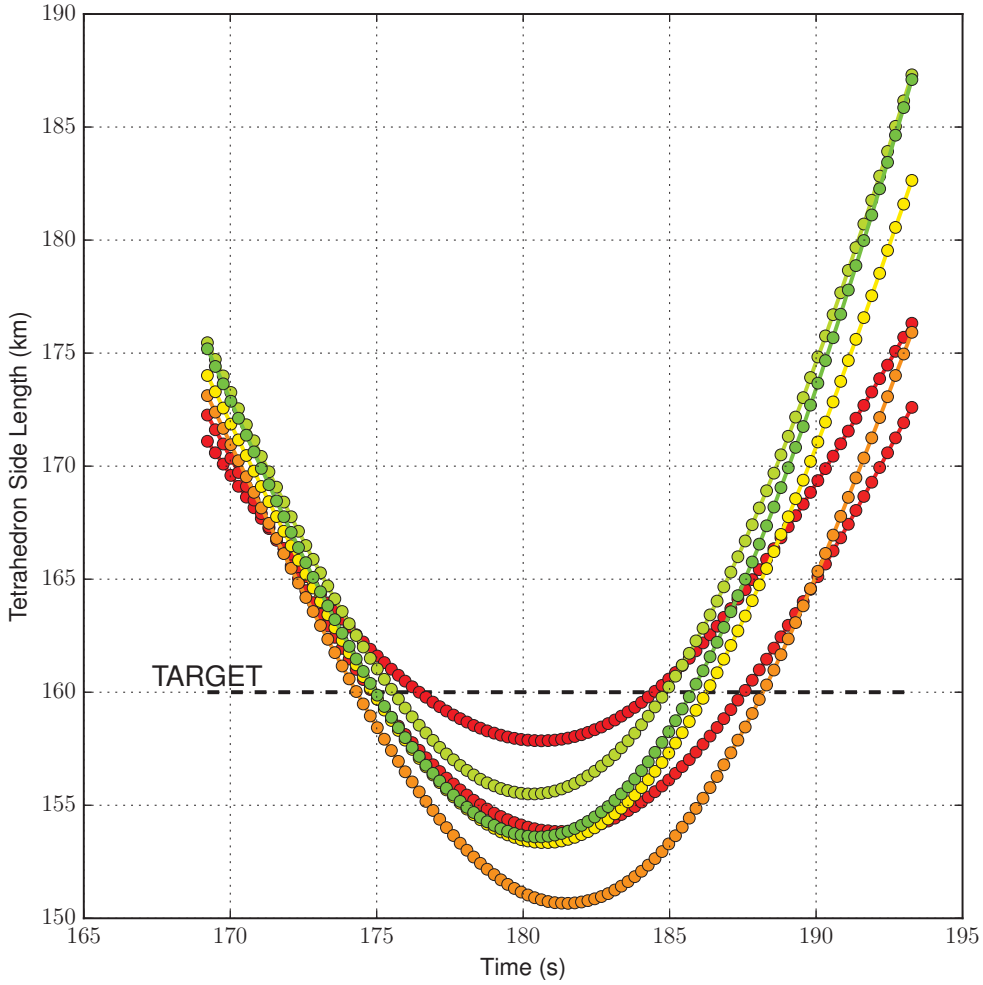

Figure 4.49: Local Optimizer : $L = 160$ km target test ; $\pm 15,000$ second ROI, Side-Length Graph

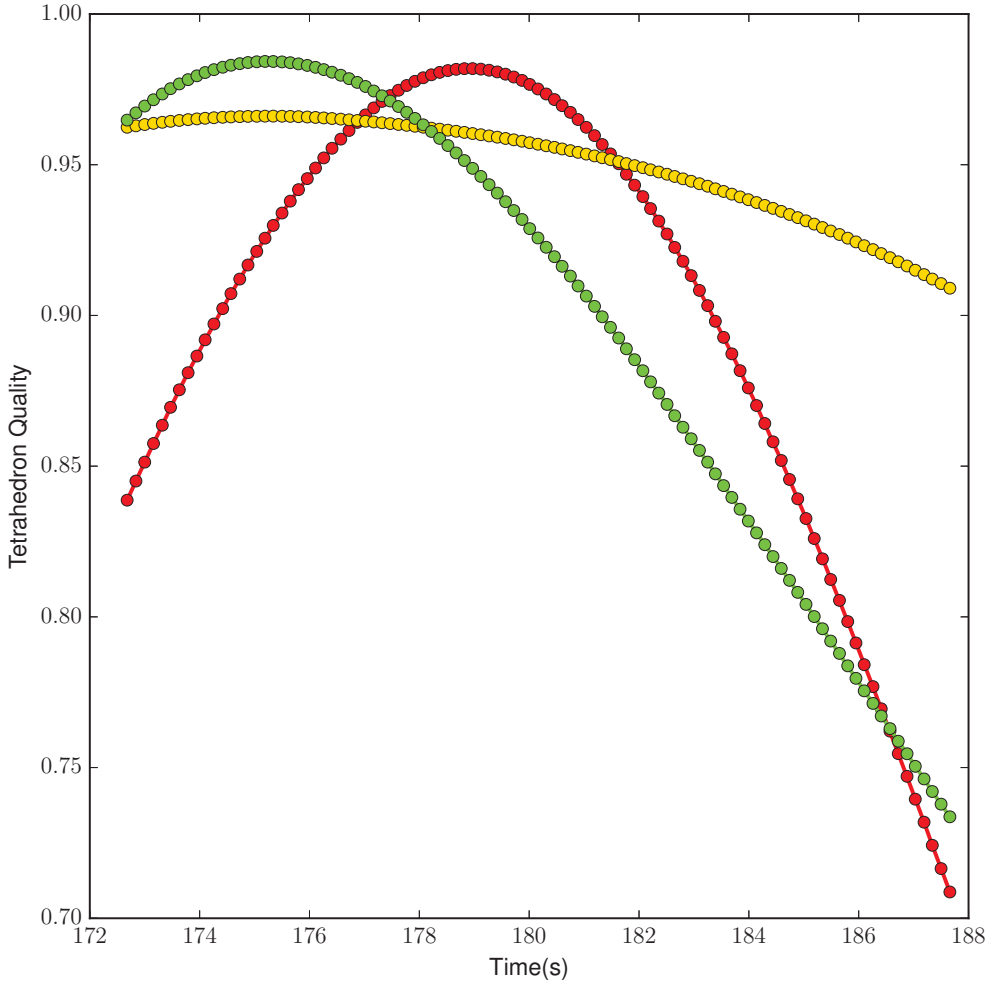

Figure 4.50: Local Optimizer : $L = 10$ km target test ; $\pm 10,000$ second ROI, Quality Graph

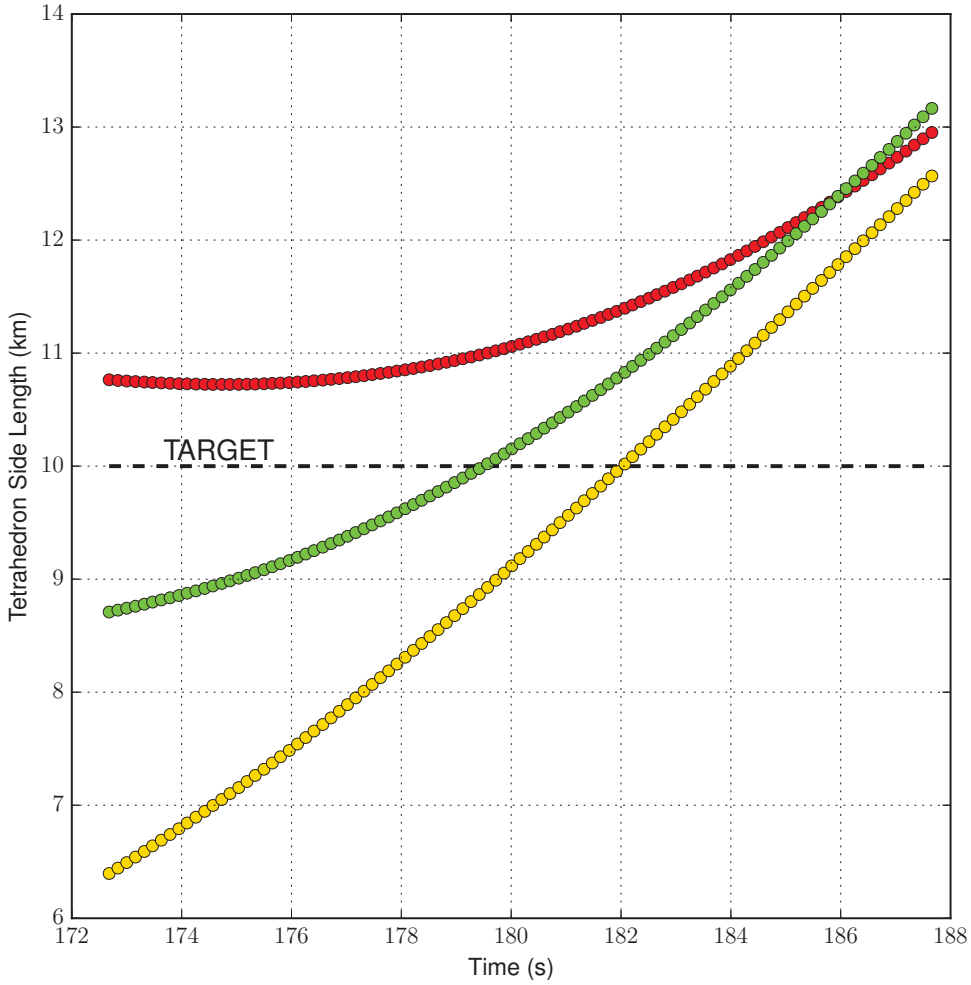

Figure 4.51: Local Optimizer : $L = 10$ km target test ; $\pm 10,000$ second ROI, Side-Length Graph

Chapter 5

Conclusions

Trajectory design that accounts for multiple craft and constraints on their relative positions is a difficult task. While much work has been conducted in evolutionary trajectory design in both the Earth-centered and Sun-centered (often interplanetary) frames, such approaches have not been applied to the simultaneous design of trajectories for multiple craft interlinked by requirements on their effective formation to the knowledge of the author. In this work Differential Evolution (DE) was applied to a multi-satellite trajectory problem modeled after the Magnetospheric Multi-Scale Mission (MMS). A process for increasing the size of the Region of Interest (ROI) in both number of revolutions and time within each revolution was outlined and shown capable of expanding along both fronts 15 fold in many of the results presented. The restriction to a single-impulse approach ultimately limited how far trajectories could be extended both in ROI time extent and the number of revolutions considered but this was necessary due to computational limitations. The set of initial configurations tested demonstrated the importance of the choice of initial configuration when restricted to this approach but the method here presented can be extended beyond this limitation since the inclusion of more maneuvers requires only amending the problem's genome. Regardless of the limitation, multi-satellite trajectory design with topological constraints was shown viable with the use of DE and the definition of fitness here presented.

5.1 Future Work

The application of this technique is not limited to 4-satellite formations. As of this writing, some light work into 5-satellite LEO formations was conducted. Generalization of fitness to any n-hedron is difficult but it can be accomplished through shape constraint and deconstructing volumes into combinations of tetrahedra; for 5 and 6 satellite formations this has been investigated and the complications rise explosively with each new satellite added. Different applications may not only require greater number of satellites but also formations aside from regular n-hedra. A tangible example is orbiting debris mitigation using a physical net. This, if one were to extend how simple nets work on Earth, would likely require a 2-Dimensional formation that is normal to the intercept path. While the current formulation is specialized to regular n-hedra, planar geometric rules applied with vector consideration (direction of travel and the plane's normal vector) could be used to arrive at an initial model of fitness without much difficulty. Arrayed measurement devices would also require similar formations for viewing the Earth, with a different direction of course. Beyond this, the possible formations are inconceivably infinite but the utility of their application is determined by their need in the industry (a smiley face is possible but not useful beyond the novelty). The last means of extension discussed here is different propulsion schemes. Due to limitations on time, only single impulsive firings were considered; to clarify, impulsive firings are the simplest description of chemical propulsion. With a sufficient computational setup, or perhaps with a more suitable method (new fitness definition or algorithm), multiple impulses can be considered which vastly expands the utility of the method as it escapes from the single ellipse trajectories of purely academic interest. This could be continued further to the finite burn model, where thrust has a finite non-singular period over which it occurs. Moving away from chemical propulsion, the expanding interest in continuous thrust could be examined. This type of problem is far more difficult than the chemical analog as

issues of non-constant available power, power distribution between systems, and a myriad of increasingly complex systems level considerations arise. The extension of this work to formations consisting of inexpensive satellites (all using continuous propulsion) would be particularly useful as, combined the concept of artificially large measurement systems, this provides a means of making advanced data acquisition from space missions a more accessible prospect; not cheap by any means since the satellites must still be carried to their destination but far less expensive than large satellites of similar capability.

Appendix A

Appendix

A.1 Governing Physics

A.1.1 Keplerian motion

The basic description of a spacecraft's motion about a planetary body is governed by Newton's Law of Gravity (16). The spacecraft's motion is often best viewed relative to the planet to whose gravity it is subject. This leads to the equation for relative two-body motion given by equation A.1.

$$\ddot{\mathbf{r}} = -\frac{\mu}{|\mathbf{r}|^3}\mathbf{r} \tag{A.1}$$

where $\ddot{\mathbf{r}}$ is the second derivative of the position vector, μ is the gravitation parameter (here for Earth), and $\mathbf{r}$ is the position vector from the center of the planetary body. A spacecraft's path about a planet following this description of gravity is described by a conic section; the most pertinent of these is the ellipse as it represents the closed orbits of interest. Closed paths about the planet are not time dependent; an object's position along the path is a function of time but the path itself is unchanging in time. This recurring path means that extending any work to consider multiple orbits as opposed to a single orbit is trivial as orbits can never differ from the original path without additional force inclusions. This is a

long studied, well understood problem with accessible solution methods for the orbit about a single planetary body.

A.1.2 The Earth's Oblateness

While Newton's Law of Gravity was derived for point masses, as an approximation it stands up reasonably well for spherical distributions of mass. This does not hold true for the Earth. While the exact mass distribution of the Earth is difficult to quantify, a better approximation than a sphere is calling the Earth an oblate spheroid. The deviation this causes in the acceleration of an orbiting body is captured by equation A.2.

$$\mathbf{a_{oblate}} = \frac{3J_2\mu R_E^2}{2|\mathbf{r}|^5}\left[x\left(5\frac{z^2}{|\mathbf{r}|^2}-1\right)\mathbf{i} + y\left(5\frac{z^2}{|\mathbf{r}|^2}-1\right)\mathbf{j} + z\left(5\frac{z^2}{|\mathbf{r}|^2}-3\right)\mathbf{k}\right] \tag{A.2}$$

where $\mathbf{a_{oblate}}$ is the acceleration caused by the oblateness perturbation, J_2 is the oblateness correction (zonal harmonic), R_E is the radius of the Earth, $[x, y, x]$ are the Cartesian coordinates of position with the Earth revolving about the z-axis, and $[\mathbf{i}, \mathbf{j}, \mathbf{k}]$ are the units vectors for the Cartesian axes. This correction alters the closed path of Keplerian motion into open paths. The J_2 correction does not appreciably affect the altitudes (perigee and apogee) of an orbit but does cause the orbit to precess about the planet.

Figure A.1 shows the how considering the J_2 correction affects the MMS reference trajectory over the course of 20 days. In the figure the red trace of the orbit widens in areas which, since each revolution about the planet traces out a thin line, shows the precession of the orbit over time. The MMS reference trajectory has a period just shy of one day so this level of effect is beyond that felt by many of the multi-revolution trials. Figure A.2 shows the same path after only 5 days; this is around the base level of the multi-revolution tests. Although not as pronounced, the same precession effects are seen in the widened path traced over time.

Although the effect does not appear to be too great an alteration of a single craft's

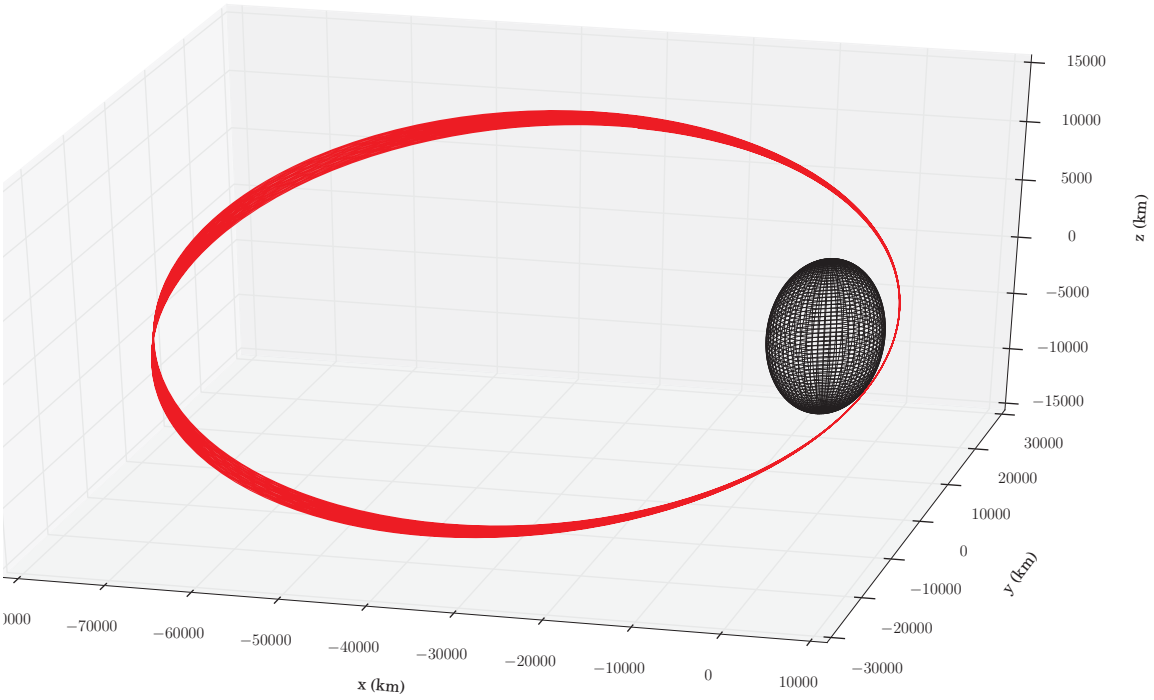

Figure A.1: The MMS reference path numerically integrated over 20 *days with oblateness effects considered*

trajectory one must remember that the problem studied here concerns the motion of multiple craft. After even a single orbit the relative motion of the satellites due to this effect are enough to greatly lower the quality of the formation during successive passes through the ROI.

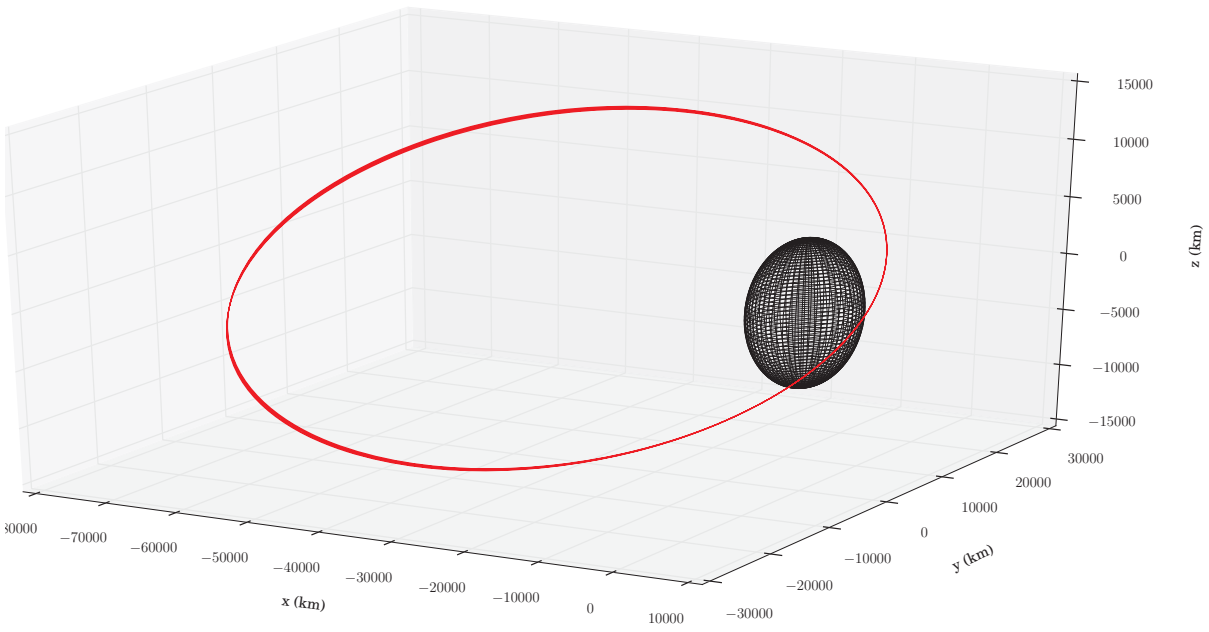

Figure A.2: The MMS reference path numerically integrated over 5 days with oblateness effects considered

A.1.3 Atmospheric Drag

Atmospheric drag is the force exerted on an object as it moves through the atmosphere of a planet. This force rapidly attenuates as the altitude relative to the planet is increased; this is due to the force being proportional to the atmospheric density which too rapidly decreases with altitude. Figure A.3 shows how atmospheric density varies as a function of altitude. Since the lowest altitude of the MMS reference path is approximately 1276km, it is clear that atmospheric drag will not be very influential over the time range considered; this will be further demonstrated later in this section.

An aspect of this drag that is not immediately apparent is the fact that the drag force has a component that points tangent to the surface of the planet in the direction of rotation since the rotations of the planet causes the atmosphere to have a bulk velocity. This means that non-equatorial orbits are steered in addition to the expected slowing effect.

Figure A.4 shows the effects of atmospheric drag as they apply to the MMS reference path over 20 days. In a region around apogee, similar to the description of the MMS ROI, the apogee of the orbit is seen gradually decreasing. As it was with the J_2 demonstration, this effect is shown for a period of time longer than the tests concern. Figure A.5 shows the same effect applied over a period of 5 days. It is hard to definitively state whether or not what is observed in the graphic is the effects of drag or simply an artifact of digital representation of images. Looking back to the density plot A.3 it would seem that for the altitude of perigee, the point most affected by this source of gravitational perturbation, that the density is not sufficient to cause appreciable affects. Drag itself, even for these distances, is not something that should be thought of as unimportant. Figure A.6 demonstrates that the effect compounds over time; the graphic shows the effect over the span of 100 days. If this work concerned longer flight durations including this effect would have been necessary but since atmospheric drag does not produce a significant effect over the time-scales studied, including it in physical considerations would have only served to slow the evolutionary progress of the method.

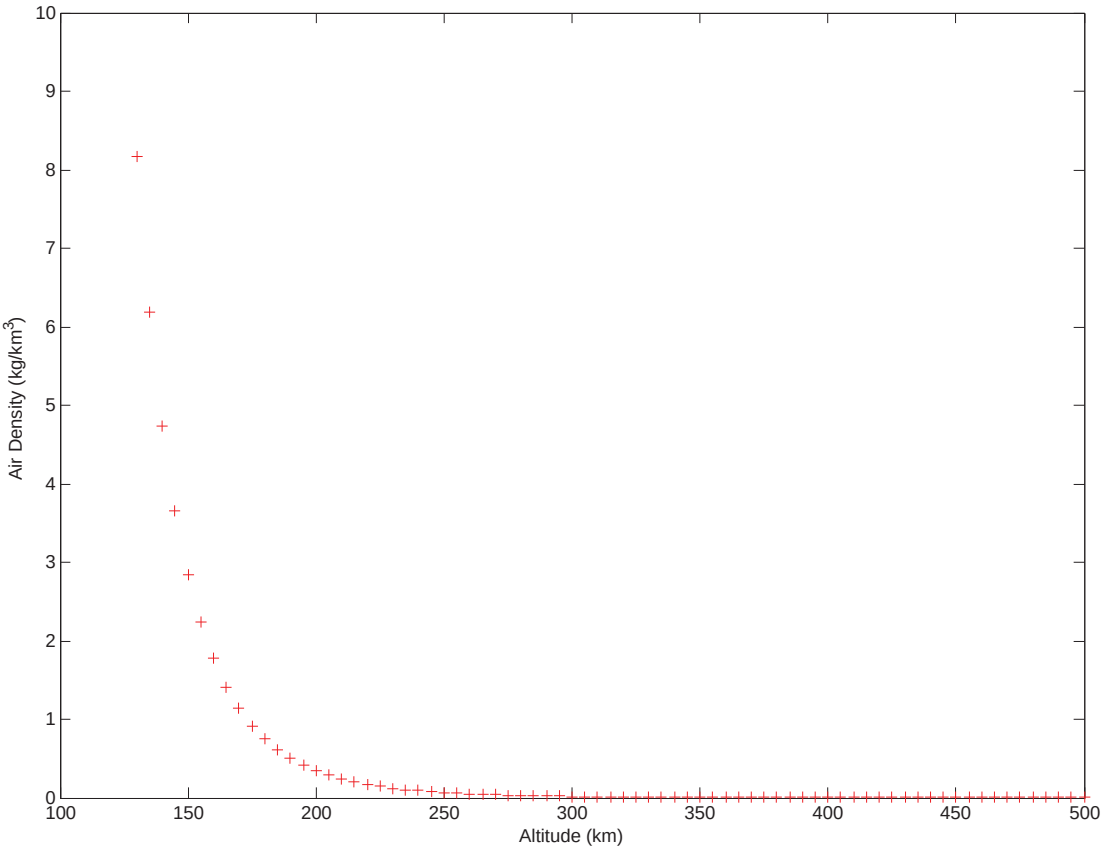

Figure A.3: Air density as a function of altitude

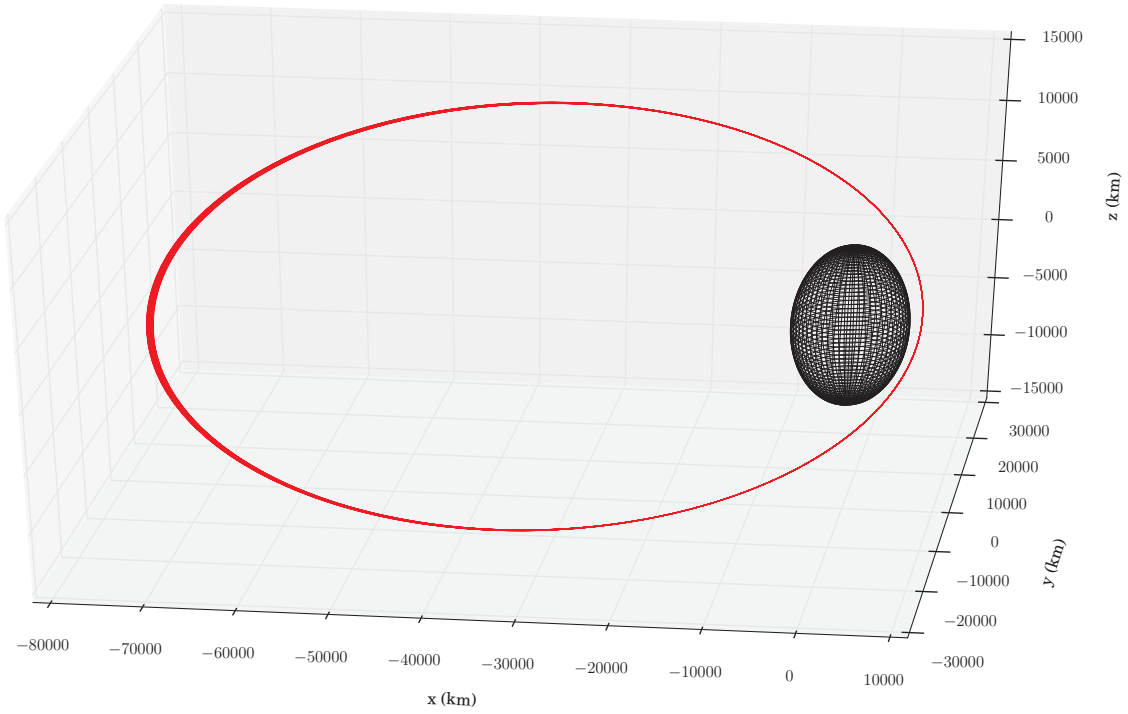

Figure A.4: The MMS reference path numerically integrated over 20 *days with atmospheric drag considered*

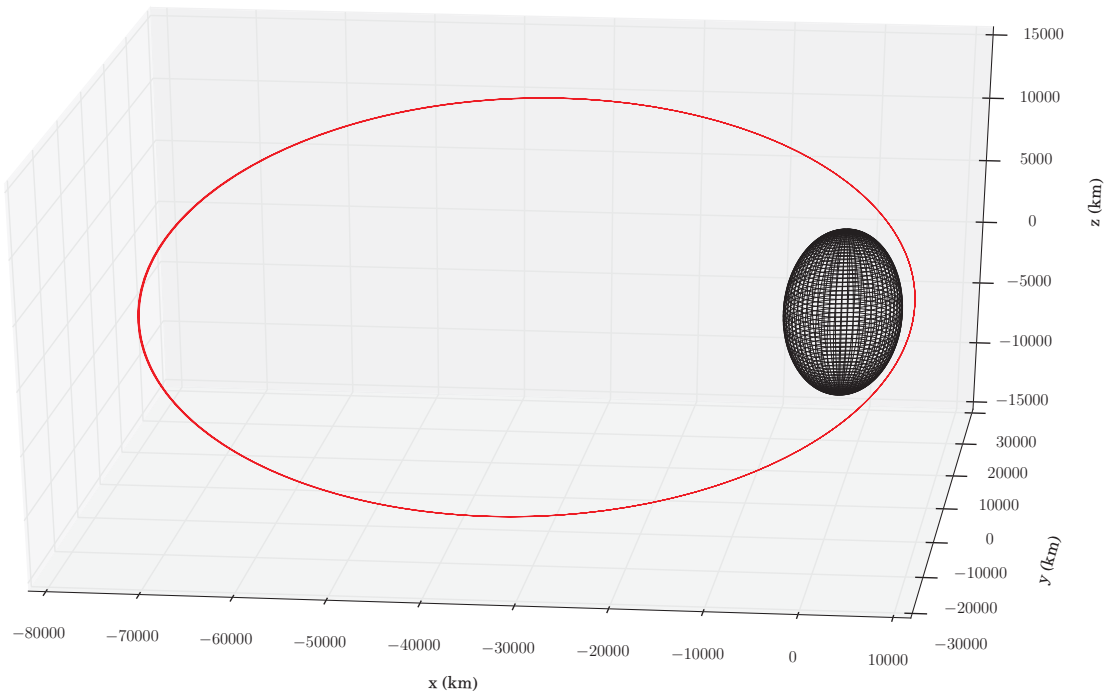

Figure A.5: The MMS reference path numerically integrated over 5 *days with atmospheric drag considered*

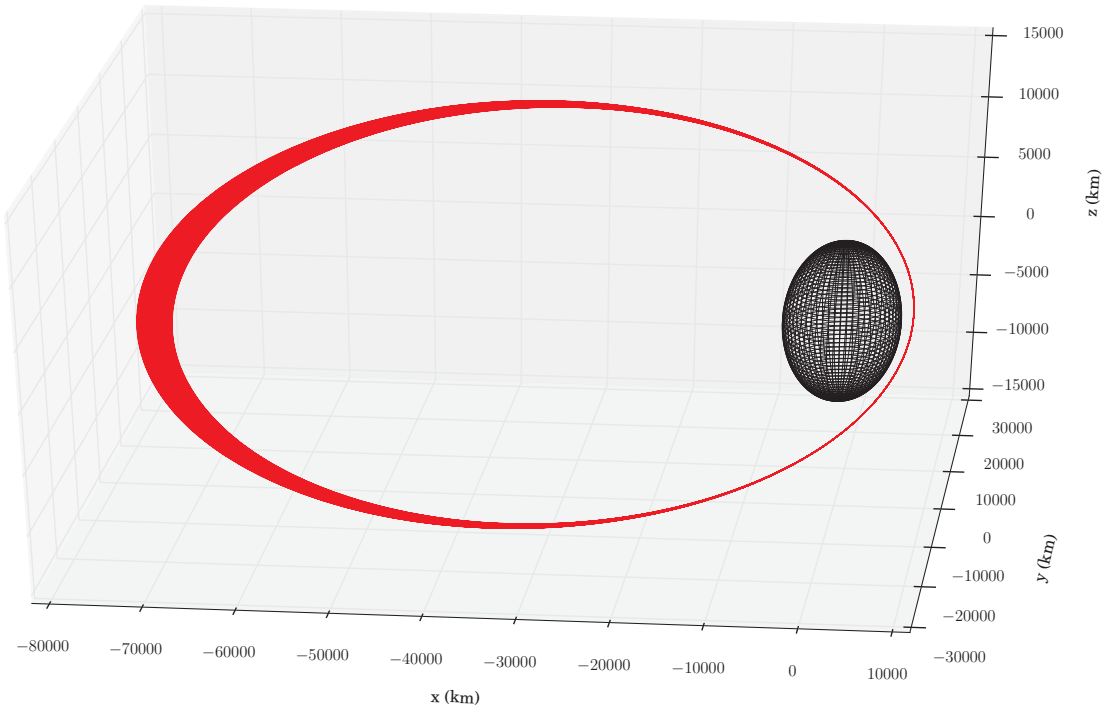

Figure A.6: The MMS reference path numerically integrated over 100 *days with atmospheric drag considered*

Bibliography

[1] J. Stiles, N. Goodman, and SiChung Lin. Performance and processing of sar satellite clusters. In *Geoscience and Remote Sensing Symposium, 2000. Proceedings. IGARSS 2000. IEEE 2000 International*, volume 2, pages 883–885 vol.2, 2000.

[2] E. Gill, P. Sundaramoorthy, J. Bouwmeester, B. Zandbergen, and R. Reinhard. Formation flying within a constellation of nano-satellites: The {QB50} mission. *Acta Astronautica*, 82(1):110 – 117, 2013. 6th International Workshop on Satellite Constellation and Formation Flying.

[3] Seungwon Lee, Paul von Allmen, Wolfgang Fink, A. E. Petropoulos, and R. J. Terrile. Multi-objective evolutionary algorithms for low-thrust orbit transfer optimization. *GECCO*, 2005.

[4] C. R. Bessette and D. B. Spencer. Optimal space trajectory design: A heuristic-based approach. *Advances in the Astronautical Sciences*, 2006.

[5] M. Vasile, E. Minisci, and M. Locatelli. An inflationary differential evolution algorithm for space trajectory optimization. *Evolutionary Computation, IEEE Transactions on*, 15(2):267–281, April 2011.

[6] L. Casalino and M. Rosa Sentinella. Evolutionary algorithm for interplanetary trajectories optimization. *Astrocon*, 2008.

[7] Francesco Cacciatore and Chiara Toglia. Optimization of orbital trajectories using genetic algorithms. *Journal of Aerospace Engineering, Sciences and Applications*,

2008.

[8] T. Vinko and D. Izzo. Global Optimisation Heuristics and Test Problems for Preliminary Spacecraft Trajectory Design.

[9] C H Yam, D D Lorenzo, and D Izzo. Low-thrust trajectory design as a constrained global optimization problem. *Proceedings of the Institution of Mechanical Engineers, Part G: Journal of Aerospace Engineering*, 225(11):1243–1251, 2011.

[10] J. Englander, B.A. Conway, and T. Williams. Automated mission planning via evolutionary algorithms. *Journal of Guidance, Control, and Dynamics*, 35(6):1878–1887, 2012.

[11] Steven Hughes. Formation Design and Sensitivity Analysis for the Magnetospheric Multiscale Mission (MMS). In *AIAA/AAS Astrodynamics Specialist Conference and Exhibit*, Reston, Virigina, June 2012. American Institute of Aeronautics and Astronautics.

[12] CWT Roscoe, S R Vadali, and K T Alfriend. Design of satellite formations in orbits of high eccentricity with performance constraints specified over a region of interest. *The Journal of the Astronautical Sciences*, 2011.

[13] Christopher William Thomas Roscoe. *Satellite formation design in orbits of high eccentricity for missions with performance criteria specified over a region of interest*. PhD thesis, Texas A&M University, 2012.

[14] Kenneth Price and Rainer Storn. Differential evolution for continuous function optimzation. http://www1.icsi.berkeley.edu/ storn/code.html, 2013.

[15] Sreeja Nag and Leopold Summerer. Behaviour based, autonomous and distributed scatter manoeuvres for satellite swarms. *Acta Astronautica*, 82(1):95 – 109, 2013. 6th International Workshop on Satellite Constellation and Formation Flying.

[16] Howard D. Curtis. *Orbital Mechanics for Engineering Students 2/e*. Elsevier, Burling-

ton, Massachusetts, 2013.